A Quantitative, Small-Scale Characterization Suite to Assess Hybrid-Manufactured Tool Performance for Composite Processes

Joshua Ilse
Department of Mechanical Engineering
McGill University, Montreal

A thesis submitted to McGill University in partial fulfilment of the requirements of the degree of Master of Science

Contents

Appendix 105

Abstract

Hybrid large-scale manufacturing (HLSM) of tooling for composite processing offers potential to address common cost and performance problems with traditional tooling, however current methods of research into their design and manufacturing are time, material, and labour-intensive resulting in unnecessary cost. This study proposes a quantitative, small-scale test suite to assess and predict key processing parameters and resultant tool properties and performance of HLSM-tooling in composite processing, which minimizes large-scale testing and consequently material and labour.

The test suite consisted of thermal characterization and a durability test plan, the latter further subdivided into pre-screening tests and a small-scale composite process. Thermal characterization used differential scanning calorimetry and thermogravimetric analysis to develop extrusion temperature processing windows for the two hybrid-manufacturing materials investigated, carbon-fibre acrylonitrile-butadiene-co-styrene (CF-ABS) and glass-fibre polycarbonate (GF-PC), determined to be 150 – 300 ℃ and 160 – 395 ℃ respectively. Thermomechanical analysis was additionally employed to determine coefficients of thermal expansion (CTE) for the materials, which revealed significant CTE anisotropy due to the material extrusion process. All thermal properties were characterized using less than 12 grams total for each material tested. Pre-screening tests used tensiometry, a custom vacuum setup, and micro-indentation testing to assess chemical resistance, vacuum integrity, and hardness of tools, which enabled the rapid screening of many different tool/coating combinations based on a calculated performance index. Small-scale composite process tests used laser profilometry and demould testing to characterize the progressive deterioration of the tools, which revealed that HLSM-tool degradation and failure predominately occurred through mechanisms of increasing roughness of the tool surface that led to increased tool-composite part adhesion.

This work demonstrates that HLSM has potential to produce low-cost, high performance tooling for composite processes competitive with traditional tooling materials and manufacturing processes, but furthermore that research into HLSM and HLSM-tooling for composite processing can be achieved through a low-cost, high fidelity approach that employs small-scale, quantitative characterization methods.

Résumé

La fabrication hybride à grande échelle (HLSM) d'outils pour le traitement des composites offre la possibilité de résoudre les problèmes courants de coût et de performance de l'outillage traditionnel, mais les méthodes actuelles de recherche sur leur conception et leur fabrication demandent beaucoup de temps, de matériel et de main-d'œuvre, ce qui entraîne des coûts inutiles. Cette étude propose une suite d'essais quantitatifs à petite échelle pour évaluer et prédire les paramètres de traitement clés et les propriétés et performances résultantes de l'outillage HLSM dans le traitement des composites, ce qui minimise les essais à grande échelle et par conséquent le matériel et la main-d'œuvre.

La série d'essais comprenait une caractérisation thermique et un plan d'essai de durabilité, ce dernier étant subdivisé en essais de présélection et un processus composite à petite échelle. La caractérisation thermique a utilisé la calorimétrie à balayage différentiel et l'analyse thermogravimétrique pour développer des fenêtres de traitement de la température d'extrusion pour les deux matériaux de fabrication hybrides étudiés, acrylonitrile-butadiène-co-styrène avec fibre de carbone (CF-ABS) et polycarbonate avec fibre de verre (GF-PC), déterminées comme étant 150 - 300 °C et 160 - 395 °C respectivement. L'analyse thermomécanique a également été utilisée pour déterminer les coefficients de dilatation thermique (CTE) des matériaux, ce qui a révélé une anisotropie significative du CTE due au processus d'extrusion du matériau. Toutes les propriétés thermiques ont été caractérisées en utilisant moins de 12 grammes au total pour chaque matériau testé. Les tests de présélection ont utilisé la tensiométrie, une installation à vide personnalisée et des tests de micro-indentation pour évaluer la résistance chimique, l'intégrité du vide et la dureté des outils, ce qui a permis de sélectionner rapidement de nombreuses combinaisons outil/revêtement différentes sur la base d'un indice de performance calculé. Des essais de traitement des composites à petite échelle ont utilisé la profilométrie laser et des essais de démoulage pour caractériser la détérioration progressive des outils, ce qui a révélé que la dégradation et la défaillance des outils HLSM se produisaient principalement par des mécanismes d'augmentation de la rugosité de la surface de l'outil qui entraînaient une augmentation de l'adhérence outil-pièce composite.

Ce travail démontre que HLSM a le potentiel de produire un outillage à faible coût et à haute performance pour les processus composites, compétitif par rapport aux matériaux d'outillage et aux processus de fabrication traditionnels, mais aussi que la recherche sur HLSM et l'outillage HLSM peut être réalisée par une approche à faible coût et à haute fidélité qui utilise des méthodes de caractérisation quantitative à petite échelle.

Acknowledgements

Contribution of Authors

The work completed in all chapters of this thesis was solely performed by the author, with the only exceptions being:

Chapter 3 For tool fabrication described in Section 3.1, all 25.4 mm x 25.4 mm "tool" specimens were fabricated in 2021 and 2022 by the industrial partner, which was given a set of manufacturing instructions.

Chapter 4 For thermomechanical analysis described in Section 4.1, the coefficient of thermal expansion data used for the aluminum specimens was produced in 2014 for a separate research project by C. Demeira, a graduate student in the McGill Composite Structures and Materials Laboratory. For Micro-Indentation/Hardness Testing described in Section 4.2, all data was collected in 2022 by Venkata Naga Vamsi Munagala, a post-doctoral fellow in the McGill Surface Engineering and Tribology.

List of Figures

XIII

List of Tables

List of Abbreviations and Symbols

HLSM: Hybrid Large-Scale Manufacturing

CNC: Computer numerical control

WLVB: Wet-Layup Vacuum Bag

R&D: Research and Development

CTE: Coefficient of Thermal Expansion

DFAM: Design for Additive Manufacturing

DFSM: Design for Subtractive Manufacturing

CAM: Computer-Aided Manufacturing

DFHM: Design for Hybrid Manufacturing

TGA: Thermogravimetric analysis

DSC: Differential Scanning Calorimetry

TMA: Thermomechanical Analysis

ARCA: Advancing-Receding Contact Angle

ACA: Advancing Contact Angle

RCA: Receding Contact Angle

2D: Two-Dimensional

3D: Three-Dimensional

AL: Aluminum

GF: Glass-Fibre

CF: Carbon-Fibre

ABS: Acrylonitrile Butadiene Styrene

GF-PC: Glass-Fibre Polycarbonate

S1: Sealant 1

U: Uncoated

C-P: Ceramic-Polymer

S2: Sealant 2

E: Epoxy-Based

TDS: Technical Data Sheet

CAD: Computer-Aided Design

ORNL: Oak Ridge National Laboratory

ASTM: American Society for Testing and Materials

FOV: Field of View

ROI: Region of Interest

mm: Millimetre

μm: Micrometre

N: Newtown

mN: Milli-Newtown

μL: Microlitre

wt% : Weight Percent

g: Grams

mg: Milligrams

DOT: Degradation Onset Temperature

Tg: Glass Transition Temperature

Tm: Melting Temperature

HV: Vickers Hardness

°C: Degrees Celsius

N_2: Nitrogen

α: Coefficient of Thermal Expansion

L_f: Final Length

L_0: Initial Length

T_f: Final Temperature

T_0: Initial Temperature

γ_{SL}: Solid-Liquid Interface Energy

γ_{SV}: Solid-Air Interface Energy

γ_{LV}: Liquid-Air Interface Energy

Sa: Arithmetic Mean Height

Sq: Root Mean Square Height

Sz: Maximum Height

Chapter 1

Introduction

In a growing materials landscape, composite materials are finding widespread use today for a myriad of applications as scientists and researchers find ways to synergistically leverage the advantages and minimize the disadvantages of each individual material used. Though many different types of composites exist, of growing prevalence is that of polymer-matrix composites which are finding widespread adoption in a range of consumer and commercial industries such as sporting goods, aerospace, automotive, and defence due to their superior properties compared to conventionally used single-phase materials (Figure 1.1) [1–4]. Some of these properties include high strength-to-weight ratio, corrosion resistance, and electrical and thermal resistivity, but what, furthermore, demonstrates their success is their design flexibility in which their highly customizable nature allows for the exact properties of the composite to be tailored specifically for the application [3, 4]. This design flexibility will ultimately be influenced by the specific composite manufacturing method used, many different composite processing methods existing to achieve various types of composite products [4]. Given this growing demand for polymer composites, however, the composite manufacturing industry must find new and innovative ways to streamline the manufacturing process to both increase production and minimize cost.
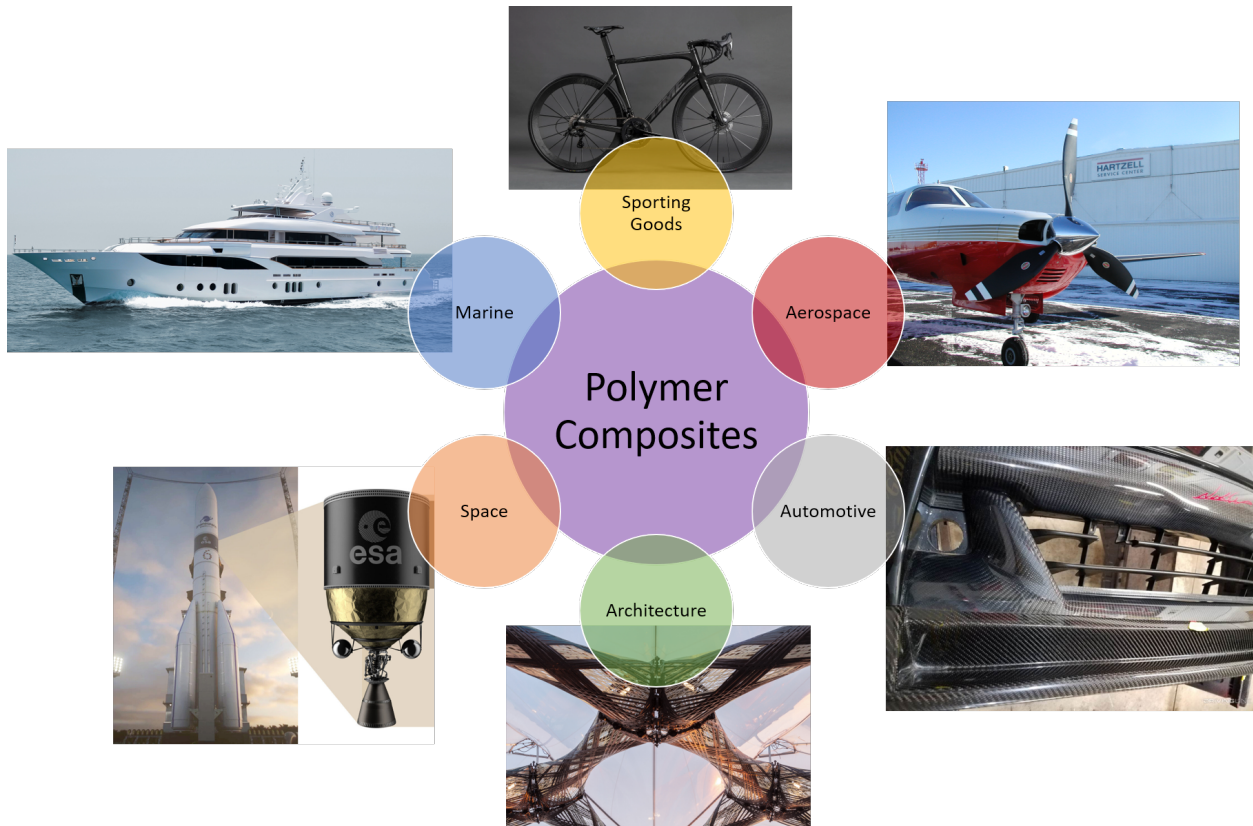
Figure 1.1: The various applications of polymer composites. From top working clockwise: bike frame, aircraft propeller, car bumper, archway, rocket nozzle, yacht. Images reproduced from [5–9].

Tooling is an essential element in almost all composite manufacturing processes in which tight control of the tool properties is required to ensure good quality composite parts [10–13]. Traditionally, these tools are manufactured using metal or composite materials (Figure 1.2), both of which offer advantages and disadvantages in properties and performance depending on the composite process employed. An underlying theme, however, among both are high costs associated with fabrication, due to either inherent material or labour costs when using high performance metal alloys or composite materials respectively [14].
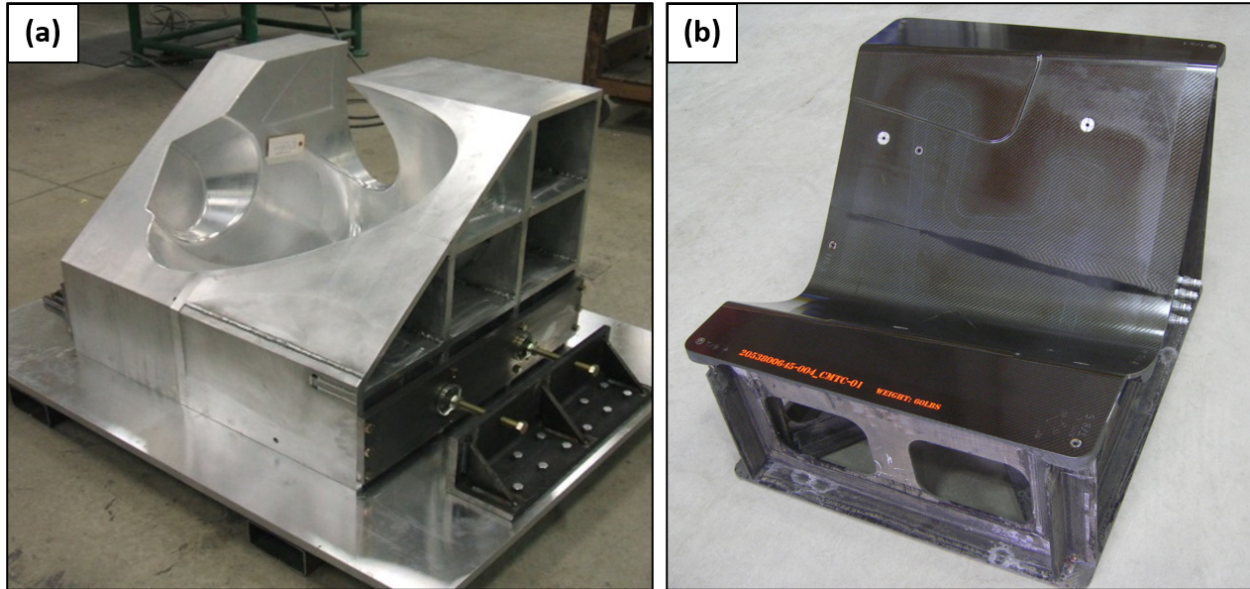
Figure 1.2: Traditional (a) metal and (b) composite tools used in composite manufacturing processes. Images reproduced from [15] with permission.

Recent studies have looked at the use of hybrid large-scale additive and subtractive manufacturing (HLSM) to address these shortcomings in tool manufacturing, in which a thermoplastic material extrusion system is combined with a conventional computer numerical control (CNC) machine which allows for large-scale printing of near net shapes and their subsequent machining to required dimensions and tolerances to take place on the same machine (Figure 1.3) [16–18]. This hybridized process allows for reduced lead time and labour enabling rapid tool development and production, however issues of tool durability due to the intrinsic properties of thermoplastic or thermoplastic composite tool materials used must be addressed [14, 16, 17, 19–27]. Furthermore, to assess the durability of tools produced through this process, most research and development (R&D) is typically performed through large-scale empirical testing which leads to superfluous time expenditure, material waste, and associated costs [14, 16, 17, 24–26]. There is a need for less time and material-intensive approach to characterize tool durability.
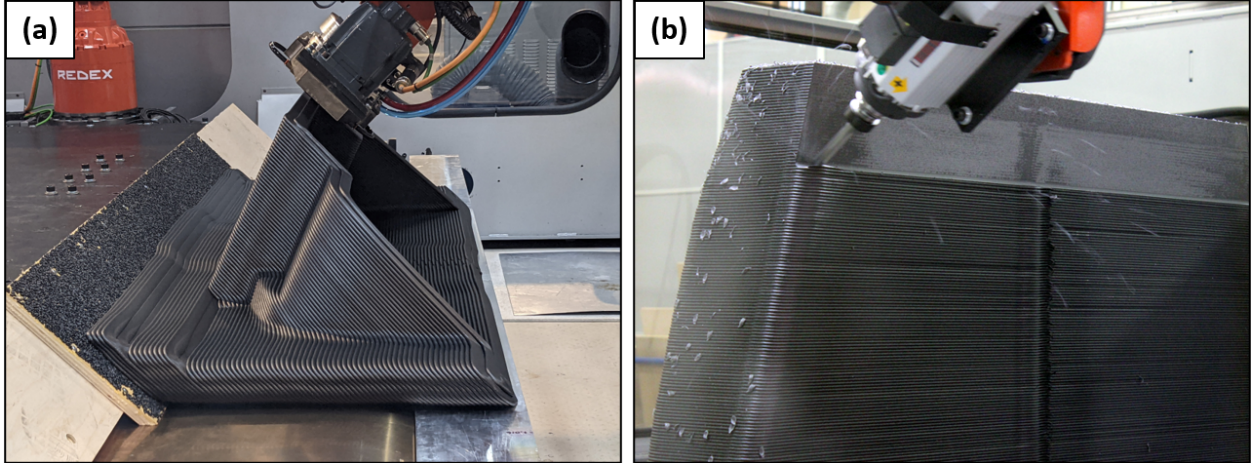
Figure 1.3: The large-scale hybrid manufacturing process, which consists of an (a) additive process followed by a (b) subtractive process. Adapted from [28].

The aim of this work was to present a small-scale suite of characterization methods to quantitatively assess and predict the performance of hybrid-manufactured tools for polymer-matrix composite part fabrication. Performance is evaluated both in terms of processing and manufactured tool performance, in which the context for the latter is a wet layup vacuum bag (WLVB) process. The results of these tests can be used as an early-stage screening process in the design and manufacturing of large-scale tooling produced through the hybrid manufacturing process before progressing onto more time, material, and cost-intensive large-scale testing methods.

1.1 Motivation & Hypothesis

For the completion of this work, there were 2 key motivations: 1) the need for "better" tooling and 2) the need for a small-scale approach to perform research and development into HLSM. The need for "better" tooling stems from issues present in traditional tool options, these issues rooted in both processing method and manufactured tool performance [10–14, 29, 30]. From a processing perspective, there is a need for a processing method that minimizes material waste, long lead times, and labour investment that would ultimately minimize cost [13, 14, 25]. Directly resulting from this processing method is the tool produced, which must not only match traditional tooling options, but offer superior properties for composite processing (ex. high durability, ability to withstand elevated temperatures for an extended time, chemically resistant during composite part curing, etc.) [10, 12, 13, 17]. Hybrid-Large Scale Manufacturing (HLSM) can potentially address the issues with traditional tool options both in process and tool performance [16, 17, 24], however further R&D into HLSM

is needed to find out how to leverage the process to produce low-cost, high-performance tools.

With HLSM offering significant potential, the method in which R&D is performed in this area needs to be highly targeted, first by identifying key properties that are required for a composite processing tool and then investigating how to achieve them in HLSM tools. Whereas the identification of key properties can be achieved through comprehensive understanding of the specific composite process employed, investigation in turn needs to employ well-established, quantitative, small-scale characterization techniques to accurately determine these properties with minimal material and labour. Of particular importance is understanding tool "durability" and what key properties influence it, as this will predominately define the practical use of the tool (i.e. How may composite parts can be produced on the tool before it fails.) [10, 16, 17]. The hypothesis of this work was therefore that through quantitative, small-scale test methods, one can determine the properties, processing, and performance of these HLSM tools while minimizing large-scale testing methods and consequently cost.

1.2 Objectives & Scope

From the motivation and hypothesis, objectives for the quantitative, small-scale test method were established based on key tool properties identified in the literature review (Figure 1.4). As there are many different properties that can define a tool's performance [10, 17], it was essential to select a small subset that would best represent tooling performance in the context of a specific composite process. As such, the process used to assess and predict tool performance was wet-layup vacuum-bag (WLVB), in which "better" tools was subdivided into 2 major objectives:

Objective 1: Maximize parts per tool.

Objective 2: Minimize cost of determining HLSM tooling performance.

The first objective was further subdivided into 2 indicators of tool performance, durability, and thermal resistance[1], in which the WLVB process was specifically chosen to further define "durability" based on specific elements present in the composite process. Thermal resistance was further divided into service temperature and thermal expansion/contraction, in which unique to the thermoplastic material used in the HLSM process, these aspects are governed by thermal properties unique to polymers [31, 32]. The cost objective comes from the second

---

[1]Contrary to the traditional definition of "resistance" in the context of electrical circuits, here "resistance" is defined simply as "opposing".

point in the motivation, in that minimizing all associated costs with R&D into HLSM (and the tools produced through it) make the entire option competitive with traditional tools. Finding the appropriate trade-off between these two main objectives is paramount to the successful transition of HLSM and HLSM tooling to industrial composite processing.
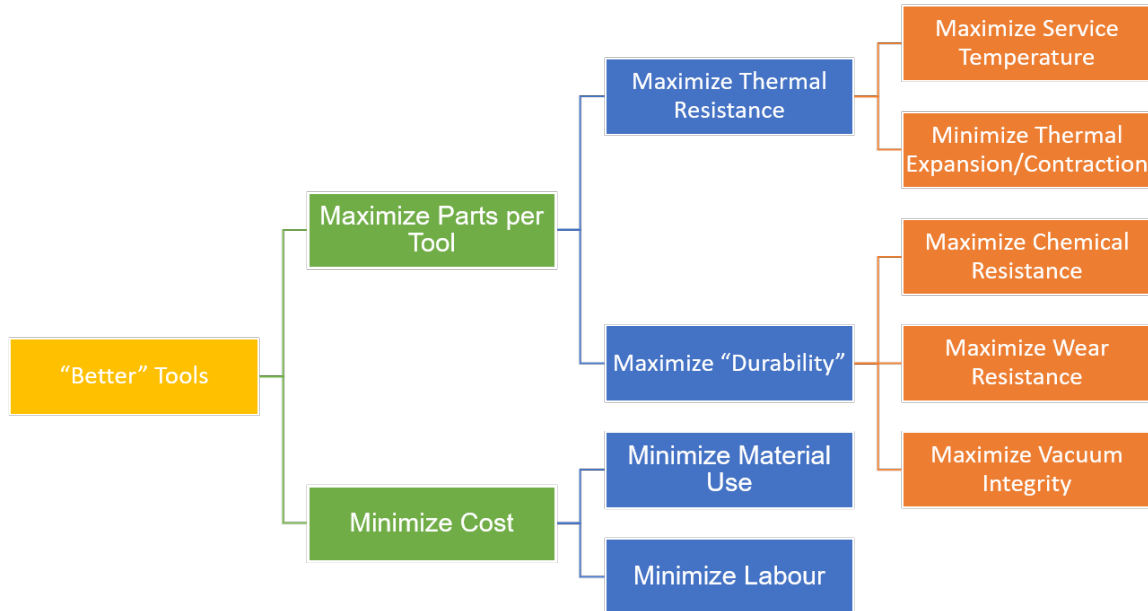
Figure 1.4: Objectives hierarchy.

1.3 Metrics

Having identified the objectives and scope, the next step was to then establish key metrics in which to assess the relative performance of HLSM tool for each relative to traditional tools. With the underlying objective of minimizing cost (and the corresponding sub-objectives), the metrics chosen for this work were predominately geared towards being quick to perform, small-scale, and preferably provided quantitative results for each specific objective (Table 1.1). The resulting data could therefore be low-cost and straightforward to acquire and interpret, allowing a unique set of data "profiles" to be assigned to a specific tool type. These data profiles could then contribute to the development of a library containing each tool type tested, which could subsequently be referred to and compared against in all future tool designs. Further details regarding each specific metric can be found in both the Literature Review (Chapter 2) and Materials & Methodology (Chapter 3).

Table 1.1: Metrics associated with each objective.

Main Objective	Sub-Objective	Metric
	Maximize Chemical Resistance	Contact angle hysteresis
	Maximize Wear Resistance	Hardness
Maximize Parts per Tool	Maximize Vacuum Integrity	Vacuum pressure "drop-test"
	Maximize Service Temperature	Glass transition temperature
	Minimize Thermal Expansion/Contraction	Coefficient of Thermal Expansion
Minimize Cost	Minmize Material Use	Mass
	Minimize Labour Time	Time

1.4 Thesis Structure

In the organization of this thesis work, the goal was to provide a structured approach for the reader that followed a logical progression of thought. This required that the thesis:

- Identify the need for hybrid manufacturing and support the motivation and chosen materials and methodologies.

- Provide detail on the materials and methods chosen to assess hybrid manufacturing process and tool performance.

- Present the results of the work for each method employed and discuss its significance both individually and holistically.

- Summarize the main findings from this thesis and what next steps could potentially be taken to further this work.

- Provide the references used to further understanding of this thesis work and the general status of the research area.

- Give additional supplementary information not contained in the main body of the thesis that the reader could consult to enrich their understanding behind the work performed.

As such, the structure of this thesis is as follows:

Chapter 2 provides a literature review on the requirements of composite processing tools, traditional tooling materials and manufacturing processes, the hybrid manufacturing process and associated materials, and finally theory behind the thermal and durability characterization techniques employed.

Chapter 3 outlines the materials and methodology used in this thesis work, beginning with a detailed description of the composite processing tools manufactured (both traditional and hybrid) followed by identification of key attributes specific to the thermal and durability characterization methods employed.

Chapter 4 presents the results of each characterization method, followed by a comprehensive discussion of the validity of each metric and their implication for the hybrid manufacturing process and production of hybrid-manufactured tools.

Chapter 5 summarizes the main conclusions drawn from the work performed, drawing on the findings presented in the results and discussion.

Chapter 6 highlights major avenues of future work, building off of the conclusion and previous chapters.

References covers the references used throughout this thesis document.

Appendix contains additional supplementary information in the form of an appendix.

Chapter 2

Literature Review

2.1 Requirements of a Composite Processing Tool

For a composite processing tool, there are many different requirements that determine tool performance which are ultimately a function of the tools properties [4, 10, 11, 13, 33]. These properties can range from thermal, mechanical, or other physical/chemical properties, each of which play a key role in the tool's performance and will consequently have significant influence on the final properties of the composite parts produced [4, 10, 11, 33]. Many of these required properties are common across almost all composite processes (ex. stiffness, strength, etc.). However many requirements are specific not only to the application but, furthermore, the specific composite process employed to fabricate parts, leading to additional properties to consider [4, 10, 11, 33]. With a growing list of properties to consider, attempting to characterize them all in the proposed small-scale test method would be ambitious, yet unreasonable as it would create an endless "laundry list" of tests that would drive up material and labour costs. As such, the properties discussed in the following sections of the literature review were selected based on their having broad applicability across most composite processes in which the model composite process used in this thesis work, WLVB, is an exemplar of their impact [4].

2.1.1 Thermal Properties

In many composite processes, precise yet dynamic processing temperatures are required to control final part properties as the thermal profile used will influence the structure and behaviour of the materials used to produce the composite part (Figure 2.1) [4, 10, 34–36]. For thermoset materials, the temperature profile will ensure proper degree of cure through regulation of the cure kinetics, whereas for thermoplastic materials, temperature will dic-

tate properties and behaviour predominately through molecular mobility and crystallization mechanisms [37–40]. Furthermore, the temperature profile will control residual stresses and deformation due to tool-part interaction that can ultimately lead to composite part warpage [33, 41–43]. It is therefore critical that the tool used remains thermally stable, and its behaviour in response to temperature is well characterized to be able to accurately predict its influence on the composite parts produced. To this end, two key thermal properties of tools used in composite processing are the maximum service temperature and coefficient of thermal expansion [4, 10, 33].
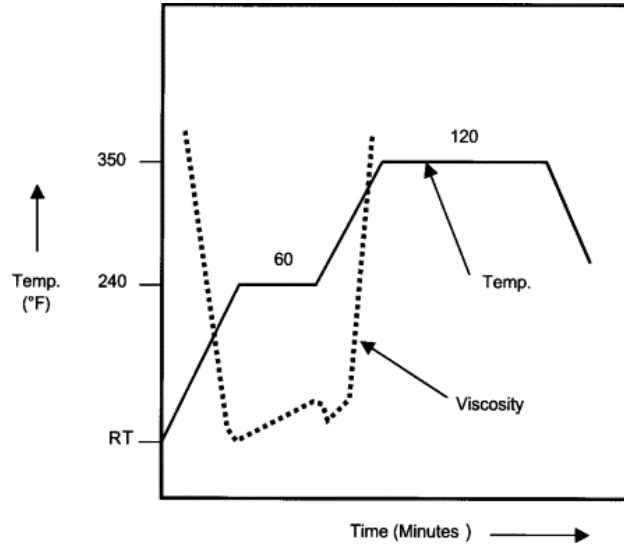
Figure 2.1: Typical cure cycle used in composite processing. Reproduced from [4] with permission.

Maximum Service Temperature

At the elevated temperatures used in many composite processes, the tool must remain thermally stable to ensure that it does not undergo any physical changes that may influence part quality [4, 44–46]. As such, for each tool type there exists a maximum service temperature which defines the limit of its use [4, 10]. This maximum service temperature is ultimately dependent on the tool material used. However it is nevertheless critical to remain below this temperature as surpassing it may lead to thermal deterioration of the tool [4, 10]. In practice, the value used as the maximum is conventionally lower than the "true" maximum service temperature to ensure that tool degradation does not occur [4, 10, 47]. Regardless, for composite processes that require elevated temperatures, it is most advantageous to maximize this value enabling its use in a wide range of processing temperatures [47].

Coefficient of Thermal Expansion

When heating or cooling during a composite process, differences in coefficient of thermal expansion (CTE) value between tool and composite part can lead to significant warpage of the part and/or tool, compromising dimensional accuracy and/or potentially causing part failure [33, 41, 48–50]. This is due to the fact that each material involved has its own unique CTE, resulting in intrinsically different thermal expansion/shrinkage in response to temperature increases/decreases respectively [4, 33, 51]. If there is a large mismatch of CTE values, this can lead to the development of residual stresses in the composite part and/or tool as the different expansion/shrinkage of each material will constrain the deformation of the other[1] (Figure 2.2). Once demoulded from the tool, these residual stresses can then lead to deformation/warpage of the part and/or tool as they are no longer constrained [33, 50]. As such, in tool design it is most advantageous to minimize the CTE such that it is in a similar range to that of the composite part, which is typically dictated by the low (or sometimes negative) CTE values of the fibre reinforcement [10, 50, 51]. By matching the CTE values, expansion and shrinkage of the tool and part is more uniform, minimizing residual stresses.
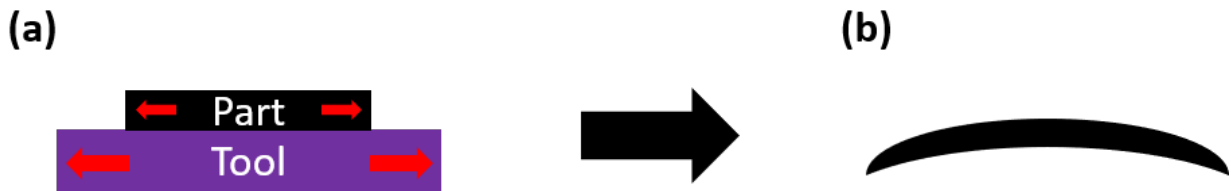
Figure 2.2: Composite part warpage as a result of CTE mismatch between part and tool. (a) Due to the CTE mismatch, the tool and part expand at different rates, generating residual stresses. (b) Once the part is demoulded from the tool, the residual stresses lead to distortion/warpage of the part. Adapted from [33] with permission.

2.1.2 Mechanical Properties

Various types of forces are commonly applied to the tool during composite processing, such as in the form of vacuum or autoclave pressure, to ensure consolidation of individual plies and tight control of the final laminate thickness (Figure 2.3) [4, 54–56]. In doing so, the tooling used must therefore have sufficient mechanical properties to endure these loads, potentially at elevated temperatures, on a repeat basis with each composite part produced. Conventionally, properties of stiffness, strength, and hardness can be used as good indicators

---

[1]Residual stresses can also occur within the laminate itself due to the differences in CTE of fibre and matrix phases. However this can be mitigated through intelligent laminate design [52, 53].

of a tool's mechanical performance [4, 10, 57], the exact values ultimately dependent on the specific composite process employed [4].
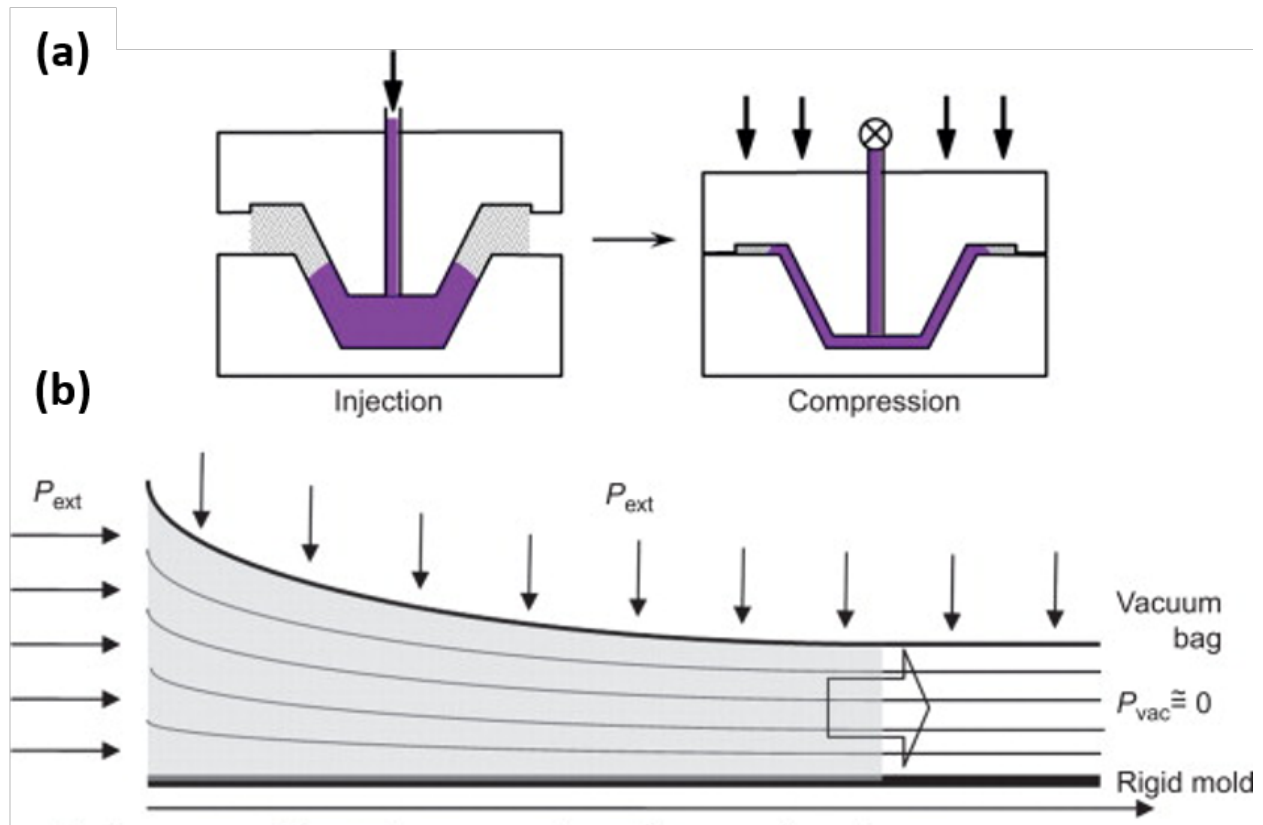
Figure 2.3: Forces acting on tool during specific composite process. (a) Compressive forces present in compression resin transfer moulding process introduced by press. (b) Compressive forces present in vacuum infusion process due vacuum/atmospheric pressure. Adapted from [56] with permission.

Stiffness & Strength

Regardless of the specific composite process, the tool used must be able to predictably withstand the forces applied without failure, ultimately corresponding to the tool's stiffness and strength. Stiffness defines the tool's ability to resist deflection, which is important to know and account for as it's deflection in response to processing force can lead to undesirable warpage of the composite part [4, 10]. Concurrently, strength of the tool is of equal importance, as it describes the maximum allowable load the tool can withstand without failure [4, 10]. Exact stiffness required will depend on the magnitude of forces present in the composite process, where for high force applications, a tool of high stiffness is typically desired to ensure minimal deflection during composite processing, and for lower force applications, a combination of tool materials can be used with stiffness values ranging from flexible (low

stiffness) to rigid (high stiffness) [4, 54–56]. When considering strength, a higher value is typically desired to ensure that the tool does not fail during composite process by exceeding this value.

Hardness

Though not explicitly a material property, hardness of the tool serves as a good indicator of its ability to resist permanent compressive deformation both during and between composite processing [17, 58]. In service, tooling is generally subject to various compressive forces as a result of both pressure applied during the composite process (where the composite part reinforcement, typically fibre, is pressed down into the tool, leaving an imprint on the surface) and/or impact due to "dropped tools" or "tool scratches" (Figure 2.4) [17, 56, 59]. If the tool material is not sufficiently hard, these compressive forces can lead to the formation of permanent localized indentations on the tool surface, significantly increasing tool wear [17]. As wear accumulates, so too does tool performance, reducing the service life of the tool [17]. It is therefore critical in tool design to ensure that the tool and tool surface is of sufficient hardness such that tool life may be extended.
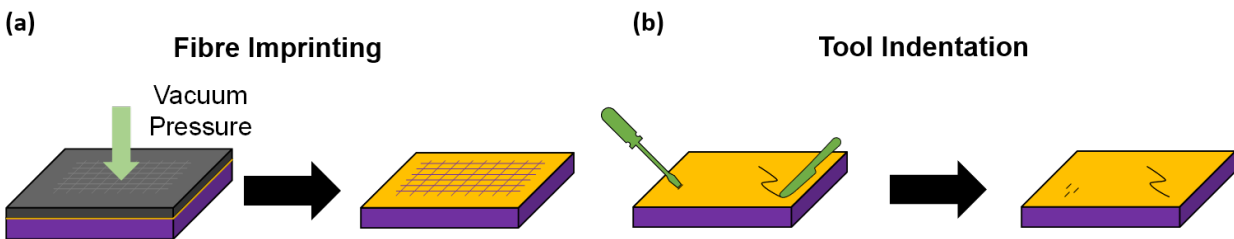
Figure 2.4: Sources of localized plastic deformation during/between composite processing. (a) Localized plastic deformation due to fibre imprinting. (b) localized plastic deformation due to (demould tool) indents/scratches.

2.1.3 Other Physical/Chemical Properties

In addition to the aforementioned thermal and mechanical properties, there are many other physical/chemical properties of tools that have been shown to have a significant impact on tool performance [4, 10, 11, 17, 60, 61]. Depending on the property, this impact on tool performance may not only influence composite part quality but, furthermore, impact tool durability with each successive part produced, necessitating their careful consideration. Two key properties that play a predominate role in tool performance are vacuum integrity and chemical resistance, which have been demonstrated to influence both composite part quality and/or tool service life [4, 10, 11, 17, 60, 61].

Vacuum Integrity

For many composite processes, vacuum is drawn within a closed (i.e. 2-part) tool to facilitate infusion of the liquid resin phase through the dry fibre reinforcement and/or introduce pressure to compact and consolidate the plies of the composite part[2] (Figure 2.3b) [4, 10, 56, 60]. In these processes, it is critical that a constant vacuum pressure is applied and maintained at a specific value, as it will influence the rate of infusion and/or pressure applied to the laminate [56, 60, 62]. Variations in the infusion rate and/or pressure applied can consequently impact the final part quality due to increased void content and/or uneven compaction [56, 60, 62, 64]. Any potential source of vacuum leakage must therefore be eliminated and/or mitigated, in which the major sources of vacuum leakage are improper seal between tool components and/or permeability of the tool [10, 60, 62]. Improper seal relates to the properties of the tool surface that are in contact with sealant tape, where it is critical that a complete seal is achieved [10, 60]. Permeability of tool dependent on its inherent structure, in which porosity will lead to avenues for vacuum pressure loss [10, 62]. As such, tools used in vacuum-assisted/mediated processes must provide a non-porous, impermeable surface that also facilitates good adhesion with sealant tape [56, 60, 62, 64].

Chemical Resistance

During the composite manufacturing process, the tool surface is exposed to a harsh external environment consisting of thermal, mechanical, and chemical factors that it must resist [4, 10, 11, 17, 61]. Though mechanical and thermal properties of the tool must be sufficient for the given process, chemical resistance becomes paramount as the tool surface must provide a chemically resistant, "non-stick" surface with each successive tool use (Figure 2.5) [17, 61, 65, 66]. This nonstick property ultimately ensures that the composite parts can be easily demoulded from the tool and that the tool surface remains in its "as-fabricated" state [17]. Conversely, if the tool surface is not chemically resistant, this can lead to the composite part bonding with the tool surface which can lead to difficulty in demoulding the part from the tool as significant force is required to overcome the bond between the composite part and tool surface or coating [17, 61, 65]. Furthermore, if the bond between the tool and composite part is stronger than the inherent strength of the base tool substrate or applied coating, this can lead to failure of the tool surface as the demoulding of the composite part strips away the tool surface/coating or even complete failure of the entire tool if it's strength is exceeded (Figure 2.6) [17]. As such, it is most advantageous that the tool/coating has high chemical

---

[2]This is achieved through a pressure differential created by the external atmospheric pressure exterior to the tool which leads to laminate compaction [4, 60, 62, 63].

resistance so as to minimize the susceptibility of the composite part bonding to the tool [10, 11, 17, 61, 65]. This is in part achieved by the use of mould release agents, typically applied before every tool use, which act as a semi-permanent "non-stick" coating [11, 61, 65, 66]. However it is nevertheless critical that the tool itself possess chemically resistant properties should the mould release agent not provide adequate coverage or in the extreme be omitted due to operator error.
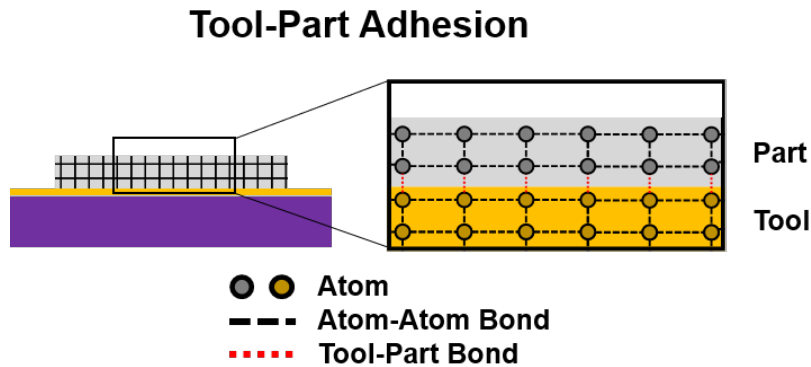
Figure 2.5: "Non-stick" properties of a composite processing tool.
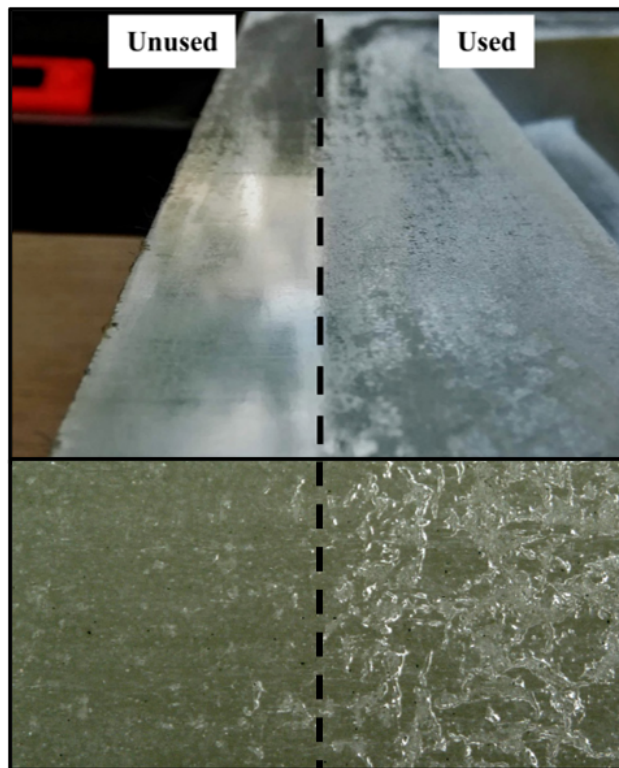
Figure 2.6: Tool surface/coating wear due to composite part bonding. Adapted from [17].

2.2 Traditional Tool Materials & Manufacturing

For most conventional composite processes performed today, similar types of tooling materials and the processes to manufacture them are traditionally used across all industries [4, 10, 11, 13]. This "tradition" is due to the fact that they have been widely demonstrated to provide reasonable and/or sufficient tool performance, meeting or exceeding most fundamental tool requirements [4, 10, 11]. Despite their widespread use however, they are by no means flawless; each tool type having its advantages and disadvantages both in terms of tool material and/or its associated manufacturing process [4, 10, 13, 67]. Traditionally, the two most commonly used tool types used for composite processing are metal or composite tools [11, 13, 67].

2.2.1 Metal Tooling

The production of metal tooling is performed through a single-step subtractive process in which a metal "billet" (i.e. block) is machined down into the final tool geometry (Figure 2.7). Machining is conventionally performed on a computer numerical control (CNC) machine which utilizes a rotating machine tool to selectively remove material from the billet and create complex features with high precision [68–71]. With this process, one can use many different metal types depending on the specific material properties required for the tool, however, traditionally aluminums or steels are used for more low-cost applications whereas invar or nickel-based alloys are reserved for high-performance due to their unique material properties [10, 11, 13]. As a single-step process, metal tool manufacturing is relatively simple and only requires the feedstock material and CNC program to machine the tool geometry. The metal materials used are relatively durable, the tools produced using them often being able to withstand repeated use before the need for repair or replacement [10, 11, 13]. As this process is entirely subtractive, it results in significant material wastage, in most cases only a small fraction (as low as 10% [69]) of the original mass of feedstock remaining after machining [68, 69]. Furthermore, the more common, less expensive metal materials such as steel or aluminum do not inherently have similar coefficients of thermal expansion to that of the composite parts being produced, which can prove detrimental to final part quality [10, 11, 13, 33]. This can be solved by utilizing more high-performance alloys such as Invar which have more comparable CTE values, however, not without a significant increase in lead times to procure the material and its associated material cost [10, 11].

Billet Feedstock   **Subtractive**
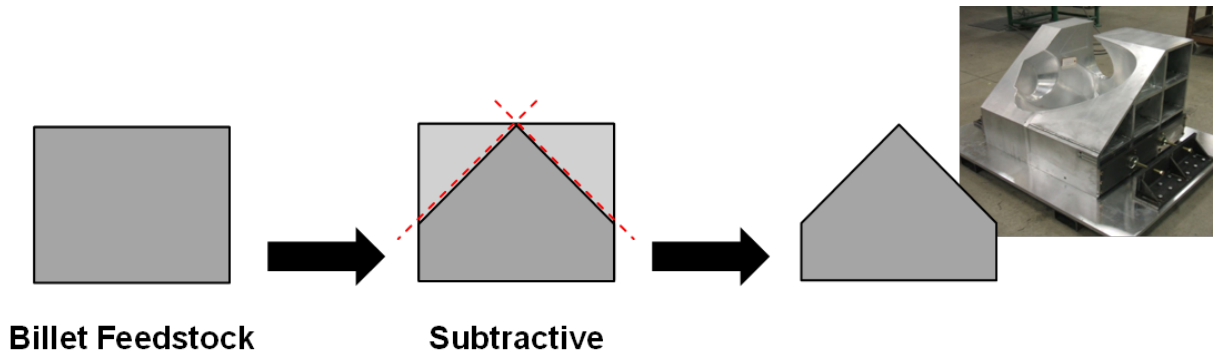
Figure 2.7: Metal tooling manufacturing steps. Image reproduced from [15] with permission.

2.2.2   Composite Tooling

Composite tool manufacturing is a multi-step process which involves the fabrication of a tool "template", which is then used to make the composite tool (Figure 2.8) [11, 13, 67, 72, 73]. This template is created using tooling board, a lightweight, easily machinable material, that is assembled into a near-net shape of the final composite tool geometry. The near-net shape is then machined on a conventional subtractive system (such as described in "Metal Tooling") before finally being used to fabricate the composite tool [67, 73]. Traditionally, the composite materials used to produce these tools are the same if not similar to that of the composite parts to be produced on it, which offers the advantage of having similar thermal expansion/shrinkage (i.e. CTE) during processing [10, 11, 13, 73]. Despite this thermal advantage, most composite tooling options suffer from having intrinsically low durability and as such are costly to produce given the manufacturing process being relatively labour-intensive [10, 13, 67, 73].

Tooling Board   **Subtractive**   **Tool Layup & Cure**
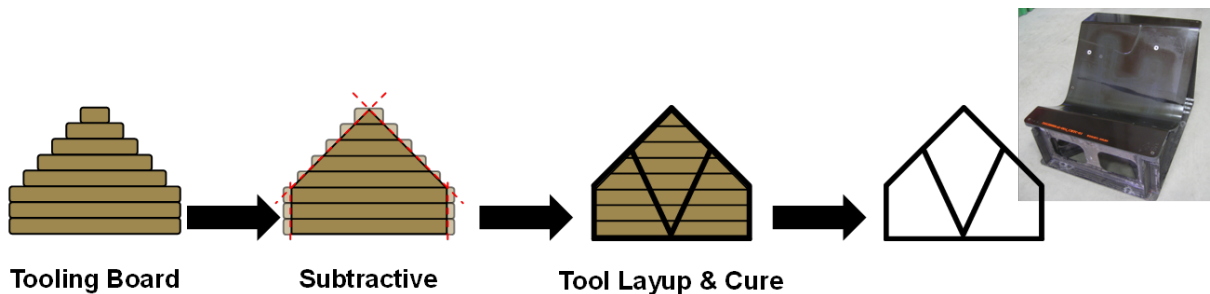
Figure 2.8: Composite tooling manufacturing steps. Image reproduced from [15] with permission.

2.3 Hybrid Tool Materials & Manufacturing

Given the current shortcomings of traditional tooling options, recent work has looked into using a new technique known as hybrid large-scale manufacturing (HLSM), which combines both additive and subtractive fabrication steps on a single machine, to address these issues and streamline the manufacturing process (Figure 2.9) [14, 16–18, 24–26, 28]. In this hybridized process, the additive element first prints the near-net shape of the tool which is then followed by the subtractive element that machines it to the final tool geometry. The result of this hybridized system allows for reduced lead time, labour, material waste, and ultimately cost, though like most other manufacturing processes it still has its own unique disadvantages that must be addressed to leverage the benefits of the process for tooling [14, 16, 17, 19–27, 74]. As such, in addition to having an intimate knowledge of the advantages and disadvantages for both additive and subtractive manufacturing processes and the associated materials, one must also consider the interplay between these two elements to ensure successful tool fabrication.
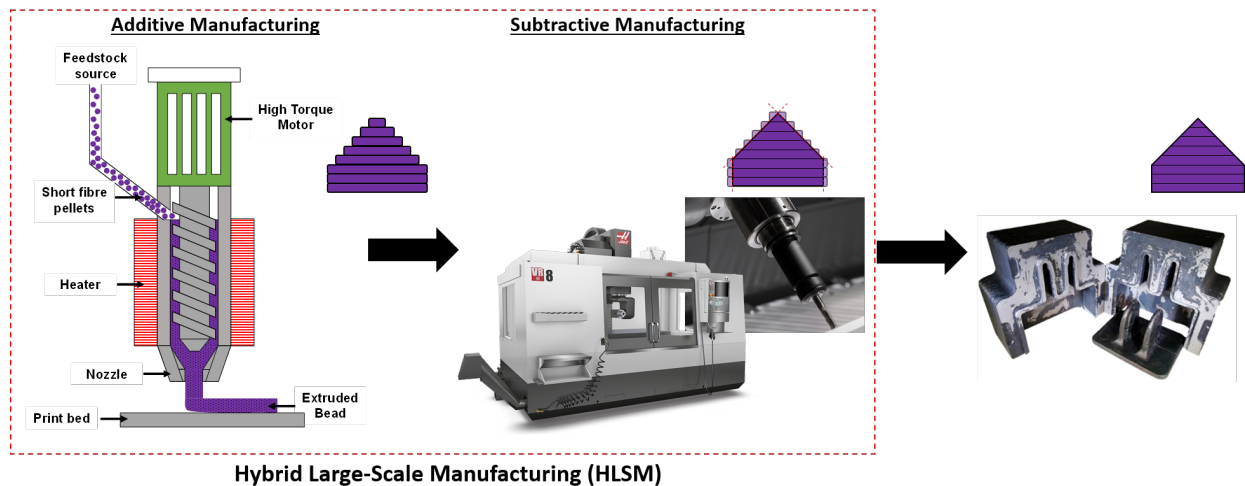
Figure 2.9: Basic hybrid manufacturing process, detailing the key components of the thermoplastic material extrusion system used for the additive manufacturing step. Thermoplastic material extrusion system schematic adapted from [75]. Images of subtractive manufacturing reproduced from [76]. Image of final hybrid tool reproduced from [74].

From a material perspective, the exact tooling material used in hybrid manufacturing is dependent on the hybrid system design, in which different types of additive systems can be used with materials ranging from metals to polymers [14, 19, 26, 75, 77–79]. In most cases however, the latter is most commonly employed due its well-established background in pre-existing polymer processing techniques and relatively low material cost [14, 80–82]. The additive element of hybrid manufacturing is typically achieved through thermoplastic ma-

terial extrusion, in which a miniaturized single-screw pellet extruder (similar to those used in traditional polymer extrusion) is used to melt and extrude a thermoplastic or thermoplastic composite pellet feedstock material (Figure 2.9). For these thermoplastic composite materials, the polymer generally acts as the matrix phase whereas the reinforcement phase can take the form of short fibres or particles [14, 26, 75, 78, 81]. Given the range of potential polymer and reinforcements possible, the properties of the resulting material systems used can be highly customized to meet the target tool application. Relative to metals (and similar to composite) tools however, hybrid manufactured tools suffer the same issues of durability with the additional issue of strength due to the weaker bond between additively manufactured layers that must be eliminated or mitigated to ensure their success [17, 24, 77].

In the first step of the hybrid manufacturing process, significant time must be spent in tool design and generation of additive and subtractive toolpaths, as successful execution of the hybrid process will ultimately require both design for additive manufacturing (DFAM) and design for subtractive manufacturing (DFSM) principles be used simultaneously. To do so, one must consider the individual settings of each process, specific design considerations for each process, and ultimately how the optimizations for both will impact the other process. It is of paramount importance that in doing so, the additive and subtractive processes variables are considered concurrently, as optimizing for one can render the execution of the other impractical or in the extreme impossible [17, 83].

From an additive perspective, one must consider the settings associated with the additive software and how they will impact the manufacturing process and resultant tool properties during print. These settings are defined in the toolpath software for the additive system commonly referred to as a "Slicer"[3], in which the number and type of settings (and consequently the degree of process control) is largely determined by the complexity of the software. Despite this complexity, in almost all software the most prevalent and conventional settings employed are print speed, bead width, layer height, print speed, and build orientation [77, 83–85]. Modification of these settings will influence both the manufacturing process through key processing parameters such as print time and material cooling rate but, furthermore, the final/resultant tool properties such as part interlayer bond strength [24, 26, 27, 77, 83, 84]. Though the main objectives are typically to achieve a "good" quality part in as short a time as possible, these two objectives commonly conflict, therefore the optimal solution is ultimately a trade-off between the two.

---

[3]The name "Slicer" comes from the fact that the software "slices" the imported model into a stack of thin layers, which it then creates toolpaths for each.

From a subtractive perspective, the impact of the process settings and how they will impact the process and resultant tool properties is similar to traditional (metal or composite) tool manufacturing, though has its nuances specific to the thermoplastic material used during the additive stage. As such, conventional settings associated with subtractive machining apply such as feed rate, spindle speed, and types of cutting tools used, all of which are programmed into the specific computer-aided manufacturing (CAM) software used. Variation of these settings have ultimately been shown to impact the subtractive process through machining time and cutting tool wear, but, furthermore, influence the final tool properties such as surface finish and structure of the tool (Figure 2.10) [16, 86–88]. Structure of the tool can be specifically influenced by overheating caused by the machining process, which can be detrimental to the printed tool given the use of thermoplastic (or thermoplastic composite) materials that have relatively low temperature resistance [16]. Therefore, similar to the additive manufacturing, the optimization of the subtractive process is ultimately a compromise between minimizing the machining time without negatively influencing the properties of the tool [16, 83].
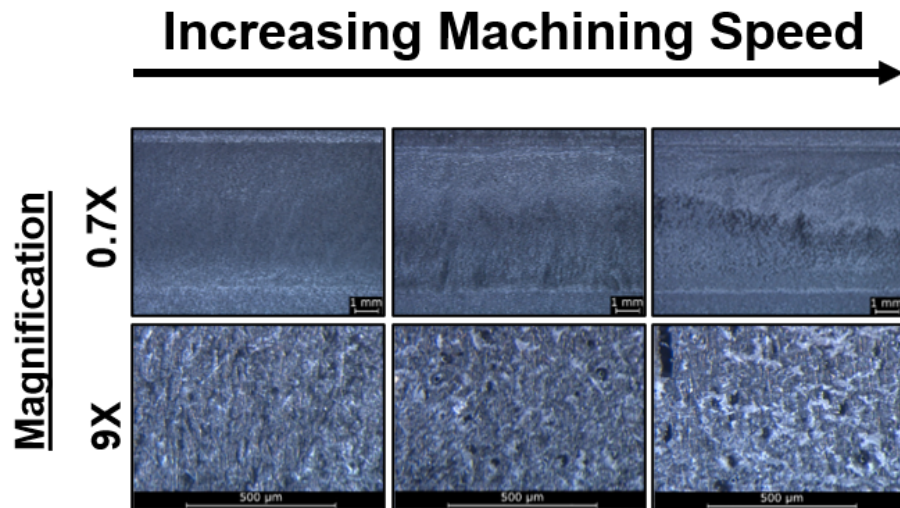
Figure 2.10: Impact of machining parameters on tool surface. Adapted from [16] with permission.

In the optimization of the additive and subtractive processes, it is of critical importance that the interplay between the two is taken into account to ensure the success of the hybrid process as optimizing for each process individually may impact the performance of the other. As such, one must consider how the structure resulting from the print process may influence the machining process from multiple aspects ranging from toolhead access, feature

creation, process stability, and final tool surface on the printed part (Figure 2.11) [17, 24, 26, 83, 89]. Toolhead access pertains to the ability of the subtractive toolhead to reach all necessary areas on the printed structure, which ultimately must be accounted for during the additive process (Figure 2.11a) [83]. Providing the cutting tool can access all areas, a subsequent concern is whether the printed structure is sufficiently stable to be machined "as is" (i.e. unsecure) or if additional fixturing needed to mitigate machining vibrations (Figure 2.11b). These vibrations are produced by the interaction of the cutting tool and printed structure, which can ultimately lead to defects or in the extreme significant movement of the printed part from the machine bed [17, 18, 90]. The remaining two design considerations of feature creation (Figure 2.11c) and chosen tool surface (Figure 2.11d) are ultimately based on personal preference and/or the required application. However there is generally a specific approach that garners the most success [24, 26, 83, 89, 91, 92]. Given the ability to manufacture the tool using two distinct processes, it must be determined whether certain complex features are easier to produce during the additive or subtractive stage. Regarding feature creation, given the strengths and limitations of each process, it is typically most advantageous to minimize complex features during the additive stage to produce a rough, near-net shape which is then fulfilled during the subtractive stage (Figure 2.11c) [83, 91, 92],. The latter choice of tool surface is of critical importance as print surface quality can vary significantly depending on the machined surface, which will impact the surface quality of the final tool (Figure 2.11d) [24, 26, 83].
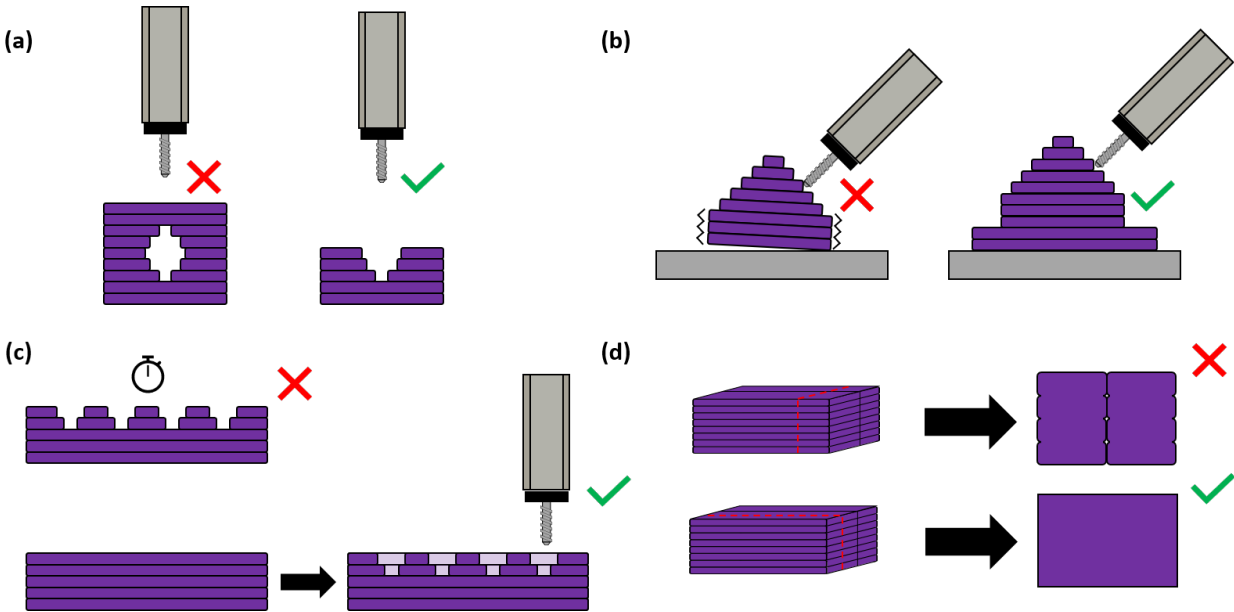
Figure 2.11: Interplay of additive and subtractive processes in hybrid manufacturing. (a) subtractive toolhead access. (b) Subtractive process part stability. (c) Feature creation. (d) Tool surface selection.

Following tool design and generation of toolpaths for the additive and subtractive processes, the next step is their execution as ultimately it is generally difficult to plan the entire fabrication process without any tangible feedback or prior experience. Therefore, once sufficiently confident in the specified settings, one must execute the toolpath codes for each respective process to confirm their performance. At this stage, modification of the processes during fabrication is relatively limited as the process steps have already been largely predetermined by the numerical control files containing the additive and subtractive toolpath instructions, though some degree of process parameters can be adjusted during fabrication (ex. print speed, feed rate). If the settings employed, however, yield undesirable or unsatisfactory results in either process, one must iterate by returning to the tool design and toolpath generation step in which with each successive iteration comes additional time, labour, and material costs (Figure 2.12) [93–95]. This highlights the need for predictive tools in hybrid manufacturing which accurately capture the additive and subtractive processes, such that iteration can be minimized and consequently time, material, and cost.
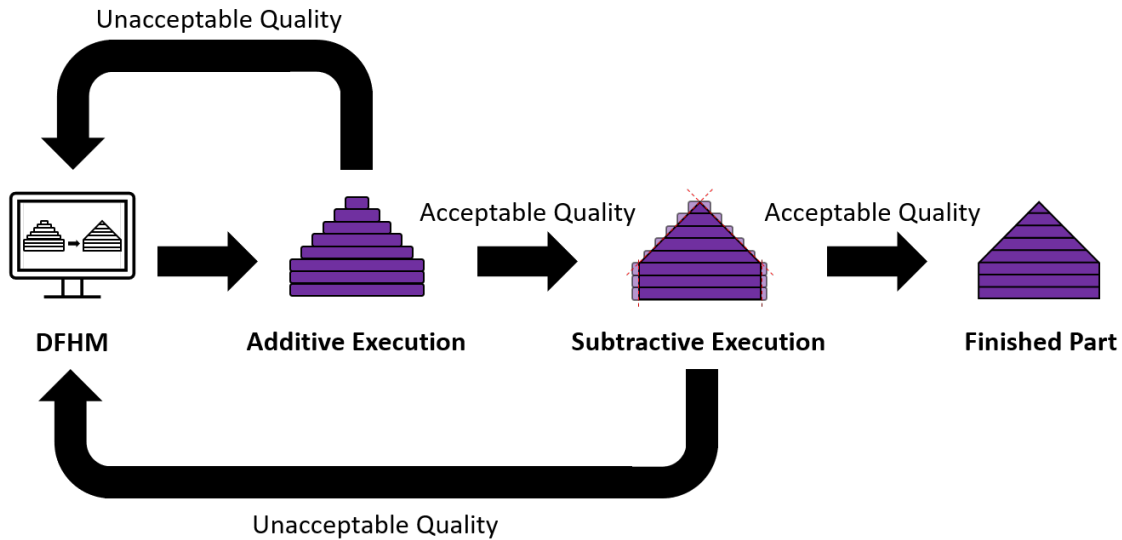
Figure 2.12: Iterative workflow in the hybrid manufacturing process. DFHM: Design for Hybrid Manufacturing.

2.4 Thermal Characterization Techniques

2.4.1 Thermogravimetric Analysis (TGA)

Thermogravimetric analysis (TGA) is a thermal characterization technique which measures specimen weight change in response to change in temperature. The setup typically consists

of a small pan which contains the specimen and is suspended by a platinum hook within an insulated ceramic furnace (Figure 2.13). The exact pan material and geometry used ultimately depend on the material type tested [96]. Once the specimen is contained within the ceramic furnace, the internal volume is filled with a gas of interest (ex. air, nitrogen, etc.) and the temperature can be ramped up or down at varying speeds or held isothermal according to the predefined temperature profile.
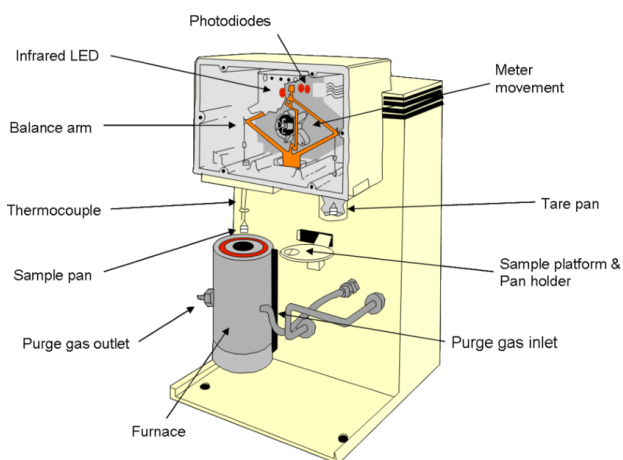
Figure 2.13: Basic components of a thermogravimetric analyzer (TGA). Reproduced from [97].

For polymer or polymer composite TGA, the technique is generally used to determine the degradation onset temperature, which can traditionally be defined as a change in weight percent ranging from approximately 1-5 weight percent [31, 98]. At this temperature the polymer begins to experience thermal degradation, which depending on the atmosphere can consist of deterioration of the physical molecular structure and/or the formation of oxidation products in the presence of oxygen respectively [31, 98]. For fibre-reinforced polymer compositions, such as carbon or glass fibre reinforced polymers, thermogravimetric analysis can, furthermore, be used to determine fibre reinforcement content of the material system [99]. This can be done when testing the thermal degradation in an inert atmosphere (i.e. N2), in which the temperature is ramped to a significantly high temperature relative to the polymer system (ex. 800°C), resulting in complete thermal degradation of the polymer component. Following this thermal degradation, one will be left with only fibres in the specimen pan providing there are no additional high temperature additives in the specific polymer material system tested [31, 99].

2.4.2 Differential Scanning Calorimetry (DSC)

Differential scanning calorimetry (DSC) is a thermal characterization technique that measures the rate of heat flow to and from a specimen with respect to time and temperature [100]. This is achieved through comparison to a reference that is inert, typically an empty specimen pan, in which the differential in heat flow between the specimen and reference is reported. Similar to TGA, the exact choice in DSC specimen pan material and geometry ultimately depends on the material to be tested, with materials and geometry is ranging from aluminum to platinum and open to hermetically sealed respectively [101].

Two major types of DSC setup exist, known as power-compensated DSC and heat-flux DSC (Figure 2.14). In the former, the general set up consists of two separate chambers, in which one chamber holds an empty specimen pan (i.e. the reference) and the other holds a pan containing the specimen. Each specimen chamber has its own individual temperature sensor and heater in which the differential heat flow is measured through the difference in energy (i.e. the power input) required to maintain both chambers at the same temperature. In the latter, the general set up consists of a single chamber and heat source, in which the heat flow is measured by comparing the temperature difference between the specimen and the reference. Both instruments have their advantages and disadvantages, the predominant difference being the faster heating and cooling rates on the power compensated DSC versus higher sensitivity on the heat flux DSC [100].
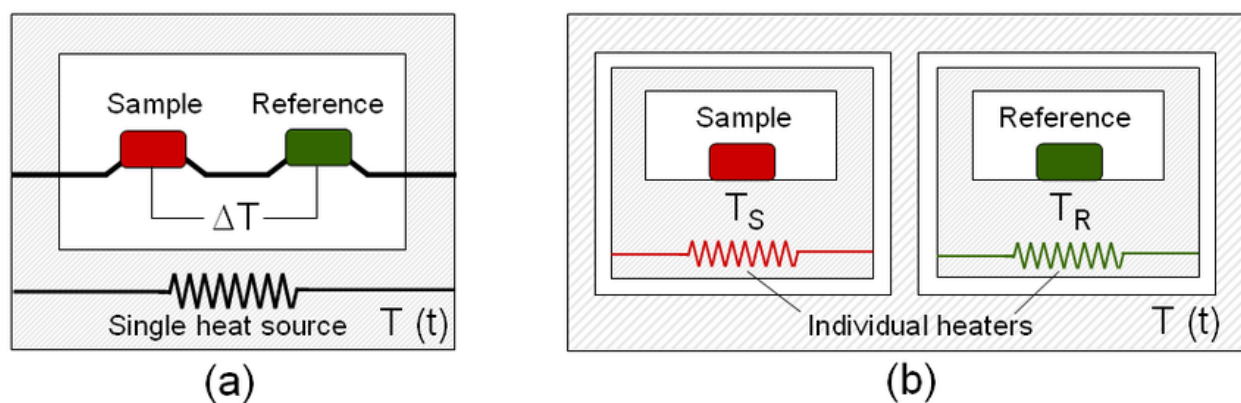
Figure 2.14: Basic designs of differential scanning calorimetry (DSC). (a) Heat-flux DSC. (b) Power-compensated DSC Reproduced from [100].

Regardless of DSC type chosen, both systems allow the measurement of specific heat capacity of a material, in addition to characterization of various exothermic and endothermic heat flow events, such as the glass transition and melting/crystallization temperatures in thermal

plastic polymers, the cure reaction in epoxies and other oxidation and decomposition [96]. Of particular interest in thermoplastic polymer material systems are the properties of glass transition temperature (Tg) and melting/crystallization temperatures as both temperatures offer key insight into the molecular mobility and structure of the polymer chains and as a result the mechanical strength of the material [37]. For the production and use of 3-D printed tooling materials, understanding these properties is paramount as they will dictate not only processing conditions (i.e. interlayer bonding of printed beads) but additionally the maximum permissible service temperature of the tool (Section 2.1).

The glass transition temperature specifically marks the transition between a glassy and rubbery state of the polymer chains which has important implications on mechanical strength (Figure 2.15). Below the glass transition temperature, the polymer chains are frozen into place, with the material exhibiting more brittle like properties. Conversely, above the glass transition temperature there is enough energy supplied to the system to allow a small degree of polymer chain movement, and the polymer exhibits more rubber/elastomeric like properties (i.e. decreased stiffness and strength). Time spent above the glass transition temperature will, furthermore, influence the interlayer bonding strength of printed beads by enabling prolonged diffusion of polymer chains across adjacent layers (Figure 2.16) [74, 102].

For a semi-crystalline polymer, the melting temperature represents the points in which there is the degradation of long-range structural order (i.e. the crystalline component) in the polymer system. Above this point the polymer chains have enough energy to be freely mobile and the polymer material exists in a liquid/melt state, resulting in a significant drop in mechanical properties [103].
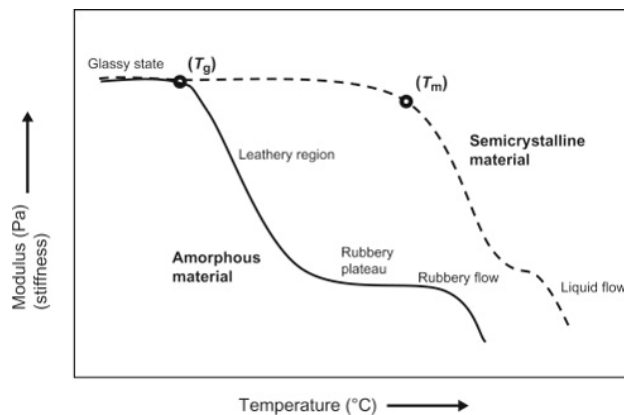
Figure 2.15: Effect of temperature on the mechanical properties of amorphous and semi-crystalline polymers. Tg: Glass transition temperature. Tm: Melting temperature. Reproduced from [103] with permission.
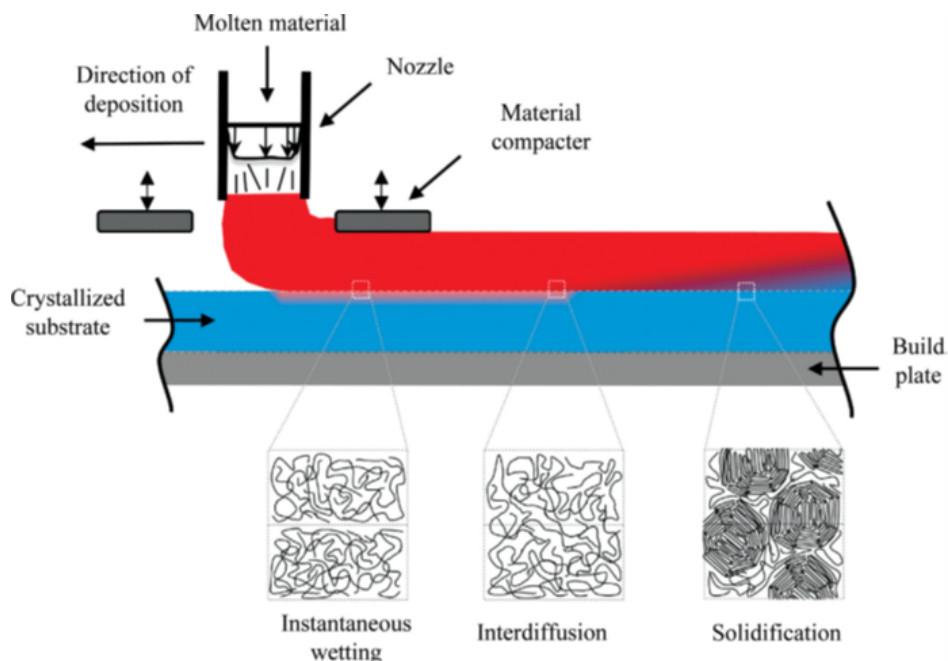
Figure 2.16: Diffusion of polymer chains across printed beads. Reproduced from [104] with permission.

2.4.3 Thermomechanical Analysis (TMA)

Whereas TGA and DSC measure key thermal transition temperatures, thermomechanical analysis (TMA) is a thermal characterization technique that measures dimensional change in response to changing temperature [105, 106]. Based on this dimensional change as a function of temperature, one is able to characterize key thermal properties such as the linear coefficient of thermal expansion and in the case of polymers the glass transition temperature [105, 106] depending on the specific set up. Much like TGA, the set up of this thermal characterization equipment consists of a small, insulated chamber, however, in this instance the chamber covers a small apparatus that consists of a specimen stage, thermocouple, and thermal probe (Figure 2.17). The exact geometry and size of the thermal probe can vary depending on the specific application, ranging from expansion, macro expansion, penetration, and more, each of which characterize a distinct property of the material [107].
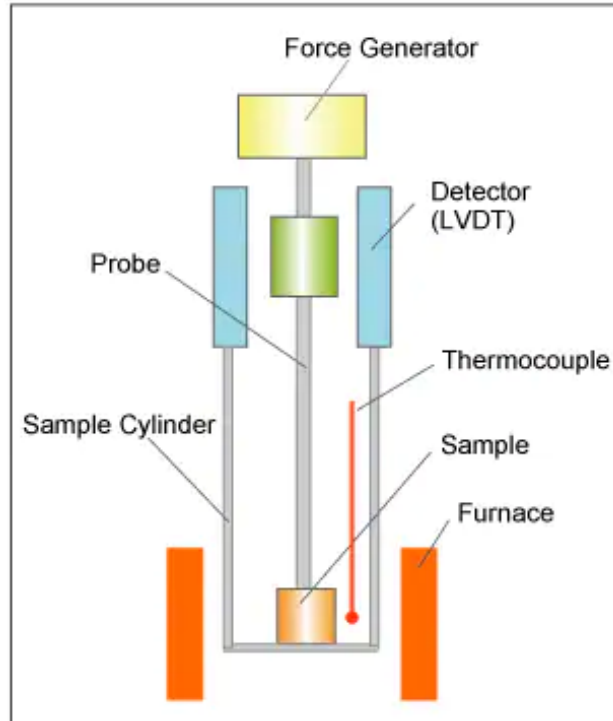
Figure 2.17: Basic elements of a thermomechanical analyzer (TMA). Reproduced from [108].

As seen previously (Section 2.1), in the application of tooling for composite of processes, and understanding of the linear CTE is paramount as it will dictate tool expansion and shrinkage, which intern will influence final composition part dimensions and tolerances as a result [33, 34, 36]. Using a TMA, the linear CTE is typically determined through the use of a macro expansion probe, in which the flat surface of this probe lies flush against a flat surface of the specimen, prepared in the form of a cube or rectangular prism, that sits on the specimen stage. Following the loading of a specimen onto the specimen stage (taking care for the probe to not come in contact with the thermocouple), the probe is lowered to rest on the top surface of the sample and the insulated chamber is closed. The temperature of the chamber is then equilibrated at the reference temperature (typically room temperature, i.e. 25°C) and the initial length of the specimen is recorded. Dimensional change of the specimen is then recorded as the temperature differs from the reference temperature, the exact curve generated depending on the temperature profile specified [105–107]. Using the value obtained for the dimensional change, the linear CTE can then be calculated according to the following equation:

$$\alpha = \frac{\Delta L}{L_0} \frac{1}{\Delta T} = \frac{L_f - L_0}{L_0} \frac{1}{T_f - T_0} \tag{2.1}$$

α: Coefficient of Thermal Expansion [1/°C]

L_f: Final Length [mm]
L_0: Initial Length [mm]
T_f: Final Temperature [°C]
T_0: Initial Temperature [°C]

For an isotropic material determination of the linear CTE generally need only to be performed once, as the CTE in the remaining orientations should be identical. However, for anisotropic materials, the linear CTE will most likely vary depending on the orientation of the specimen therefore all directions of interest must be tested [31].

2.5 Durability Characterization Techniques

2.5.1 Pre-Screening Tests

Tensiometry

Optical tensiometry is a characterization technique that characterizes the interaction between a fluid and the substrate surface of interest by measuring the contact angle which can be used to predict or estimate the free surface energy of the substrate material (Figure 2.18). This property can then be directly related to the substrate materials ability to resist bonding with fluids that come in contact with its surface [86]. As one of the issues with tool durability is the chemical resistance of the tool surface to the resin used to fabricate the composition part (Section 2.1), it is the goal that this technique may therefore be used to predict the ability of the tool surface to resist bonding with the resin used in the composite part. A tool that possesses a low surface free energy will potentially resist bonding with resin from composite parts, which will allow for longer preservation of the tool surface finish in its as-fabricated state by preventing tool-part adhesion [109]. As this surface-free energy is influenced by both chemistry and inherent surface morphology (i.e. surface roughness) [109, 110], the longer the as-fabricated tool maintains this "as-fabricated" after each successive use, the greater the tool durability.
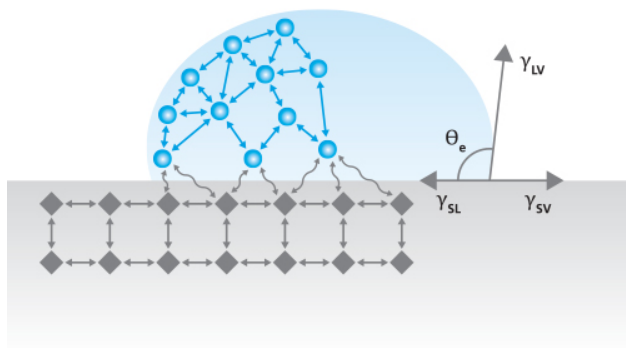
Figure 2.18: Contact angle measurement performed through tensiometry. Θ_e: contact angle, $\gamma_{SL}, \gamma_{LV}, \gamma_{SV}$: surface energy of the solid-liquid (SL), liquid-air (LV), and solid-air interfaces (SV). Reproduced from [111] with permission.

One particular version of this technique is known as advancing-receding contact angle (ARCA) measurement, which measures the dynamic contact angle of an advancing/receding drop (Figure 2.19). In this technique, an initial droplet is first formed on the surface of the substrate with the needle positioned in its centre and close to the substrate surface. Additional fluid is then pumped from the needle onto the surface of the prescribed amount increasing the droplets volume over time. Initially, during this increase in volume, the droplet edges are pinned at their respective positions and the droplet increases in size through an increase in the contact angle. The droplet, however, eventually reaches a critical size in which the contact angle no longer increases, but instead the baseline positions becomes unpinned and advances to a more favourable position before becoming again pinned. This unpinning (and subsequent pinning) reduces the contact angle of the droplet which then returns to increases in size through increasing contact angle. The contact angles associated with this point (that is, the underpinning of the droplet edges and the subsequent advance) is what's known as the advancing contact angle (ACA), this pinning and underpinning occurring multiple times until the prescribed amount of addition of fluid has been fully pumped on to the surface, allowing for the measurement of multiple advancing contact angles [109, 112]. Similarly, the receding contact angle (RCA) is the opposite of the advanced contact angle in which the prescribed amount of fluid is then drawn back into the needle and the baseline edges begin pinned, however, eventually reach a point in which they become unpinned and recede in which contact angles associated with this baseline unfitting and subsequent receding of the droplet what is known as the receding contact angle [109, 112].

Advancing CA   **Receding CA**
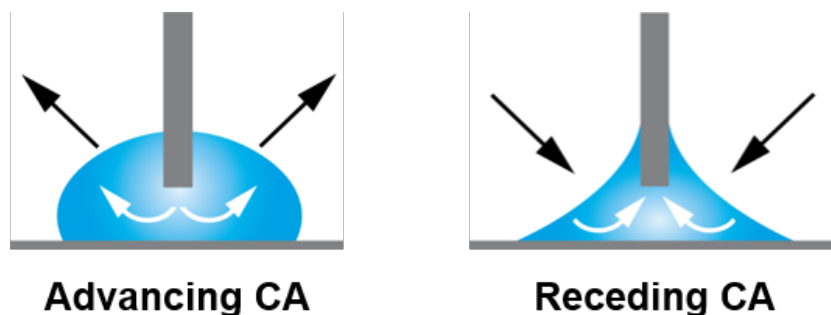
Figure 2.19: Advancing and receding contact angle (ARCA) measurement. Reproduced from [112] with permission.

Vacuum Integrity

As discussed in Section 2.1, the ability of the tool coating combination to hold the vacuum is critical to ensure proper pressure is applied to the lab ensuring its consolidation upon cure. To this end, it is paramount that the tool is non-porous and impermeable to air. Once a bag has been formed on a tool and vacuum is drawn, one method in industry commonly used to assess the vacuum integrity of a tool is to perform what is known as a "drop test" [113]. In a drop test, the vacuum bag is first worked while the vacuum source is active to obtain the maximum potential vacuum for the given tool-coating combination. Once it is predicted that the maximum possible pressure has been reached, the vacuum source is deactivated and the pressure is monitored over a set time to assess whether there is any vacuum pressure change. In theory, there should be no change in vacuum pressure over the prescribed interval which would suggest that there is a perfect seal of the vacuum bag on the tool surface. However, in reality there are multiple potential sources of vacuum leakage including but not limited to holes in the vacuum bag, insufficient adhesion of the tacky tape to the bag/tool, and/or porosity in the tool itself [113].

Micro-Indentation/Hardness Testing

Micro-indentation/Hardness testing is a mechanical characterization technique in which an indenter of known size and shape is applied to a surface at a prescribed force (in the micro range) and the resulting indentation is analyzed. From this indentation one is able to ascertain many different properties of the material of interest, most commonly a hardness value being reported. Though not explicitly a material property, the hardness value is a relatively fast, sufficient, and easy to perform characterization which provides an indication of the materials stiffness and strength [114]. Many different hardness test types exist (Figure 2.20) such as the Vickers, Barcol, Shore, and more, defined by the type of indenter geometry used

and the class of materials tested (i.e. metals, ceramics, polymers, elastomers, etc.) [115].
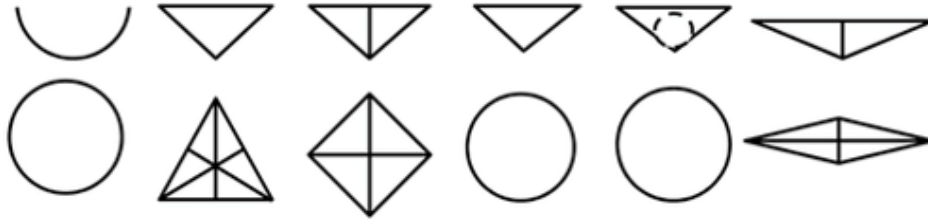
Figure 2.20: Indenter types used in hardness testing. Reproduced from [116] with permission.

2.5.2 Small-Scale Composite Processing Tests

Laser Profilometry

Laser profilometry is a non-contact, non-destructive, optical characterization technique that measures the surface roughness of a specimen by projecting a laser light onto the surface of interest, the reflected light then detected by camera. The exact method used to capture the reflected light can vary depending on setup. However the most predominant method is coherence scanning interferometry which is demonstrated to provide robust characterization of complex surfaces [117–119]. In this method, a light source scans two surface: one reference surface and the surface of interest; the resulting reflections merged at the camera detector to produce an "interference pattern" that is processed into a two-dimensional (2D) "slice" of the surface. Multiple 2D slices are produced by performing multiple scans perpendicular to the surface (for a defined scan depth), after which the 2D slices are then combined to form a three-dimensional (3D) representation of the surface topography [120].

From the laser profilometry method, one is able to ascertain three key parameters regarding the topography of the surface which have important implications on tool durability (Figure 2.21): arithmetic mean height (Sa), root mean square height (Sq), and maximum height (Sz). Arithmetic mean height (Sa) is average difference in height of the surface to the calculated mean plane, most commonly taken as the metric for surface roughness. Closely related is the root mean square height (Sq), which is the standard deviation of height relative to the arithmetic mean height. Lastly, as the name suggests, the maximum height (Sz) is the difference in height between the lowest point relative to Sa and the highest point relative to Sa [121–123]. As previously mentioned, high surface roughness can lead to increased adhesion of the composite part with the tool, therefore characterizing this property is essential to predicting tool-part adhesion.
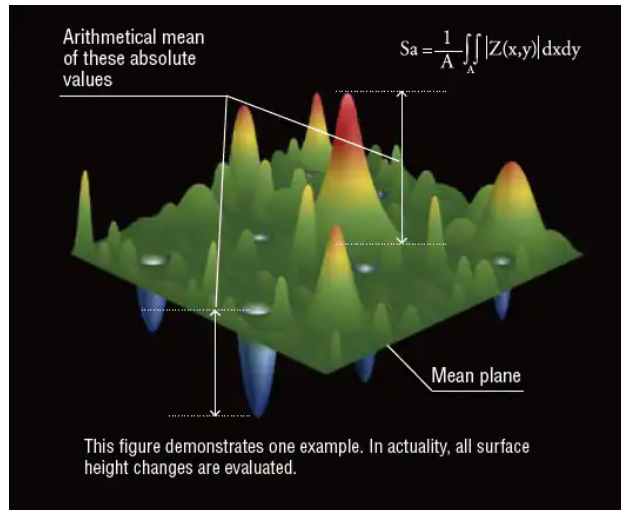
Figure 2.21: Fundamentals of surface roughness. Reproduced from [121].

Psuedo Wet-Layup Vacuum Bag Process

The wet-layup vacuum bag composite process is a relatively straightforward composite processing technique that relies on the manual assembly of resin and dry fabric plies followed by the application of vacuum bag to apply compact and consolidation [4]. During the WLVB process, the uncured composite part is first assembled layer-by-layer, in which a dry fabric ply is placed into the mould and wetted with resin which is spread across the ply via "squeegee" or roller to ensure complete wetting of the dry fabric (Figure 2.22). Traditionally, the tool is also pre-treated prior to each cycle with a "mould release" agent, that acts to enhance the "non-stick" properties of the tool and prolong its durability [61]. This process is repeated for the total number of plies required, and then the tool is bagged and vacuum is drawn to compress/consolidate the plies through atmospheric pressure (101.3 kPa). These conditions are maintained, potentially at elevated temperatures, until the composite part is sufficiently cured before removing it from the tool [4]. As seen through this process, the tool is subject to both mechanical (i.e. atmospheric pressure) and chemical (i.e. resin curing) conditions that it must withstand repeatedly with each part produced. Consequently, the quantity of parts produced (of sufficient quality) will ultimately define the durability of the composite processing tool.
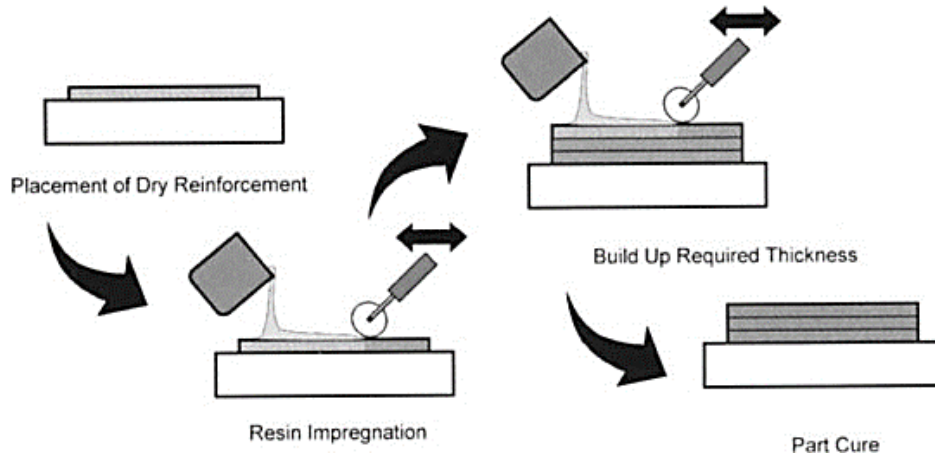
Figure 2.22: Steps of the wet-layup vacuum-bag process. Reproduced from [4] with permission.

Demould Testing

Tool demould testing is commonly performed through repetitive use to produce parts (Figure 2.23), in which with each subsequent demould of a composite part from a tool after processing, the surface roughness of the tool gradually increases due to mechanical and chemical wear (Section 2.1), leading to an increase in the force required to demould composite parts [17]. The incremental increase of this force will inevitably lead to a threshold value where "failure" occurs, potentially taking the form of tool failure, part failure, or failure to demould the composite part. For this first case (i.e. tool failure), tool failure can be further subdivided, the root cause attributable to either failure of the base tool substrate and/or failure of the bond between the base tool and any applied coating. In this scenario the force of adhesion between the composite part and tool/coating exceeds the mechanical strength of the tool itself and/or the strength of the bond between the coating and base tool substrate respectively [17, 89]. Alternatively, should these strengths be sufficient, the process can fail through part failure, in which the force required to demould the composite part exceeds that of the part's mechanical strength [89]. This mechanical strength is dependent on the composite part design, which is ultimately dictated by its intended application [4, 10, 17, 89].

Figure 2.23: Tool durability testing through repetitive use of tool to produce parts. Adapted from [17].

Though failure of the tool will ultimately occur when the force of adhesion between the composite part and tool/coating exceeds that of the tool/coating or part strength, in reality there exists a more realistic failure criterion: failure to remove the composite part from the tool. This criterion is practically defined by the maximum force that the operator can apply when attempting to demould the part, which once exceeded defines "failure" of the tool. The exact value used for this criterion may ultimately vary depending on the operator. However it is expected that the specified value will generally be lower than that of the tool and/or coating's mechanical strength . As such, the "optimal tool" is one that is mechanically "sufficient" in terms of strength while concurrently minimizing the adhesion of the composite part to the tool [4, 10, 17, 89].

Chapter 3

Materials & Methodology

3.1 Tool Fabrication

For all testing excluding thermal characterization, a single type of test specimen was fabricated, hereafter referred to as a "tool" or "specimen". These tools consisted of base substrate tool material followed by the application of a coating or left uncoated (Figure 3.1). A total of 4 different tool materials and 5 coating combinations (including uncoated) were fabricated for a total of 11 unique tool-coating combinations. The exact test matrix can be seen in Table 3.1 below. The dimensions of the tool were 25.4 mm x 25.4 mm in terms of length and width with varying heights depending on the tool material and its associated manufacturing method. For all tests performed, tool thickness was not important as it did not influence any of the test results. Following the fabrication of the base tool substrates, one 25.4 mm x 25.4 mm surface on each was milled and polished to a surface finish of 500 grit (0.18 μ m) prior to the application of any coating. This was done with the intent that the surface roughness fell between two standards commonly used in the plastics industry for mould finish, B3 (0.28 – 0.32 μ m) and B1 (0.05 – 0.15 μ m), which correspond to a semi-gloss surface finish [124, 125], but, furthermore, to ensure that the surface roughness for all tools was equal and did not influence test results.

Four unique tool substrate materials were used: Aluminum (AL), glass-fibre epoxy (GF-Epoxy), carbon-fibre acrylonitrile-butadiene-co-styrene (CF-ABS), and glass-fibre polycarbonate (GF-PC). Aluminum and GF-Epoxy tools were traditional tooling options with the exception of GF-Epoxy (C-P), which was a variation on the traditional composite tooling option (see Section 3.1.3 for further details). CF-ABS and GF-PC tools were alternatively produced through the hybrid manufacturing process. The manufacturing process for each material type is discussed in the following subsections, with additional detail regarding the

tool materials and their preparation prior to any coatings. Following fabrication of the base tool substrates, 4 different coatings were applied to the specimens: Sealant 1 (S1), Ceramic-Polymer (C-P), Sealant 2 (S2), and Epoxy-based (E), while an additional set of tool substrate materials were left uncoated (U). The details regarding these coatings are discussed in Section 3.1.3.
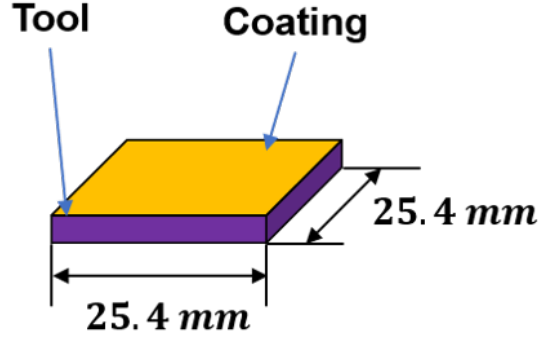
Figure 3.1: Tool geometry.

Table 3.1: All possible tool-coating combinations and the associated tool material and coating. S1: Sealant 1, U: Uncoated, C-P: Ceramic-Polymer, S2: Sealant 2, E: Epoxy-Based.

Specimen ID	Tool Material	Tool Type	Coating
AL (S1)	Aluminum	Traditional (Metal)	Sealant1
GF-Epoxy (S1)	GF-Epoxy	Traditional (Composite)	Sealant1 Ceramic-Polymer
CF-ABS (U)	3D-CFABS	Hybrid	None
CF-ABS (C-P)			Ceramic-Polymer
CF-ABS (S2)			Sealant 2
CF-ABS (E)			Epoxy
GF-PC (U)	3D-GFPC	Hybrid	None
GF-PC (C-P)			Ceramic-Polymer
GF-PC (S2)			Sealant 2
GF-PC €			Epoxy

3.1.1 Traditional Tooling

For the traditional tooling materials, metal and composite substrates that had already been coated were received from the industrial partner (Figure 3.2). Metal tooling received was an aluminum, presumably prepared according to the manufacturing process specified in Section 2.2.1. The composite tooling material provided was GF-Epoxy, which consisted of

a continuous glass-fibre reinforcement and epoxy-based resin. These tools were similarly presumed to be prepared according to the manufacturing process specified in Section 2.2.2. Furthermore, both of these tooling materials were coated with Sealant 1 mould sealant according to the procedure outlined in the technical data sheet (TDS). As these traditional tools (and those of similar make) are what is commonly used by the industrial partner and other aerospace and composite processing companies [10, 13, 30] in the manufacture of composite parts, they were used as benchmarks during all durability testing.
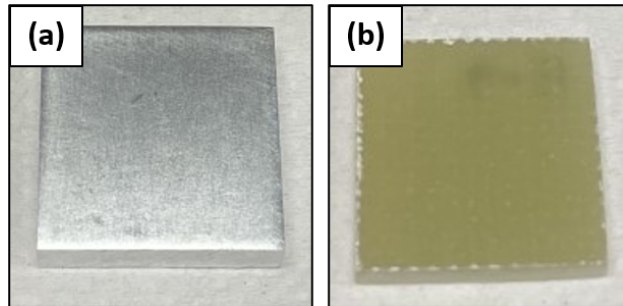
Figure 3.2: Tool geometry.

3.1.2 Hybrid-Manufactured Tooling

As seen in Section 2.3, the production of hybrid-manufactured tooling is a multi-step process that consists of multiple software's and file types. In the first step of the manufacturing process, a hexagonal structure was designed in Fusion360 computer-aided design (CAD) software (AutodeskTM). This hexagon had a width of 152.4 mm and height of 101.6 mm which corresponded to a width and height of 76.2 mm and 101.6 mm respectively for each side of the hexagon (Figure 3.3). This design was then exported in .stl file format for slicing and toolpath generation.
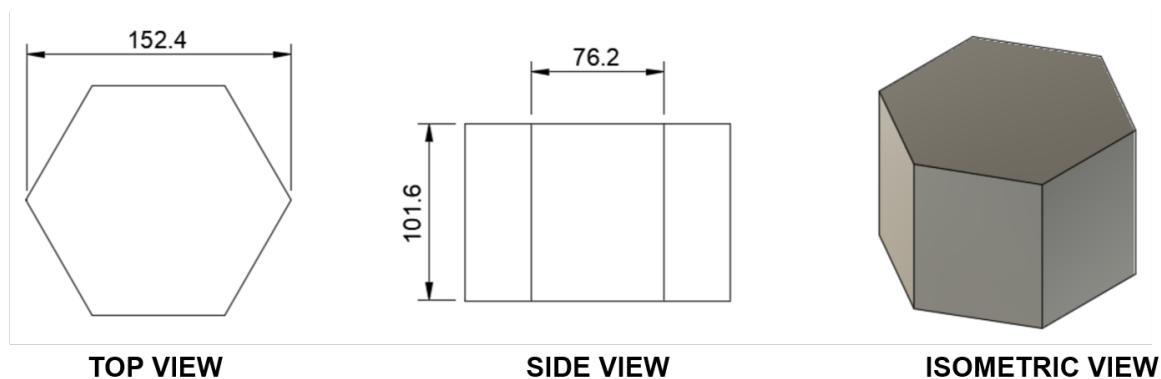
Figure 3.3: Design of hexagon in CAD software (dimensions are in mm).

The .stl file containing the hexagonal design was then imported into the Oak Ridge National Laboratory (ORNL) Slicer 2 (Oak Ridge National LaboratoryTM), an open-source research and development (R&D) CAD slicer tool that is largely designed around its use for slicing parts in large-scale additive manufacturing [126]. Due to ORNL Slicer 2 predominantly being a R&D tool, there are numerous settings that one can modify to change the details regarding the print. However many of them result in minor changes to the overall print quality. Therefore, for the purposes of this thesis, only a select few were adjusted which are known and have been shown to have the most significant effect on the resulting 3-D print structure [17, 83]. These settings can be seen in Table 3.2 below. For the major settings aforementioned, the exact values used for CF-ABS and GF-PC can be seen in Table 3.3. These print settings were used to generate the g-code files that were then imported to the hybrid machine.

Table 3.2: Major print settings in ORNL Slicer 2 and their associated function.

Setting Name	Function
Layer Height	Defines the layer height for the given bead type.
Bead Width (Perimeter, Inset, Brim)	Defines the bead width for the given bead type.
Number of Beads (Perimeter, Inset, Brim)	Defines the number of beads for the given bead type.
Exruder Speed (Perimeter, Inset, Brim)	Defines the extruder speed for the given bead type.
Print Speed (Perimeter, Inset, Brim)	Defines the print speed for the given bead type.
Minimum Layer Time	Defines the minimum time spent printing each layer.
Brim Width	Defines the width of the brim.

Table 3.3: Print settings used for the fabrication of CF-ABS and GF-PC hexagons.

Setting Name	CF-ABS	GF-PC
Layer Height [mm]	2	2
Bead Width (Perimeter, Inset, Brim) [mm]	8	8
Number of Beads (Perimeter) [mm]	1	1
Number of Beads (Inset) [mm]	2	2
Number of Beads (Brim) [mm]	2	2
Exruder Speed (Perimeter, Inset, Brim) [mm]	80	60
Print Speed (Perimeter, Inset, Brim) [mm/s]	25.4	30.5
Minimum Layer Time [s]	45	45
Brim Width [mm]	16	16

Using the g-code files generated in ORNL Slicer 2, the resulting structure printed for both materials was a two beads thick (approx. 16 mm) hollow hexagonal structure of approxi-

mately the same major dimensions specified in the original CAD (Figure 3.4). However, it was noted that the total height of the hexagon was slightly less than that of the original CAD, which could potentially be explained due to "sagging" of the printed beads thermal mass. The physics behind this are well described by Duty at all in [127].
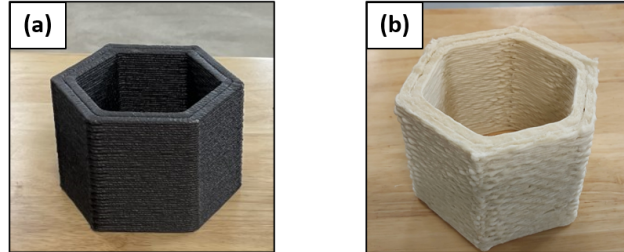
Figure 3.4: Printed (a) CF-ABS and (b) GF-PC hexagons.

After the 3-D printed hexagonal structures were fabricated, they were then machined and polished into the 25.4 mm x 25.4 mm tools (Figure 3.5). It should be noted that at the time of completion of the thesis, the subtractive component of the hybrid system was not fully operational, therefore the machining step was performed on separate subtractive systems (Struers Sectom-50 or CNC). The hexagonal structure was first cut into six individual plates and then milled on one side perpendicular to the print direction to be used as the tool surface. Doing so removes the 3-D print layer lines that are characteristic to the layer by layer deposition process, which is critical to ensure a relatively flat tool surface by revealing the most significantly fused sections between each layer (Figure 3.6) [24, 89]. If this is not done, the resulting tool surface will have inherently poor surface roughness as seen in Figure 3.6b. The milled plates were then polished to a surface finish of 500 grit using an orbital sander, starting at 200 grit and then working up to 500 . After polishing, each plate was then cut into six 25.4 mm x 25.4 mm tools on a Sectome-50 or CNC machine, resulting in a total of 36 tools produced per hexagonal structure.
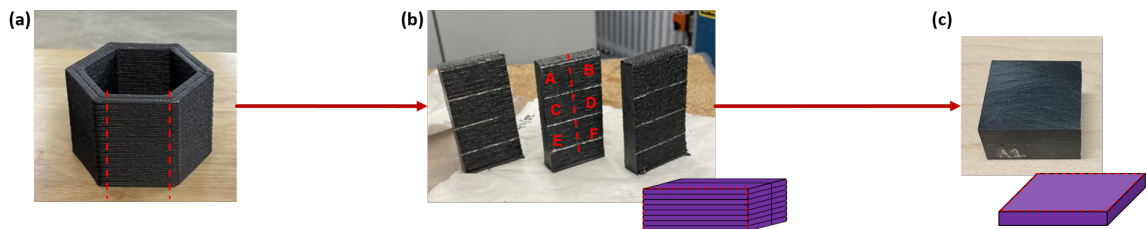
Figure 3.5: Manufacturing steps for tools produced through the hybrid manufacturing process. (a) A 2-beads thick hexagon is first printed in which the six sides are then cut to form (b) plates and subsequently (c) the 25.4 mm x 25.4 mm tools.
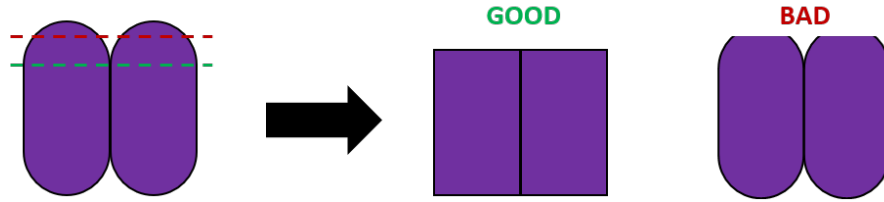
Figure 3.6: Importance of machining step on tool-coating surface finish. If the layer lines produced during the addivite manufacturing stage are not completely eliminated, the tool surface will have significant surface roughness.

3.1.3 Coatings

Once the tool substrates were manufactured and polished, four different coatings were applied to the tool substrates: Sealant 1, Ceramic-Polymer, Sealant 2, and Epoxy. The intended function of these coatings was to improve tool overall performance in terms of composite processing, performance being defined and assessed as seen in the durability test plan (Section 3.3). The following subsections outline some of the key details regarding each coating's reported properties, and how they were applied to the tool substrates.

Sealant 1

Sealant 1 is a naptha-based mould sealant by a company well-known for producing mould cleaners, primers, sealants, and release agents commonly used in the aerospace industry. This product is specifically designed to fill in tool micro-porosity, resulting in a high modulus film that chemically and physically bonds to the tool surface when exposed to atmospheric moisture. There is no mention on the product's data sheet what tool substrates this sealant is intended for. However this sealant was chosen as it is what the industrial partner currently uses for both metal and composite tooling. As such, four coats of the sealant were applied to the Aluminum and GF-Epoxy tools each according to the TDS directions prior to tool use.

Ceramic-Polymer

Ceramic-Polymer is an epoxy-based, thin-film coating containing ceramic nanoparticles, which has demonstrated use in industries ranging from aerospace, healthcare, and automotive in addition to finding a market for consumers. Advertised as having high wear resistance, hardness, and corrosion resistance, this product was consequently chosen as a potential to coating as it was expected to lead to better tool durability. Furthermore, recent literature using a similar coating was shown to have potential in the production of

hybrid-manufactured large-scale tooling [16]. The Ceramic-Polymer coating was applied to all hybrid tool materials in addition to a set of traditional tooling GF-Epoxy specimens (Figure 3.7) as per the manufacturer's training manual.
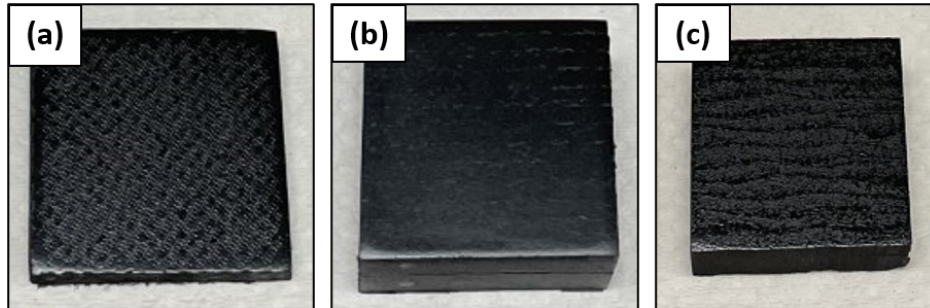
Figure 3.7: Ceramic-Polymer-coated tools. (a) GF-Epoxy (C-P), (b) CF-ABS (C-P), (c) GF-PC (C-P).

Sealant 2

Similar to Sealant 1, Sealant 2 is a naptha-based, semi-permanent mould sealant which is commonly applied to metal or epoxy tools. If used on composite or polymer mould materials, it is recommended that the mould be treated with a primer prior to the application of Sealant 2. For this MSc work, Sealant 2 was applied only to the hybrid tooling materials (i.e. CF-ABS and GF-PC) in which no primer was applied prior to the application of the sealant. This coating was chosen specifically due to previous literature in the area of large-scale hybrid tooling showing reasonable performance in terms of durability [17]. Following preparation (i.e. cleaning) of the mould, four coats of the sealant were applied (Figure 3.8) according to the directions specified in the technical data sheet.
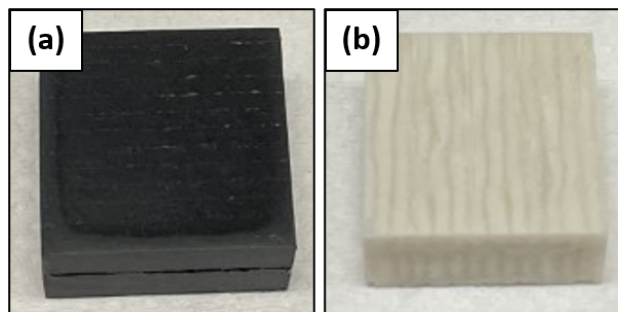
Figure 3.8: Sealant 2-coated tools. (a) CF-ABS (S2), (b) GF-PC (S2).

Epoxy

Epoxy is an epoxy-based coating specially designed for the post-processing of 3-D printed parts. Compatible with many different 3-D printing materials, this coating is applied through the use of a paintbrush, in which it creates a high gloss, smooth surface by filling in the layer line surface roughness characteristic of a 3-D printed layer-by-layer process. This product was chosen to be included in the test matrix due to its specific development for 3-D printed materials, and offered a relatively inexpensive alternative to traditional aerospace mould sealants. The Epoxy coating was applied to all hybrid tool materials (Figure 3.9) according to the manufacturer's guidelines.
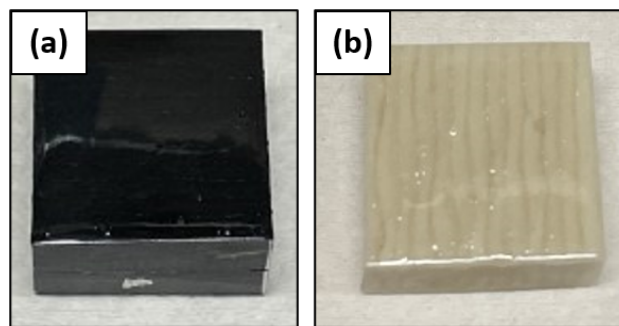
Figure 3.9: Epoxy-coated tools. (a) CF-ABS (E), (b) GF-PC (E).

3.2 Thermal Characterization of Hybrid-Manufactured Tools

As the additive manufacturing technique used in the hybrid manufacturing processes is thermoplastic extrusion, an understanding of the thermal properties of the materials used is essential. These thermal properties are not only useful in predicting the manufactured tools performance in service (Section 2.1.1), but will have a direct influence on the thermoplastic material extrusion process itself and can be the difference between a successful or failed print [19]. As such, the following subsections highlight three specific thermal characterization techniques - thermogravimetric analysis (TGA), differential scanning calorimetry (DSC), and thermomechanical analysis (TMA) - and how the results obtained can be used to predict both the thermoplastic material extrusion processing parameters and tool thermal properties. A specific benefit of these thermal characterization techniques is that they are small-scale, requiring minimal material use to determine key thermal properties.

3.2.1 Thermogravimetric Analysis (TGA)

For this thesis work, both the CF-ABS and GF-PC hybrid manufacturing materials were tested on a thermal analysis instruments (TA) TGA Q800 (Figure 3.10). Literature was first consulted to determine an estimated degradation onset temperature for similar polymer systems such that the appropriate specimen pan material could be selected. Based on this literature review, it was determined that the degradation onset temperatures of both CF-ABS and GF-PC were approximately 277 °C and 292 °C respectively [31], therefore a platinum specimen pan was chosen which is able to withstand temperatures up to 1000°C [101, 128]. The temperature profile used in this thermal characterization was based on the procedure employed by other researchers testing similar polymer composition systems [31], in which following an initial temperature equilibration at 25°C the temperature was ramped up to 800°C at a rate of 10°C per minute for both the CF – ABS and GF – PC material systems. Both materials were subsequently tested in both inert (i.e. Nitrogen) and air atmospheres for a total of four different test types, with five specimens being tested per procedure for a total of 20 specimens. Average initial specimen mass for CF-ABS and GF-PC tested in N_2 and air atmospheres can be seen in Table 3.4, in addition to the total mass used for each material.
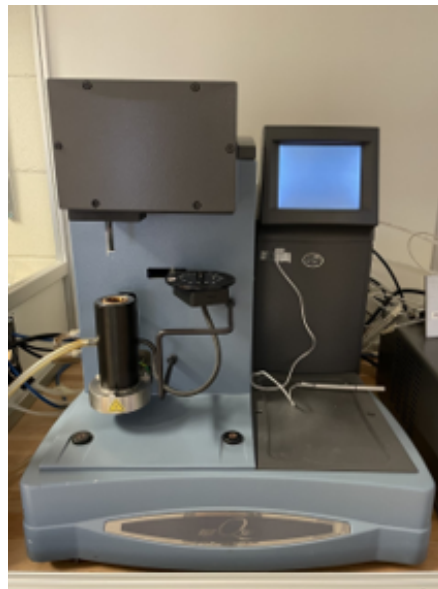
Figure 3.10: TGA Q800 used for thesis work.

Table 3.4: Average initial specimen mass for CF-ABS and GF-PC as well as the total mass for each material used in TGA.

Material	Atmosphere	Initial Mass [mg]	Total Mass [mg]
CF-ABS	N_2	21.77 +- 2.10	236.3
	Air	25.50 +- 0.68	
GF-PC	N_2	22.65 +- 0.70	201.20
	Air	21.94 +- 1.17	

3.2.2 Differential Scanning Calorimetry (DSC)

For this thesis work both the CF-ABS and GF-PC hybrid manufacturing materials were tested on a thermal analysis DSC Q300 (Figure 3.11), in which the glass transition temperatures were determined according to American Society for Testing and Materials (ASTM) standard D3418–15 [129]. Hermetically sealed aluminum pans were used to contain the specimens, as well as to create the inert reference. The exact temperature profile followed can be seen in Table 3.5 below. In this temperature profile the specimens undergo one heating cooling cycle at a rate of 20°C per minute first to illuminate any previous thermal processing history followed by a final secondary heating at a rate of 20°C per minute in which the resulting curve was used to determine the glass transition temperature.

Figure 3.11: DSC Q300 used for thesis work.

Table 3.5: Temperature profiles used for DSC characterization of CF-ABS and GF-PC.

Step	CF-ABS	GF-PC
1	Initial temperature: 25.00°C	Initial temperature: 25.00°C
2	Ramp 20.00°C/min to 300.00°C	Ramp 20.00°C/min to 400.00°C
3	Isothermal for 5.00 min	Isothermal for 5.00 min
4	Ramp 40.00°C/min to 25.00°C	Ramp 40.00°C/min to 25.00°C
5	Isothermal for 5.00 min	Isothermal for 5.00 min
6	Ramp 20.00°C/min to 300.00°C	Ramp 20.00°C/min to 400.00°C

3.2.3 Extrusion Temperature Processing Window

For the production of additively manufactured tooling, Ajinjeru et al. have demonstrated a quick, compact method to define the extrusion temperature processing window using DSC and TGA results combined (Figure 3.12) [21]. In this method, the glass transition temperature in degradation onset temperature determined through the small-scale bench top level tests define key minimum and maximum bounds for the extrusion temperature. By staying above the glass transition temperature one can avoid the risk of the polymer material existing in its glassy state during extrusion which can cause unwanted wear on the extruder motor due to increased torque requirements [21]. By staying below the degradation onset temperature, one can avoid the risk of thermal degrading or oxidizing their polymer material system which can lead to extruder clogging [21]. For this work, this method was employed to determine the extrusion processing temperature window for the CF-ABS and GF-PC hybrid manufacturing materials. However, the processing window was further narrowed to be slightly above (+20°C) the glass transition temperature and slightly below (-20°C) the degradation onset temperature, as it is known that potential variation in a polymer molecular weight can lead to variations in both the glass transition and the degradation onset temperatures [37].
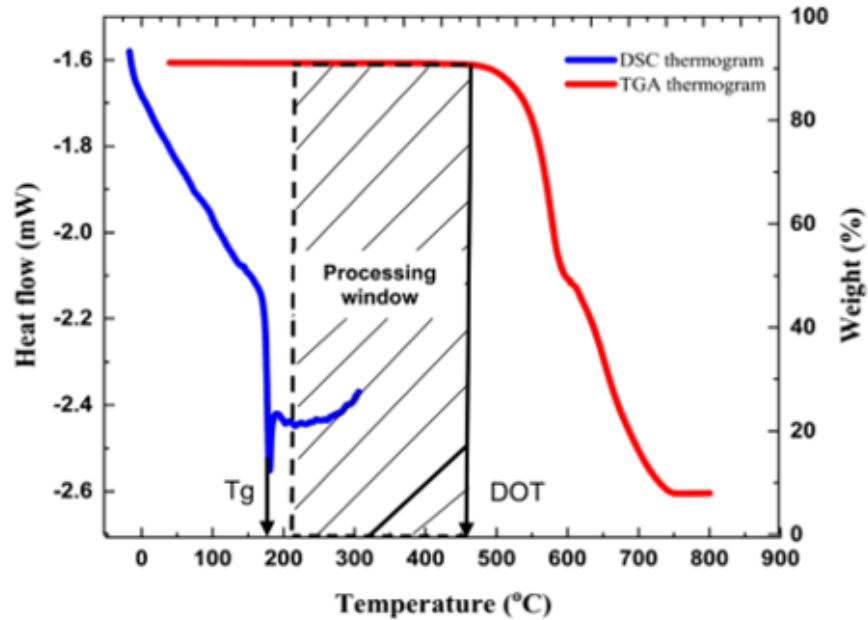
Figure 3.12: Determination of extrusion temperature processing window using DSC and TGA data. Reproduced from [19] with permission.

3.2.4 Thermomechanical Analysis (TMA)

In the following thesis work, a macro expansion thermal probe was used to determine the linear CTE of the CF-ABS and GF-PC hybrid manufacturing materials. These measurements were performed on the thermal analysis instruments TMA Q400 (Figure 3.13). The values obtained were also compared against linear CTE measurements previously performed in this laboratory for aluminum [130], which was used as a benchmark for traditional metal tooling. 3-D printed specimens were first manufactured by cutting a 12 mm x 12 mm x 12 mm cube from a previously printed structure[1]. A total of 3 different specimen types were prepared for each material to characterize the three principal directions (i.e. X, Y, and Z-direction). For hybrid manufactured materials, this corresponded to the direction of print, laterally perpendicular to the direction of print, and vertically perpendicular to the direction of print respectively (Figure 3.14). After specimen preparation, a modified version of ASTM method E831–12 was followed to determine the linear CTE of the materials [131]. Per test, a preload force of 0.02 N was first applied and the specimen was equilibrated at 25°C which was the maintained isothermally for one minute. Following this isothermal equilibration,

---

[1]In some cases, the initial geometry of the printed specimen was not large enough to be cut to the aforementioned dimensions. Instead, the specimens were prepared such that in the direction of linear CTE measurement the surfaces in contact with the specimen stage and thermal expansion probe were prepared to ensure that they were both flat and parallel.

the temperature is then ramped to 120°C at a rate of 5°C per minute, after which the test is complete. The resulting dimensional change versus temperature curve is then used to determine the linear CTE according to Equation 1.
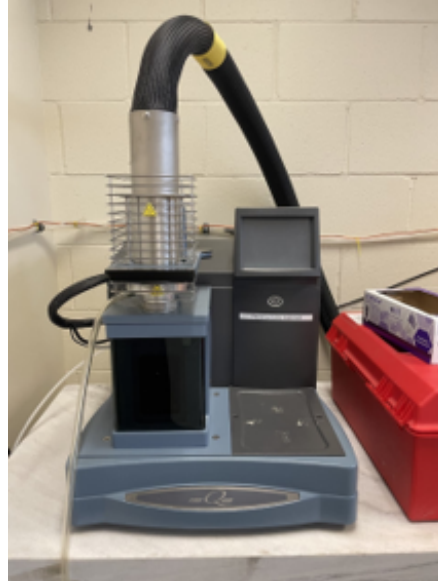
Figure 3.13: TMA Q400 used for thesis work.
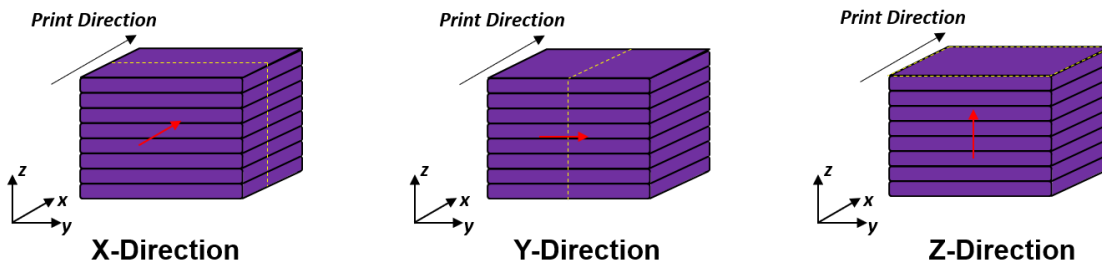
Figure 3.14: Orientation of the hybrid manufactured materials relative to the principal TMA test directions.

3.3 Durability Test Plan

The durability test plan is a multistage characterization process which was used to quantitatively assess the durability of tooling at the small scale. This multistage characterization process consists of three major stages beginning with the tool fabrication which is then followed by a set of pre-screening tests and lastly the small-scale composite process testing. The following subsections will discuss in detail the specifics regarding each of these stages and how the data is collected, generated, presented, and ultimately interpreted.

3.3.1 Pre-Screening Tests

The proposed quantitative small-scale test method begins with a series of pre-screening tests to determine the performance of a tool-coating combination on three specific fronts: chemical resistance, vacuum integrity, and mechanical resistance. These aspects were chosen based on the literature review of fundamental tool properties as seen in Section 2.1, and their analysis is accomplished through the use of tensiometry, a custom vacuum fixture, and hardness testing as quantitative metrics respectively. By evaluating a tool's performance on these three fronts, one is able to get a preliminary idea as to whether the unique combination of tool material and it's associated coating will be successful as a composite processing tool and therefore be worth spending further time and money investigating further. The relative ease in performing these three pre-screening tests, furthermore, enables the rapid identification of the best tool-coating candidates from a larger set and any new tool-coating combination developed which can quickly be analyzed and compared to a database of previously analyzed tool-coating combinations.

Upon collection of all the pre-screening test results, the analysis to determine the most optimal tool for the given application is accomplished in two distinct steps. In the first step, for each of the three pre-screening tests the results of each tool are ranked on an integer numeric scale ranging from 1 to the maximum number of tools ("n"), where 1 is the worst performing for the given test and "n" is the best performing for the given test. Following this ranking, the next step is to assign the relative weight of each of the three given pre-screening tests as a decimal number ranging from 0.0 (not important) to 1.0 (very important). The exact weight will depend on the specific application of the tool. The final step is to then calculate a performance index for each tool according to Equation 1:

$$Performance = \Sigma(TestRank)_i(TestWeight)_i \ , \ i = \#oftestmethods \qquad (3.1)$$

For each tool a single performance index is calculated by taking the summation of the rank obtained for each test by the associated test weight. The calculated performance indices can then be ranked in order of magnitude, with the highest value performance index representing the best tool for the given application based on the weights given for each of the three pre-screening tests. Should the application change, the waiting can be reassigned for each test and the performance in the seas recalculated for each tool and re-ranked to determine the new best tool.

Tensiometry

Advancing-receding contact angle (ARCA) optical tensiometry was employed to characterize the chemical resistance of the tools, correlating results to the tool's ability to resist bonding with composite parts during processing. Chemical resistance was specifically measured through dynamic contact angle hysteresis, in which a lower hysteresis value can then be attributed to the greater ability of the tool's surface to be nonstick [109, 110]. The ARCA setup consisted of a 100 μL syringe (McMasterCarr) fitted with a 32-gauge needle (Nordson), with flow controlled by a syringe pump run using a custom Arduino script (Figure 3.15a). Reverse osmosis (RO) water was used as the droplet fluid, in which for each test a 2 μL droplet was first formed on the surface of each tool prior to the ARCA test (Figure 3.15bi). During each ARCA run, an additional 5 μL of RO water was injected during the advancing phase, followed by all water being drawn back into the syringe during the receding phase (Figure 3.15bii,iii). A high-speed camera (Infinity3-1UM) paired with standard video capture software (Lumenara Infinity Capture) was used for video acquisition of the advancing and receding droplet, the resulting data then processed (Photron FastCam Viewer 4) and analyzed (Dataphysics SCA 20) using tangent leaning fitting method to determine the advancing contact angle (ACA), receding contact angle (RCA), and hysteresis (i.e. difference between ACA and RCA) for each tool. A total of 2 samples were tested per tool, in which 3 ARCA measurements were performed on each.
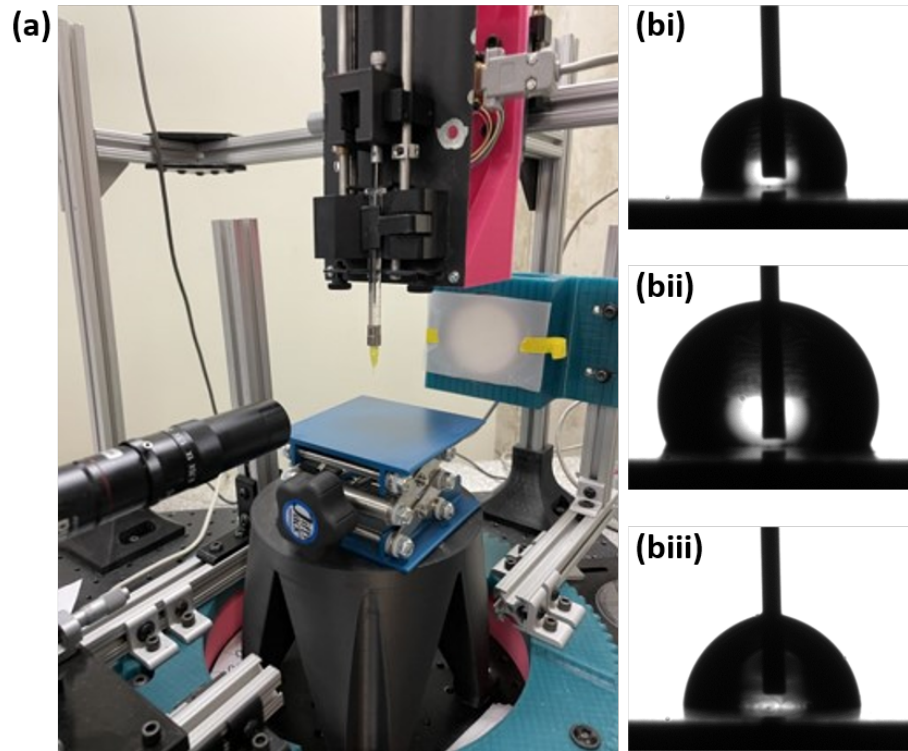
Figure 3.15: (a) Custom optical tensiometry setup. (bi-iii) The ARCA procedure beginning with (i) the initial droplet, (ii) the advancing droplet, and (iii) the receding droplet.

Vacuum Integrity

To assess the vacuum integrity of the fabricated tools a 5-minute "drop test" was performed on a custom vacuum fixture (Figure 3.16a). This fixture consisted of a small circular chamber of approximately 50.8 mm in diameter connected to a vacuum source controlled by an open close valve, a vacuum pressure gauge, and one other opening with a 19.05 mm x 19.05 mm to place the tool of interest. To use the fixture, at this opening, the tool of interest was secured using vacuum tape (General Sealants) as seen in Figure 3.16b, sealing off the cylindrical chamber when the vacuum source was closed. Vacuum was then drawn, and the tool was further pressed into the vacuum tape to ensure a good seal. After maximum potential vacuum pressure was reached for a given tool, determined after no appreciable pressure change was observed for 2 minutes prior, the vacuum source was closed and the pressure was monitored over the 5-minute interval to obtain a "vacuum drop" value, calculated by taking the vacuum pressure at the start and end of the interval. A low vacuum drop was taken to be indicative that the given tool is impermeable to air, demonstrating good vacuum integrity (the converse being true for a tool with poor vacuum integrity). A total of 3 specimens were tested per tool. Prior to analysis of any tools, the fixture was first verified to have no other sources of

vacuum pressure leak using nylon vacuum bag (Airtech).
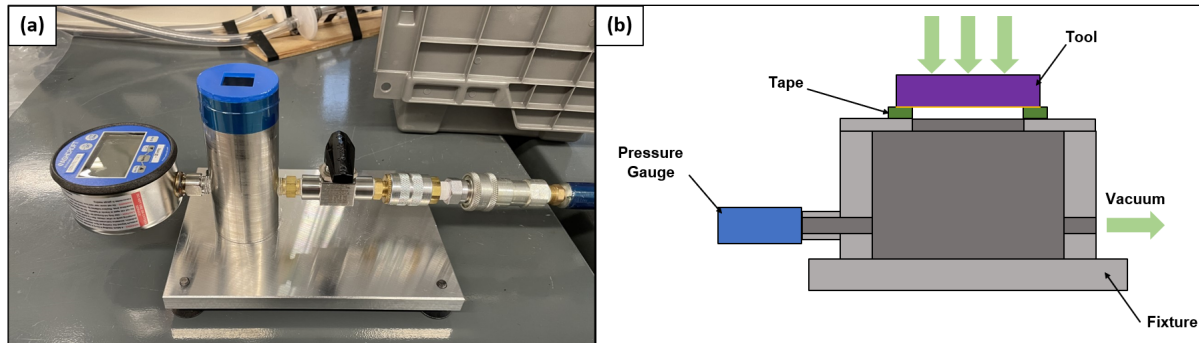
Figure 3.16: (a) Custom vacuum integrity setup and (b) its basic function. When vacuum is drawn in the chamber, the taped-down tool acts as the final wall of the chamber, any subsequent vacuum losses being attributed to permeability through the thickness of the tool.

Micro-Indentation/Hardness Testing

Hardness values obtained through Vickers micro-indentation were correlated to the tool's ability to resist mechanical wear, with a specific focus on indentation caused by the fibre reinforcement in composite parts during processing (Figure 3.17). A greater hardness would suggest greater resistance of the tool's surface to indentation. For each specimen, indentations into the surface were performed with a force of 50 mN, in which the loading time, holding time, and unloading time were each 30 seconds. These values were chosen based on literature previously reporting Vickers indentation on composite materials [132]. One specimen was tested per tool, in which twelve indentations were performed on each specimen in a 3 x 4 grid with indentation points separated by 100 microns in both the X and Y directions. Following each indentation, the geometry of each indentation was then analyzed to determine the hardness values.
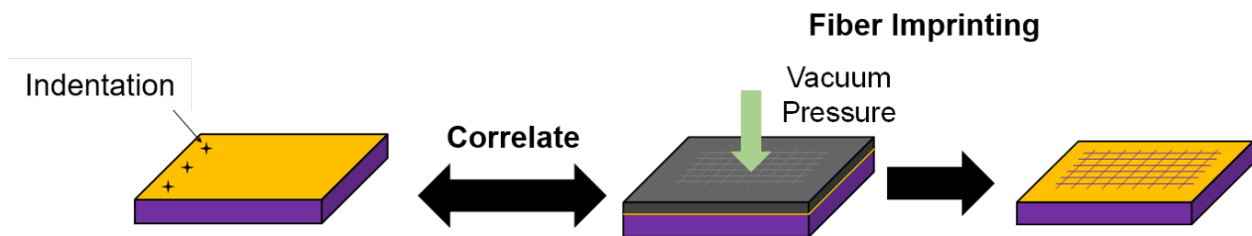
Figure 3.17: Correlation of tool hardness to mechanical resistance. During a composite process involving vacuum pressure, the vacuum pressure exerts a force that pushes the composite part into the tool. If the tool is not of sufficient hardness, this can lead to the imprinting of the fibre reinforcement into the tool surface, leading to excessive mechanical wear.

3.3.2 Small-Scale Composite Process Testing

Following the pre-screening tests, the top five performing tool-coating combinations were then subject to a small-scale composite process test method to assess the screened tools durability in an actual composite part production process and to validate the pre-screening test results. This small-scale testing consisted of three distinct elements: laser profilometry, a pseudo-wet layup vacuum bag (WLVB), and a demould test (Figure 3.18). Following specimen fabrication, the specimens were first scanned via laser profilometry to characterize the "as-fabricated" surface roughness of the tool surface. After the scans were complete, the tools were then subject to the pseudo-WLVB process such that the tools were subject to wear conditions present in actual composite processing. Once the cycle was complete, the composite parts were attempted to be demoulded from the tools without failure and the entire process (beginning with profilometry) was repeated. Further information regarding each of these elements can be found in the following subsections. The purpose of this test method was to give a holistic picture into the progressive deterioration of each tool-coating combinations durability in a practical composite processing application, characterized through the gradual increase in surface roughness and eventual failure of each tool-coating combination [17].
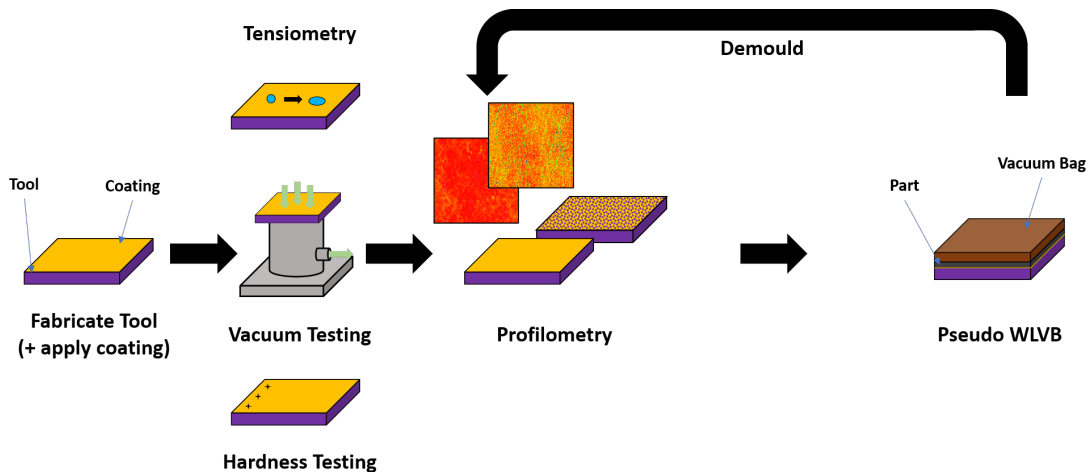
Figure 3.18: Workflow for small-scale composite process testing.

Laser Profilometry

In the small-scale composite process testing, laser profilometry was used as the primary metric to assess tool-coating wear with each successive cycle. To characterize the surface roughness of the durability test specimen, a Zygo NewView Profilometer was used which captures both surface roughness and an optical image. A 2.75x magnification was used at 1x zoom to capture a 3 mm x 3 mm field of view (FOV) with a lateral resolution of 2.97

mm. For each tool, one scan was performed after each cycle[2] until the tool was eliminated from the composite processing trial according to the criteria outlined in Demould Testing. For each scan, the region of interest (ROI) was chosen at random and in turn gave the surface profile of the 3 mm x 3 mm region on the tool surface, in addition to the Sa, Sq, and Sz. The exact settings used during scan acquisition can be found in Table 3.6. Of particular importance was scan depth, which was chosen based on the specimen type tested to minimize regions where the roughness exceeded the scan depth resulting in no data. If the surface roughness was outside the scan depth specified, this would result in what was known as "voids" that were represented as black pixels. As a first strategy, voids were first attempted to be eliminated by increasing the scan depth at the expense of longer acquisition times. If voids still remained after reaching the basic scan depth limits of the machine for the given settings, they were secondarily addressed in data analysis by using a "fill all voids" post-process which extrapolated the surface roughness of the voids relative to its nearest neighbour pixels.

Table 3.6: Major settings used in laser profilometry.

Setting Name	Value
Lens	2.75 Mich. NA 0.08
Zoom	1X
Field of View	3.00 mm x 3.00 mm
Lateral Resolution	2.927 μm
Measurement Mode	Coherence Scanning Interferometry
Z Resolution	High
Scan Depth	20 μm - 145 μm

Pseudo Wet-Layup Vacuum Bag Process

In the composite processing component of this test method, the goal was to re-create the key processing conditions found in a wet-layup vacuum bagging (WLVB) process to re-create the chemical and mechanical wear that would occur during composite part processing [4]. As such, for the small-scale composite process testing performed in this work, a pseudo-WLVB process was employed with the general assembly of materials as seen below (Figure 3.19). In this process, 25.4 mm x 25.4 mm (L x W) composite parts were repeatedly manufactured on each tool-coating combination until they were eliminated from the test as specified by Demould Testing. The composite parts consisted of 4 plies of [0/90] dry biaxial plain weave

---

[2]In addition to the one scan performed prior to any cycle, i.e. in the "as fabricated" state.

carbon fibre wetted with an epoxy-based liquid resin system mixed 100:12 (Resin:Hardener) by weight according to the manufacturer's guidelines[3]. For each cycle, dry plies were first wet-ted off-tool with an excess of mixed epoxy to ensure complete wetting before being assembled on the tool-coating combinations surfaces and covered with non-stick composite release film (A4000R, Airtech), breather (Airweave N10, Airtech), and vacuum bag (742601M, Airtech). No mould release agent was used for any processing to accelerate the wear conditions of the tool-coating combinations and, furthermore, eliminate any variability due to additional reagents use during processing (ex. quantity of mould release used, repeatability of applica-tion). The entire assembly was then placed in an oven held at 90 C, covered with two 9.3 kg stone slabs (pre-heated in the oven) to simulate atmospheric pressure, and left to cure for 1 hour. After the hour had elapsed, the assembly was removed from the oven and the composite parts were demoulded from the tools according to the procedure specified in the following section.

Figure 3.19: General assembly for the WLVB process.

Demould Testing

For the work performed in this thesis, a 2-stage procedure was employed to track the de-mould performance of each tool-coating after use[4]. In the first stage, the composite part was attempted to be removed from the tool using varying degrees of effort, ranging from "easy" (hands-only) to "hard" (considerable effort required while using an assistive tool) (Table 3.7). If the composite part was successfully removed from the tool, it remained for subse-quent small-scale composite processing. However, if this was not possible it was deemed to have "failed", the tool eliminated from subsequent small-scale tests and assigned a 2-letter demould code to qualitatively characterize the associated failure mode. As the focus of this work was to predominately characterize the performance of hybrid-manufactured tooling, demould testing was continued until all hybrid tool-coating combinations had failed, the last remaining hybrid tool-coating combination representing the most durable hybrid tool.

---

[3]Composite part configuration was not deemed important for this work as the predominate focus was on the interaction of the tool and part surfaces.

[4]At the start of this work, a qualitative method to assess demold force was designed, however preliminary testing of this setup yielded inconclusive results which made its further use futile. Details regarding this method and the preliminary results can be found in Appendix A.1.

Table 3.7: Demould code used for the characterization of tool demolding performance and failure.

Stage	Identifier	Description
1	E	Easy to demould. Can be done by hand.
	M	Some effort required to demould. Requires some use of assistive tool.
	H	Hard to demould. Requires excessive use of chisel.
2	TF	Tool failure. Specify mode of failure.
	PF	Composite part failure. When demoulding part from tool, if any part remains tool surface.

Chapter 4

Results & Discussion

4.1 Thermal Characterization

The high-level results of the thermal characterization testing are presented in Table 4.1 below alongside the total material required to perform each specific test. From these results, it can be seen that minimal material was required to determine these key thermal properties of the hybrid manufactured tool materials, a total of 11.34 g and 3.08 g used for CF-ABS and GF-PC respectively. This demonstrates the utility that small-scale quantitative testing can provide when determining key tool properties, while minimizing the upfront initial material requirements and associated costs. The following subsections go into greater details regarding each specific thermal characterization, highlighting important aspects regarding the determination of each respective property.

Table 4.1: High-level results of thermal characterization for hybrid tool materials.

Setting Name	CF-ABS	GF-PC
Degradation Onset Temperature, N_2 [°C]	322.11 +- 3.46	434.45 +- 0.89
Degradation Onset Temperature, Air [°C]	313.49 +- 2.03	412.90 +- 1.40
Glass Transition Temperature [°C]	102.66 +- 0.49, 136.60 +- 0.33 (Styrene, Acrylonitrile)	141.13 +- 0.57
Extrusion Processing Temperature Window [°C]	150 - 300	160 - 395
CTE, X-Direction [μm/m.°C]	25.87 +- 1.00	45.38 +- 1.91
CTE, Y-Direction [μm/m.°C]	35.38 +- 1.37	46.23 +- 4.00
CTE, Z-Direction [μm/m.°C]	123.69 +- 7.50	80.00 +- 8.47
Total Material Usage [g]	11.34	3.08

4.1.1 Thermogravimetric Analysis (TGA)

TGA, N_2 Atmosphere, CF-ABS & GF-PC

In a nitrogen atmosphere, for each material it can be seen that there was good repeatability in the T-wt% profile produced, in which all specimens exhibited a single distinct transition which corresponded to the 1 wt% degradation onset temperature (Figure 4.1,Table 4.2). After this transition, the wt% of CF-ABS and GF-PC fell to approximately 21 wt% and 40 wt% respectively. As both materials contain 20 wt% fibre reinforcement, it was interesting to discover that only the CF-ABS material reached this weight percent by the end of the test. The GF-PC specimens instead appeared to plateau at approximately 40 wt% by the end of each test, which might suggest the presence of additional compounds (ex. additives, plasticizers, etc.) included in the material to aid in its processing [31, 96, 99, 128]. As such, if fibre reinforcement content is to be determined by TGA characterization, a complete understanding of the material composition is essential to rule out the presence of any additional compounds that may interfere.
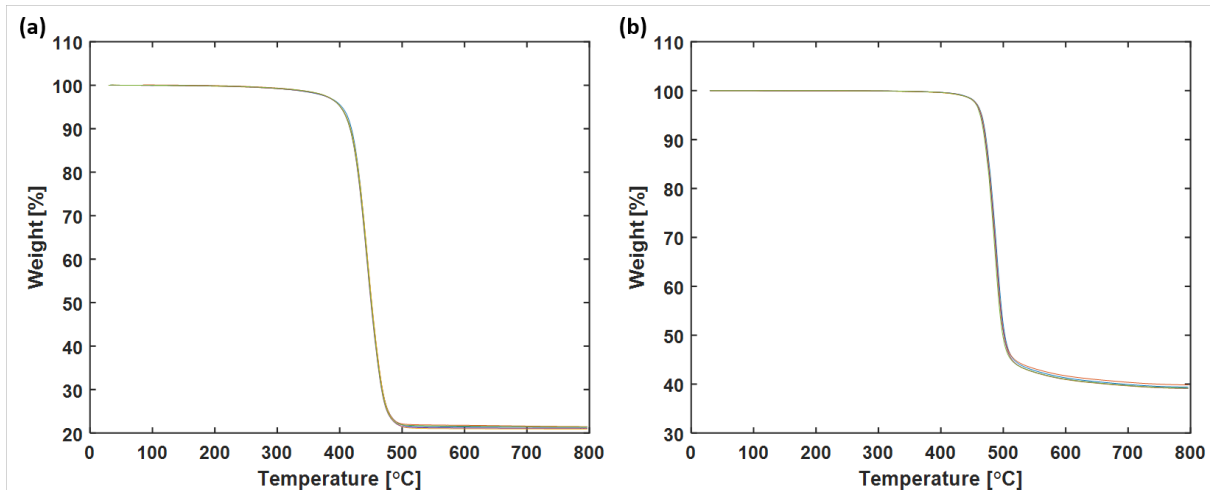
Figure 4.1: TGA Curves for (a) CF-ABS and (b) GF-PC in nitrogen atmosphere.

Table 4.2: Degradation onset temperatures for CF-ABS and GF-PC in nitrogen atmosphere.

Setting Name	CF-ABS	GF-PC
Degradation Onset Temperature, N_2 [°C]	322.11 +- 3.46	434.45 +- 0.89
Degradation Onset Temperature, Air [°C]	313.49 +- 2.03	412.90 +- 1.40
Glass Transition Temperature [°C]	102.66 +- 0.49, 136.60 +- 0.33 (Styrene, Acrylonitrile)	141.13 +- 0.57
Extrusion Processing Temperature Window [°C]	150 - 300	160 - 395
CTE, X-Direction [μm/m.°C]	25.87 +- 1.00	45.38 +- 1.91
CTE, Y-Direction [μm/m.°C]	35.38 +- 1.37	46.23 +- 4.00
CTE, Z-Direction [μm/m.°C]	123.69 +- 7.50	80.00 +- 8.47
Total Material Usage [g]	11.34	3.08

TGA, Air Atmosphere, CF-ABS & GF-PC

Results from air atmosphere TGA indicated that thermal degradation behaviour varied in a reactive environment (Figure 4.2, Table 4.3). Though both CF-ABS and GF-PC materials maintained good repeatability between tests, all profiles showed two distinct transitions in weight percent. The first transition in each corresponded to the 1 wt% degradation onset temperature. Though interesting, the second degradation onset temperatures corresponded to the second transition were not characterized as they would not translate to useful values in a practical setting. In a practical application, once the initial degradation onset temperature (DOT) is reached, the inherent material structure is compromised and therefore no longer usable for most applications [133]. Any further degradation only further compromises the material structure and is irrelevant.

Table 4.3: Degradation onset temperatures for CF-ABS and GF-PC in air atmosphere.

Material	Degradation Onset Temperature, Air [°C]
CF-ABS	313.49 +- 2.03
GF-PC	412.90 +- 1.40
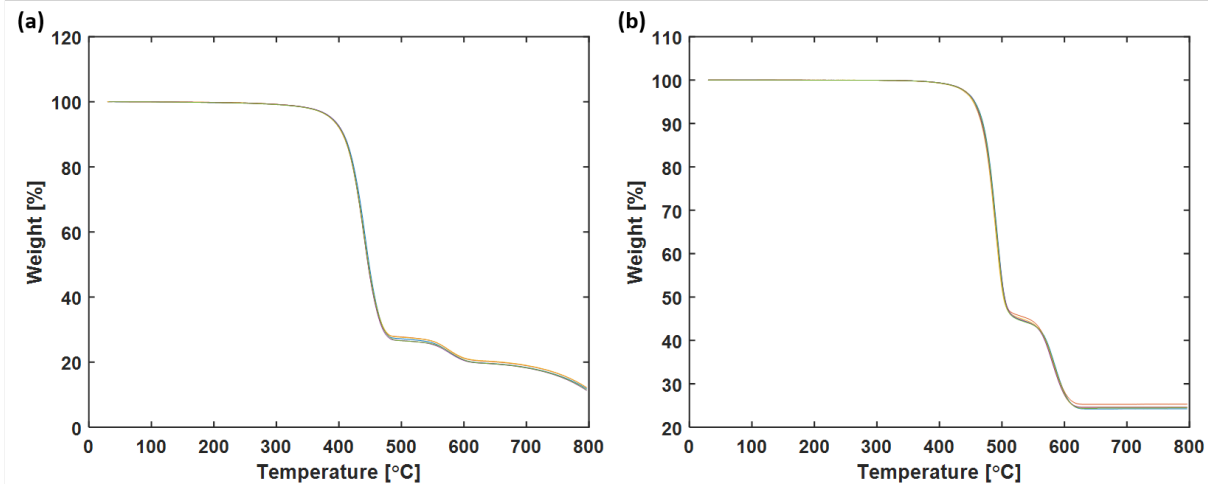
Figure 4.2: TGA Curves for (a) CF-ABS and (b) GF-PC in air atmosphere.

TGA, Comparison of N_2 and Air Atmospheres

Holistically, for the TGA work performed the goals were to determine the degradation onset temperatures as well as verify the fibre reinforcement content of the materials used in hybrid manufacturing while minimizing the amount of material used required for testing. Using this thermal characterization method, most of these properties were obtained in both nitrogen and or air atmosphere using only 297.5 mg of material which demonstrates the benefits of small-scale quantitative testing. However, though DOTs for the hybrid manufacturing materials can be determined from the TGA results in inert atmosphere, it is not the most accurate value replicative of the hybrid manufacturing process and subsequent tool use. In both of these applications, material thermal degradation does not generally occur in an inert atmosphere but instead that of air [21, 23, 27, 31, 77, 84, 134], which can ultimately lead to variations in the temperature weight percent profile [21, 23].

Comparison of the temperature profiles for each material in nitrogen and air atmospheres showed distinct differences in the DOTs (Figure 4.3), highlighting the importance of considering environmental effects. In both cases, though the temperature profiles remained largely the same when tested in different environments, however minor variations did exist. Most notably, the degradation onset temperature for the initial transition of both materials decreased by approximately 313.49°C and 412.90°C for CF-ABS and GF-PC respectively (Table 4.4). In a practical setting, such as the determination of an extrusion temperature processing window, knowing this difference in DOT relative to the testing atmosphere is paramount as it can be the difference between failure and success of the process [21, 23].
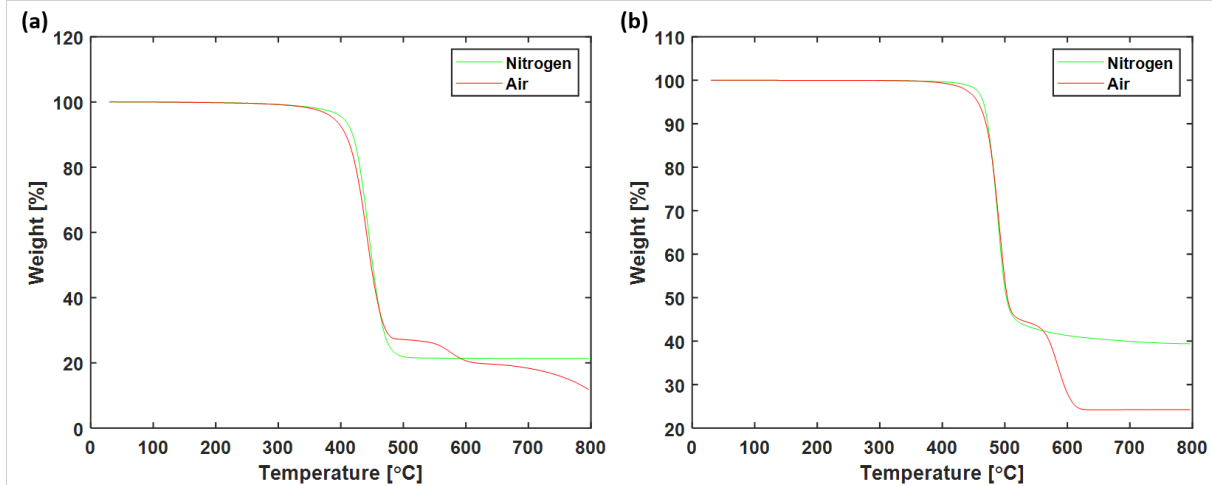
Figure 4.3: Comparison of TGA Curves for (a) CF-ABS and (b) GF-PC in nitrogen vs. air Atmosphere.

Table 4.4: Comparison of degradation onset temperatures for CF-ABS and GF-PC in nitrogen vs. air Atmosphere.

Material	DOT, N_2 [°C]	DOT, Air [°C]	Change in DOT [°C]
CF-ABS	322.11 +- 3.46	313.49 +- 2.03	8.62
GF-PC	434.45 +- 0.89	412.90 +- 1.40	21.55

4.1.2 Differential Scanning Calorimetry (DSC)

Differential scanning calorimetry (DSC) results for the second heating cycle of CF-ABS indicated the presence two distinct transition temperatures in the tested temperature window (Figure 4.4). For these two given transitions, the calculated glass transition temperatures were 102.66°C and 136.6°C, which can be attributed to the glass transition temperatures of styrene and acrylonitrile components of ABS [135]. ABS is a tri-block co-polymer consisting of three distinct units: acrylonitrile, butadiene, and styrene; and as such each subunit has its own distinct glass transition temperature, and as such have their own distinct transition. The third subunit, butadiene, additionally has its own unique glass transition temperature. However this occurs at approximately -85.5°C [135] and therefore falls outside the temperature range probed with the procedure used. This implies that for all temperatures greater than -85.5°C (i.e. most common tooling applications), the butadiene component of ABS is in its rubbery state and therefore the ABS is of lower stiffness and strength compared to if the ABS were below -85.5°C [103]. However, it is common knowledge that ABS is widely used above this temperature, in which the mechanical properties have been demonstrated to

be sufficient for most applications [136].
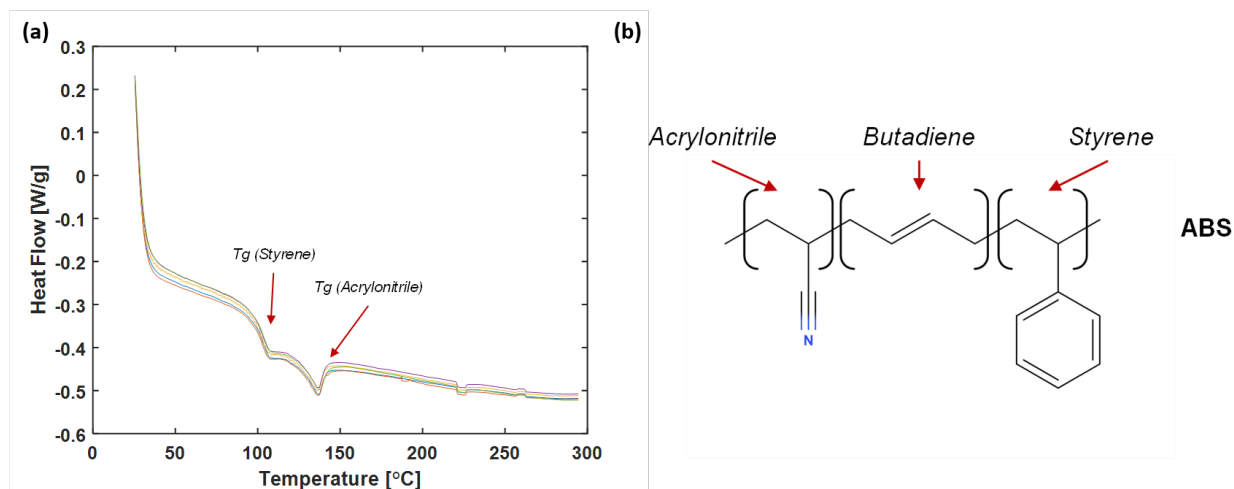
Figure 4.4: (a) DSC Curves for CF-ABS and (b) the associated molecular structure.

DSC, GF-PC, N_2 Atmosphere

DSC results for the second heating cycle of GF-PC show a single temperature transition despite minor fluctuation in heat flow values pre-and post-transition (Figure 4.5). Furthermore, it appeared that specimen four did have some minor fluctuations in the heat flow prior to the glass transition temperature. However it is expected that this is due to minor disturbances of the test cells during the test, caused by vibrations of the lab work bench. All temperature heat flow curves regardless appeared to experience a single transition, which correlated to a transition temperature of 141.13°C +- 0.57°C. This value is in good agreement with that reported in literature [137, 138].
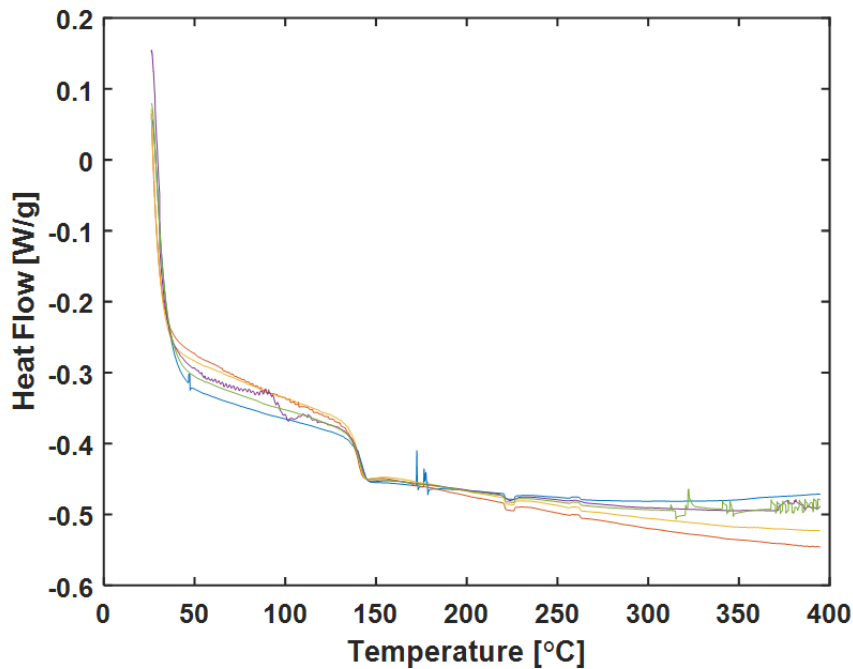
Figure 4.5: DSC Curves for GF-PC.

DSC, CF-ABS & GF-PC Summary

As previously mentioned, determining the maximum permissible service temperature of the tool is essential for defining the limits of its application (Section 2.1.1). For the production of hybrid-manufactured tooling using polymer-based materials, this maximum service temperature can be defined using glass transition temperatures determined through DSC. Above the glass transition temperature, the mechanical properties of the tool would significantly decrease due to the glass to rubbery transition of the polymer component rendering the tool unusable, therefore a value is chosen below this point. In reality, the maximum service temperature chosen would be slightly lower than the glass transition temperature to ensure no fraction of the polymer undergoes transition [139]. As such, the maximum service temperature for the CF-ABS and GF-PC material was therefore defined as 75°C and 113°C respectively. These key properties were obtained using only 51.57 milligrams and 48.21 milligrams of material total for CF-ABS and GF-PC respectively, again demonstrating the utility of small-scale quantitative testing. Based on the maximum service temperatures of the two hybrid manufacturing materials used for tooling, it appears that GF-PC would be better suited for higher temperature applications. However this is still on the lower end of processing temperatures used [4] which would suggest further hybrid manufacturing materials should be investigated.

4.1.3 Extrusion Temperature Processing Window

Combined DSC and TGA results for CF-ABS and GF-PC to form individual extrusion temperature processing windows shows the utility of small-scale characterization methods (Figure 4.6,Table 4.5). From small-scale quantitative thermal characterization equipment, proposed extrusion temperature processing windows for thermoplastic materials used in the hybrid manufacturing process can be established prior to any use of the large-scale system. Eliminating the use of the large-scale system results in a significant reduction in material used, consequently resulting in a significantly lower material cost. However, the processing windows proposed both covers a relatively broad range of temperatures (approximately 150°C and 235°C) which demonstrates the need for further narrow this range. This could be accomplished by further small-scale thermal characterization methods that capture specific conditions of the actual extrusion process. One such technique would be rheology, which could capture the influence of thermo-rheological effects present in the extrusion process and therefore further narrow the processing temperature window by identifying optimal thermo–rheological processing temperatures [19].
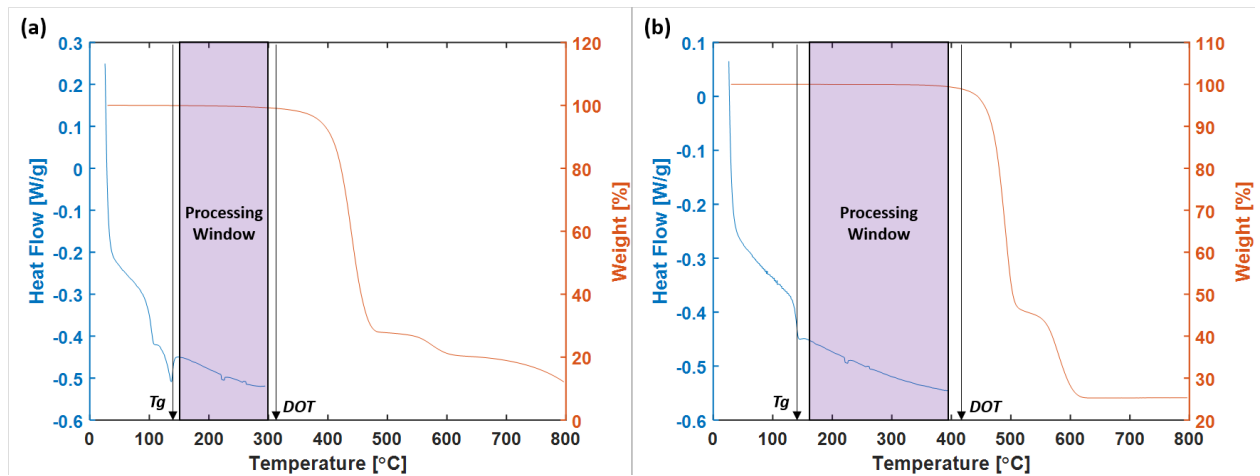
Figure 4.6: Combined TGA and DSC curves to determine extrusion temperature processing window for (a) CF-ABS and (b) GF-PC.

Table 4.5: Extrusion temperature processing windows and the relevant degradation onset and glass transition temperatures from TGA and DSC testing.

Setting Name	CF-ABS	GF-PC
Degradation Onset Temperature, Air [°C]	313.49 +- 2.03	412.90 +- 1.40
Glass Transition Temperature [°C]	136.60 +- 0.33 (Acrylonitrile)	141.13 +- 0.57
Extrusion Processing Temperature Window [°C]	150 - 300	160 - 395

4.1.4 Thermomechanical Analysis (TMA)

TMA, General Results

Compared to the aluminum reference, TMA results showed significant differences in CTE of both hybrid manufactured materials depending on the direction tested, suggesting highly anisotropic behaviour (Table 4.6, Figure 4.7). The resulting CTE in the X and Y direction showed relatively similar CTE values. However the CTE in the Z direction was approximately an order of magnitude greater. Temperature dimensional change curves for the CF-ABS and GF-PC hybrid manufacturing materials showed good agreement between specimens, in which two distinct regions were apparent: a linear regime of steady thermal expansion followed by a sudden inflection where shrinkage occurs (Figure 4.7). This initial linear regime was used to determine the linear coefficient of expansion (CTE). The deviation in linearity at the upper end of the temperature range can be explained due to the polymer materials exceeding their glass transition temperatures (as determined in Section 4.1.2), which results in a significant change in their mechanical properties [31, 103]. As the focus of the TMA tests were to determine the linear CTE, this deviation at higher temperatures was not subject to further study.

Table 4.6: CTE Values from TMA Analysis, in which AL (* = Benchmark) data was obtained from [130].

CTE [µm/m.°C]	AL*	CF-ABS	GF-PC
X-Direction	22.9	25.87 +- 1.00	45.38 +- 1.91
Y-Direction	22.9	35.38 +- 1.37	46.23 +- 4.00
Z-Direction	22.9	123.69 +- 7.50	80.00 +- 8.47
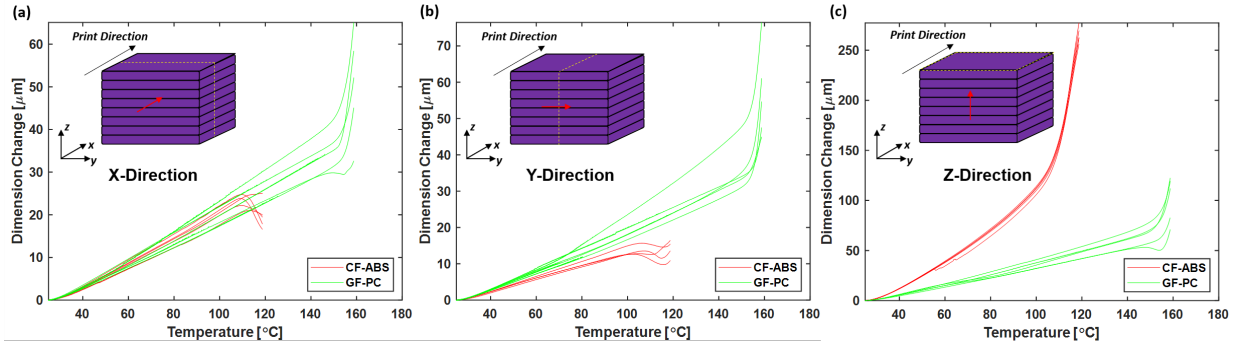
Figure 4.7: TMA curves for hybrid manufactured specimens in the (a) X-Direction, (b) Y-Direction, and (c) Z-Direction.

TMA, Anisotropy of Additively Manufactured Tooling

The anisotropy of the CTE for the hybrid manufacturing materials is a direct result of the thermoplastic material extrusion process, in which the fibre reinforcement becomes preferentially aligned in the direction of extrusion during deposition (Figure 4.8) [78, 127]. As such, the preferential alignment of the fibre phase leads to a low CTE in the x-direction as it is highly influenced by the negative CTE of fibres [78, 127]. Conversely, the CTE in the Z direction is largely dominated by the polymer matrix component that has a much higher CTE [78, 127].
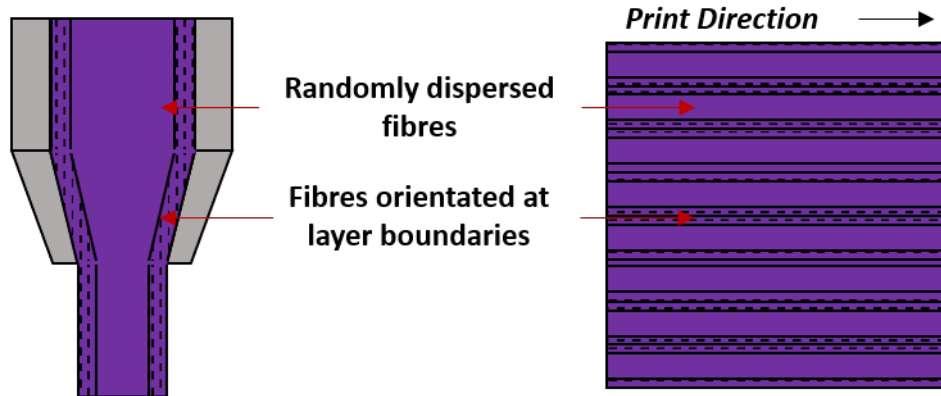
Figure 4.8: Preferential alignment of fibre reinforcement during the thermoplastic material extrusion process.

Interestingly, the CTE in the Y direction was similar to the CTE in the X direction despite no preferential alignment of fibres. This similarity can potentially be explained due to the precise location one harvest samples from the 3-D printed bed, which may impact the extent in which fibre alignment influences the CTE (Figure 4.9). Due to the nature of flow during

extrusion, the preferential alignment of fibres occurs predominantly on the exterior surface of the printed beads whereas the interior largely remains homogeneously dispersed [140–142]. As such, the region tested from the printed bead can largely influence the measured CTE value, with higher and lower values obtained from the interior or exterior respectively [140–142]. For this work, all samples were taken from an interior location, therefore it is expected that CTE values in the X-direction would potentially be lower if TMA specimens were alternatively taken from the exterior region.
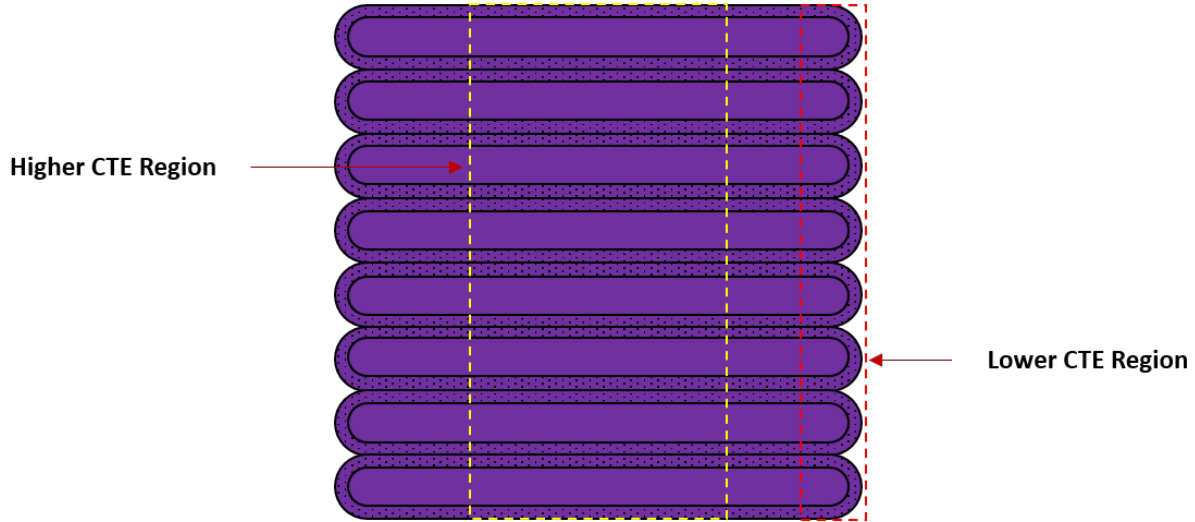
Figure 4.9: Influence of specimen harvesting location on CTE for hybrid manufactured specimens.

TMA, Summary

As seen through the TMA results, the coefficient of thermal expansion can be isotropic or anisotropic depending on the choice of material. This has significant implications for the production of composite processing tools, in which understanding the CTEs is paramount in determining its resulting effect on the composite parts produced (Section 2.1.1) [33, 41, 43]. For materials such as the aluminum reference, the homogenous structure of the material results in an isotropic CTE leading to relatively predictable tool performance [10, 11]. For hybrid manufactured tools, however, significant anisotropy exists due to the material extrusion process, which though less predictable, can be taken advantage of to produce highly complex tool geometries with variable CTE. Regardless, in the design of hybrid manufactured tools, careful consideration must be given to the deposition path to understand an account for this variable CTE.

4.2 Durability Test Plan

4.2.1 Pre-Screening Tests

Results from the pre-screening tests show that though a tool could excel in one of the afore-mentioned categories (i.e. chemical resistance, vacuum integrity, mechanical resistance), it did not necessarily imply its equal performance across all (Figure 4.10). Many of the tools, both traditional and hybrid, appeared to vary significantly in performance across the tensiometry, vacuum integrity, and hardness/micro-indentation tests, highlighting the importance of a small-scale test suite that characterizes tool durability on multiple fronts. The following subsections discuss findings relevant to each specific test before finally providing a structured framework in which to obtain a holistic interpretation of the results.
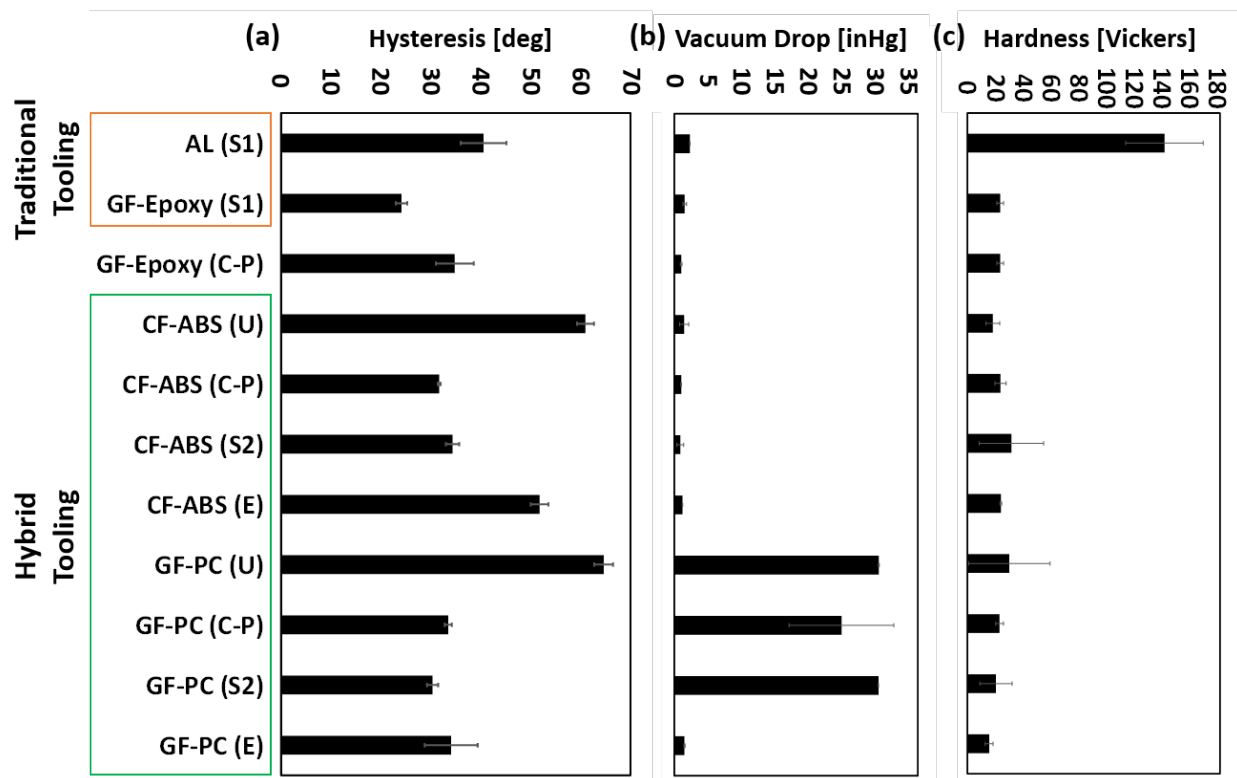
Figure 4.10: Pre-Screening Test Results. (a) Hysteresis, (b) Vacuum Integrity, (c) Hardness/Micro-Indentation.

Tensiometry

As seen in by the tensiometry results (Figure 4.10a), there was a spread of hysteresis values for tools suggesting varying degrees of chemical resistance. GF-Epoxy (S1) tools had the lowest hysteresis suggesting good nonstick properties, whereas the uncoated hybrid tools (i.e.

CF-ABS (U) and GF-PC (U)) had the highest hysteresis and potentially the poorest non-stick properties. It was interesting to note that that identical coatings did not always imply identical hysteresis values across tools, as AL (S1) and GF-Epoxy (S1) tools had a large difference in hysteresis despite having the same coating applied. Conversely, tools coated with Ceramic-Polymer or Sealant 2 also appeared to have similar hysteresis values regardless of substrate tool material, potentially suggesting substrate independence. These phenomena were not true for the remaining coatings, the hysteresis of tools coated with Epoxy varying significantly on each substrate.

Differences in performance of coated tools can potentially be explained by chemical resistance and/or physical heterogeneity of the applied coating (i.e. an uneven/defective coating). For the latter, physical heterogeneity of the applied coating can be due to surface roughness imparted by the underlying substrate [61, 86, 110] and/or repeatability of coating application, the resulting coating defects potentially leading to higher hysteresis values, and therefore lower chemical resistance [109]. This would potentially explain why the tools coated with Epoxy did not perform similarly, as closer observation of the coated surfaces show the presence of various bubbles that formed during the application of the coating which could influence the measurement of advancing and receding contact angles. Furthermore, the Ceramic-Polymer-coated tool substrates all appeared to have a distinct surface roughness as seen in the optical tensiometry imaging (Figure 4.11), which in literature has been demonstrated to affect surface adhesion properties [16]. Regarding the former, if the coatings are applied to the tool substrates uniformly and homogeneously, during tensiometry tests the water droplets interact solely with the coating and not the substrate and the tool/coating combinations performance should depend exclusively on the chemical composition of the coating and its interaction with the probe liquid [61].
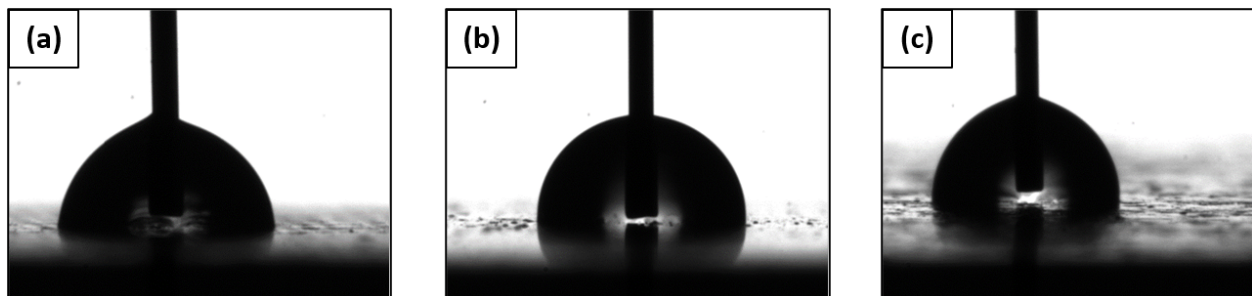
Figure 4.11: Surface roughness of Ceramic-Polymer-coated tools as seen through optical tensiometry.

Measurement of the advancing contact angle and receding contact angles on the GF-PC

specimens, irrespective of coating, proved significantly difficult as there appeared to be some degree of attraction between the droplet and the tool surface and/or repulsion between the droplet and syringe needle (Figure 4.12). Upon droplet formation on the tip of the needle, the drop appeared to be pulled towards a random position on the specimen surface (Figure 4.12a), which in the extreme would jump off the needle and adhere to the specimen (Figure 4.12b). A modified procedure was employed to prevent this issue (as documented in Appendix A.2), however, despite these modifications for many subsequent tests the droplet would have a tendency to "jump" to the side of the needle during each ARCA measurement. Furthermore, during the RCA portion of the procedure, the receding edge of the dropper on GF-PC (U) and GF-PC (S1) tools did not appear to recede uniformly like droplets on other tool/coating combinations, instead receding in a "tendril-like" fashion (Figure 4.13). This can potentially be explained by the effect tool/coating surface heterogeneity previously discussed, in which these higher energy sites have greater surface energy and therefore higher wettability [109].
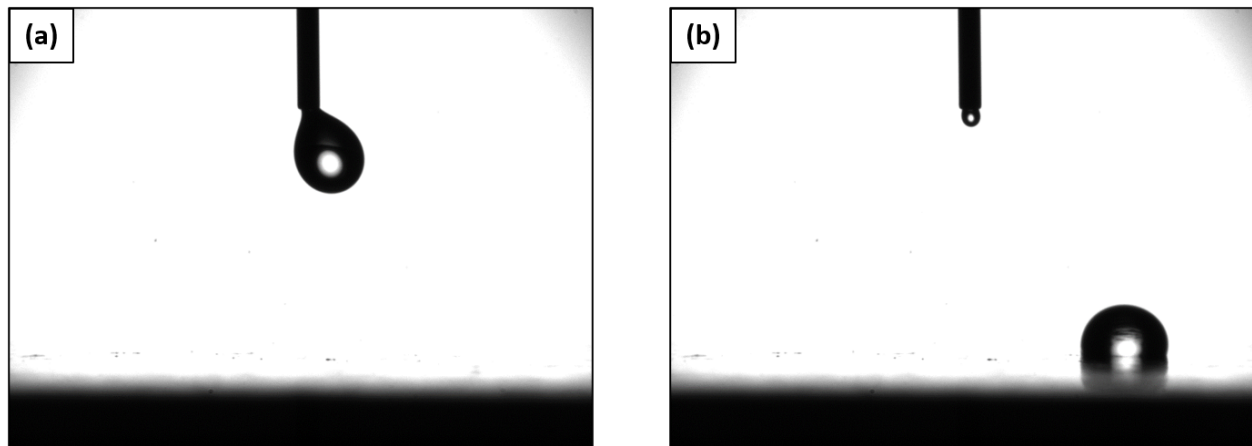
Figure 4.12: Attraction of droplet to GF-PC tool surface during droplet formation.
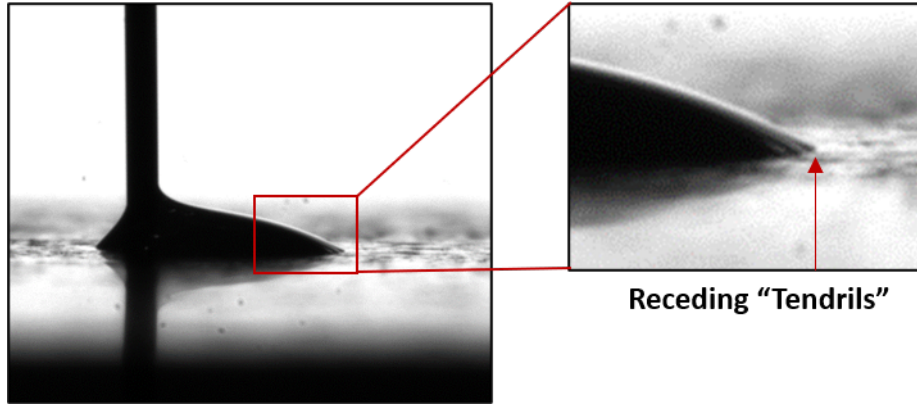
Figure 4.13: Tendril-like behaviour of droplet on GF-PC tools during the RCA phase of ARCA measurement.

Vacuum Integrity

Initial results of vacuum integrity testing showed that most GF-PC tools had significantly poor performance, in most cases the tools completely losing all vacuum pressure (i.e. venting to atmosphere) (Figure 4.10b). This can most likely be attributed to incomplete removal of the layer lines of the additively manufactured structure during tool fabrication. As seen in the fabrication process for hybrid tools (Section 3.1.2), when machining the 3D printed structure, if the surface is not milled sufficiently deep to reach the completely fused section of the layers there will be high surface roughness. This high surface roughness in turn could lead to easy access points for air ingress between the tool surface and sealant tape at the edges of the tool. For the tools coated with Ceramic-Polymer and Epoxy, the effect of surface roughness was potentially mitigated due to the inherent thickness of these coatings.

Filtering out the GF-PC outliers, the vacuum integrity results across all remaining tools showed that CF-ABS (S2) had the lowest vacuum pressure drop, whereas AL (S1) tools had the highest (Figure 4.14). Similar to the GF-PC tool results, the large standard deviation of CF-ABS (U) and CF-ABS (S2) is most likely due to incomplete layer line removal during tool fabrication (Figure 4.14). Again, AL (S1) and GF-Epoxy (S1) tools had a large difference in performancedespite having the same coating, with AL (S1) tools experiencing almost complete vacuum drop for all tested tools. This was surprising as the AL (S1) tool is currently an industry standard, demonstrating minimal vacuum pressure change over long time periods [10, 143]. Variation between the two tools could instead potentially be explained by the same conclusions drawn for their performance in tensiometry (i.e. tool/coating surface heterogeneity). If the coating uniformity is compromised by poor coating application and/or influenced by underlying tool substrate roughness, this could lead to the ingress of

air through the tool (if permeable) or between the tool and sealant tape due to high surface roughness that could create channels not sealed by the sealant tape. Regarding the latter, it is additionally probable that the adhesion between sealant tape and the tool surface was inherently poor as the bonding surface that the sealant tape was applied to was also treated with the S1 coating, which may also possess inherent nonstick properties. This could be relevant to all coated tools, and as such suggests that minor modification to the tools surface should be performed to keep the outer edges of the surface nonstick, promoting adhesion with the sealant tape.
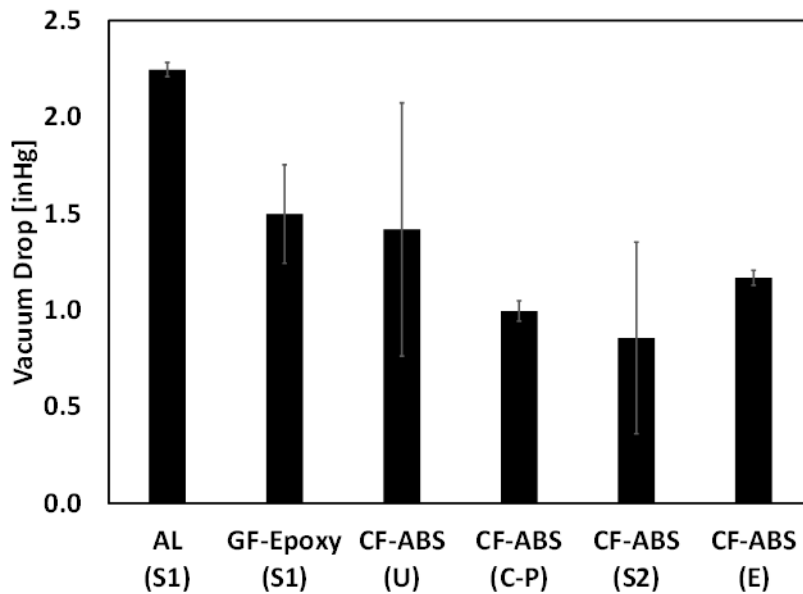
Figure 4.14: Vacuum integrity results minus GF-PC outliers.

Hardness Testing

Hardness/micro-indentation results showed that excluding the AL (S1) tools, the hardness values were relatively competitive across all remaining tool types, which suggested that the hybrid tools were comparable to the traditional GF-Epoxy tools (Figure 4.10c). The high hardness of the AL (S1) tool was expected, as it was the only tool material that was metal [144]. It was not expected that S1 or S2 coatings provided much (if any) additional hardness to the tool substrates, as their primary function was to seal micro-porosity of the tool surface. However, it was interesting to note that CF-ABS and GF-PC tools coated with Ceramic-Polymer exhibited similar tool hardness regardless of base tool material[1].

---

[1]GF-Epoxy (C-P) tools were not included in this comparison due to issues with hardness measurement. See following paragraphs for explanation.

The CF-ABS (S2) tool had the highest hardness of the hybrid manufactured tools. However their validity is questionable as the results had high standard deviation. High standard deviation of CF-ABS (S2) hardness values were thought to be a result of the location of indentation points for the given indenter type. When performing an indent on the hybrid manufactured tools, it is possible to indent on pure matrix, pure fibre, or a combination of both components (Figure 4.15). In the first two cases, the hardness would vary significantly due to the intrinsic hardness values of each material (i.e. matrix vs. fibre), ultimately leading to significant deviation for the final reported mean. This could potentially be mitigated in future work by utilizing an indenter type of sufficient size to ensure that each indentation point captures a similar distribution of fibres and matrix [145].
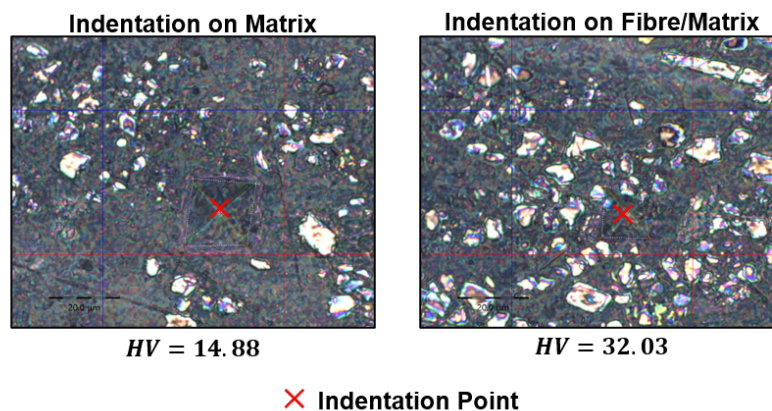
Figure 4.15: Variation of hardness due to indent location. Scale bar = 200 µm.

GF-Epoxy (C-P) tools were unable to be characterized by Vickers hardness testing as the indentations into the sample did not yield good quality points to analyze in post-processing. This is most likely due to inherent heterogeneity of the surface which led to poor indent geometries (Figure 4.16). As such, for subsequent analysis in the overall pre-screening test method, the hardness values obtained for GF-Epoxy (S1) were used as they represented a "worst-case scenario" for the GF-Epoxy (C-P) tool[2]. In other words, if the Ceramic-Polymer coating was to be completely stripped from the GF-Epoxy tool, it would most likely have similar hardness values to that of the GF-Epoxy tool coated with Sealant 1 given that Sealant 1 does not appear to significantly affect hardness.

---

[2]One could alternatively use the hardness value obtained for CF-ABS or GF-PC coated with Ceramic-Polymer, as it appears that the hardness of tools coated with Ceramic-Polymer was independent of tool material.
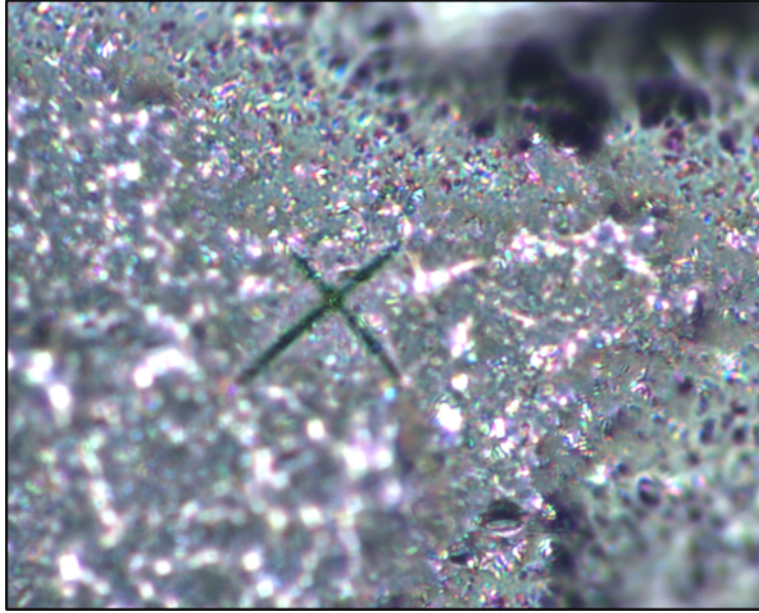
Figure 4.16: High heterogeneity of GF-Epoxy (C-P) tools. Scale bar = 200 µm.

Analysis of Pre-Screening Test Results

The analysis of the pre-screening tests is presented in Table 4.7. Looking at the rank columns, it is apparent that the top-performing tool varied between each test. However, it did appear that some tools such as CF-ABS (C-P) and carbon CF-ABS (S2) did consistently rank higher than others. Using an equal weight for all tests (i.e. an application where all three properties characterized but each test are equally important), the performance index was calculated for each tool. From these performance indices, it can be seen that CF-ABS tools were ranked in the top two positions followed by a three-way tie by AL (S1), GF-Epoxy (S1), and CF-ABS (E) for third place.

Table 4.7: Analysis of the pre-screening test results.

Tool	Tensiometry Rank	Vacuum Integrity Rank	Hardness Rank	Performance
AL (S1)	4	4	11	19
GF-Epoxy (S2)	11	5	6	22
GF-Epoxy (C-P)	5	10	6	21
CF-ABS (U)	2	7	3	12
CF-ABS (C-P)	9	9	7	25
CF-ABS (S2)	6	11	10	27
CF-ABS (E)	3	8	8	19
GF-PC (U)	1	1	9	11
GF-PC (C-P)	8	3	5	16
GF-PC (S2)	10	2	4	16
GF-PC (E)	7	6	2	15

A closer look at the performance indices shows that for some tools, despite having a high ranking, they did not perform significantly well in all tests. AL (S1) did not perform well in tensiometry or vacuum integrity . However it performed the best in hardness testing which significantly boosted its performance index. Similarly, GF-Epoxy (S1) did not perform well in vacuum integrity or hardness testing, but as the top-performing tool in tensiometry testing it likewise had an inflated performance index.

CF-ABS (S2) and CF-ABS (C-P) were the only tool that consistently ranked high for all three tests. These inflated performance indices are due to the fact that, for the given decision criteria, if a tool performs exceptionally well in at least one of the tests, it will have a high performance index even if it performs poorly in the others. As such, and improved decision criteria is needed to better assess tool results that considers the consistency in which the tool performs across all tests.

4.2.2 Small-Scale Composite Process Testing

Combined results profilometry, WLVB, and demould tests revealed that success and, furthermore, the exact ranking of a tool/coating combination in the pre-screening tests did not guarantee its successful performance in small-scale composite processing highlighting the importance of validating these small-scale metrics in a practical application (Figure 4.17). Despite being ranked the top-performing tools in the pre-screening tests, the hybrid manufactured tools, regardless of coating, were the first to fail during small-scale composite processing, with all being eliminated by the third composite process cycle. Conversely, both AL

(S1) and GF-Epoxy (S1) tools showed no appreciable signs of failure, with composite parts remaining easy to demould for all tests. GF-Epoxy (C-P) tools showed the most peculiar performance, maintaining minimal wear despite composite parts being difficult to demould after all cycles. Key findings of each individual test type (i.e. laser profilometry, WLVB, demould testing) are presented in the following sections, with a final section discussing their combined results.
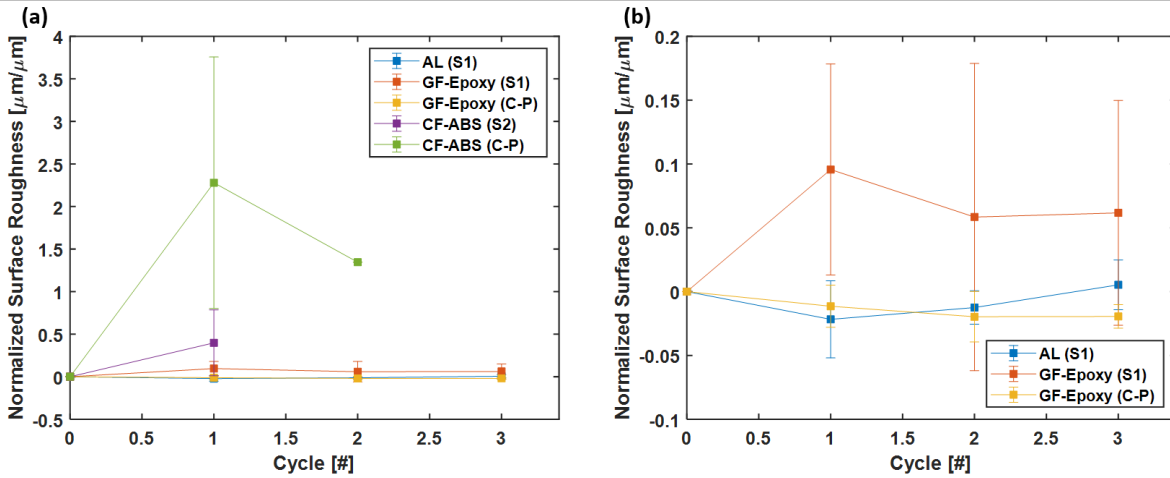
Figure 4.17: Combined small-scale processing results for (a) including and (b) excluding hybrid tool types.

Laser Profilometry

Profilometry of all tools prior to any infusion (i.e. in their "as-fabricated" state) showed that, despite 500 grit (0.18 μm) polishing, all had surface roughness values that varied greatly from the target B1/B3 mould surface finish (Figure 4.18). Not only this, the variation of surface roughness between each tool-coating combination was significant, with varying degrees of surface homogeneity. GF-Epoxy (C-P) had a very unexpected surface topography ("egg carton" shape). As the final coating and polishing of all tools was performed by the industrial partner, the exact cause for surface roughness variation is unknown. However it is most likely due to the combined effects of material, manufacturing method, and/or technician skill when polishing and/or coating the tools [86, 113–115, 146]. For the GF-Epoxy (C-P) tools specifically, one potential explanation could be that the work surface used to prepare the tools may have imparted the specific surface roughness seen [86].

AL (S1)	GF-Epoxy (S1)	GF-Epoxy (S1)	CF-ABS (S2)	CF-ABS (C-P)
0.808 μm	**0.730 μm**	**5.762 μm**	**0.538 μm**	**0.804 μm**
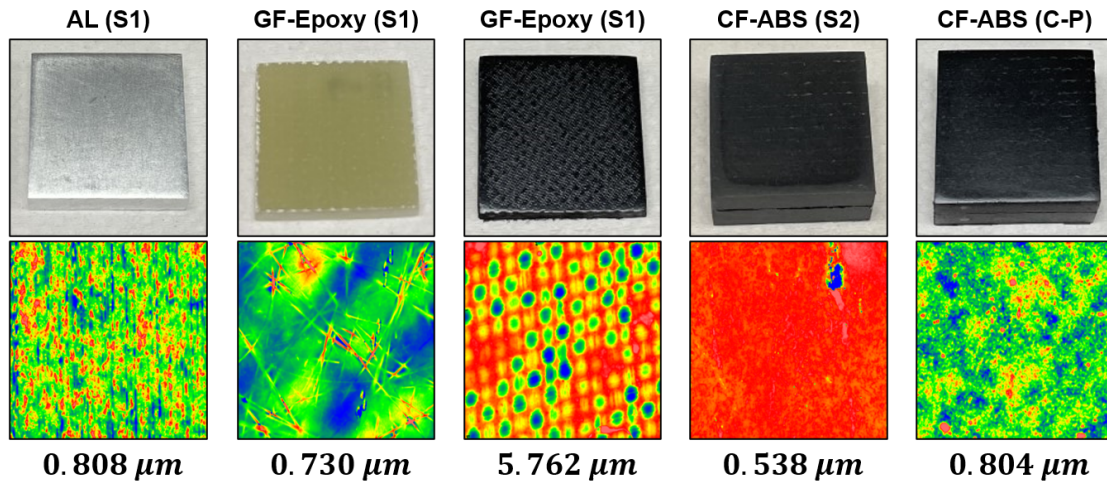
Figure 4.18: Surface roughness of "as-fabricated" tools.

Looking at the surface profiles of all tools with each subsequent infusion, it can be seen that whereas some tools maintained a generally consistent topography, others experienced significant change due to the composite process (Figure 4.19 – Figure 4.21). AL (S1), GF-Epoxy (S1), and GF-Epoxy (C-P) looked the same after all cycles (Figure 4.19), whereas the CF-ABS (S2) and CF-ABS (C-P) tools were significantly affected due to the composite process (Figure 4.19). CF-ABS (S2) tools clearly showed signs of fibre imprinting after each infusion, with indents that appeared to be transferred from the individual tows of the composite part fabric (Figure 4.20). This ultimately shows the importance of sufficient tool surface hardness to resist indentation and maintain an "as-fabricated" surface finish. CF-ABS (C-P) showed clear signs of the C-P coating being stripped away from the tool after being demoulded, which would suggest that the bond between the tool and coating was relatively poor compared to the bond between the coating and the composite part. (Figure 4.21). This could be clearly seen visually, however, due to the size of the laser profilometry scan, it was possible to miss these signs of tool wear. As such, future work should potentially use a larger scan area to capture the wear of the entire surface after each infusion.
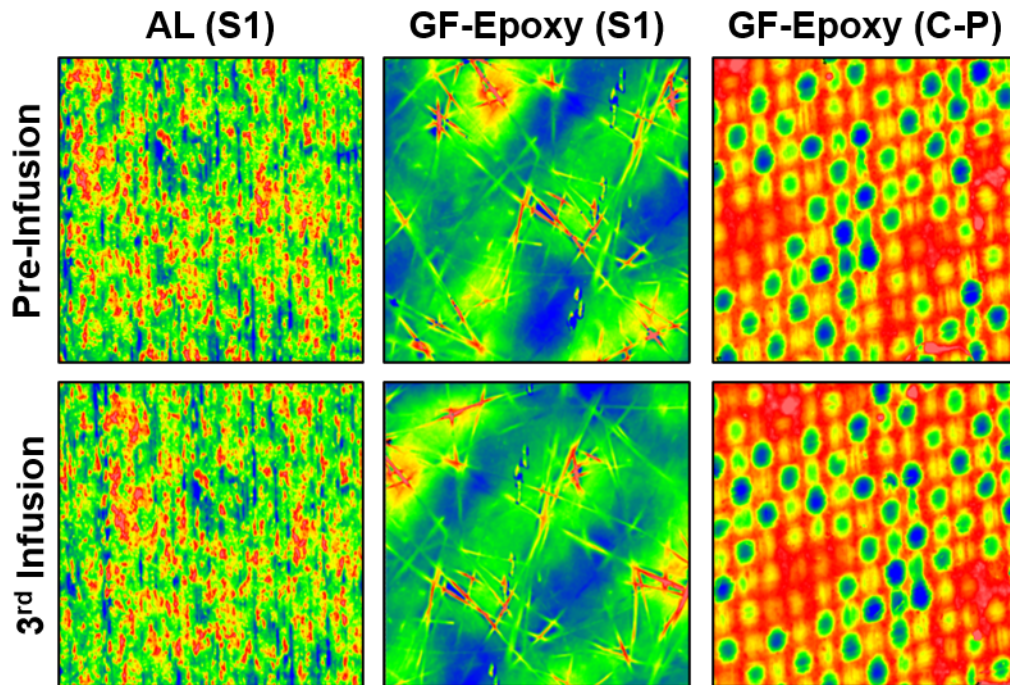
Figure 4.19: Laser profilometry scans of AL, GF-Epoxy (S1), and GF-Epoxy (C-P) tools at start and end of small-scale composite process testing.
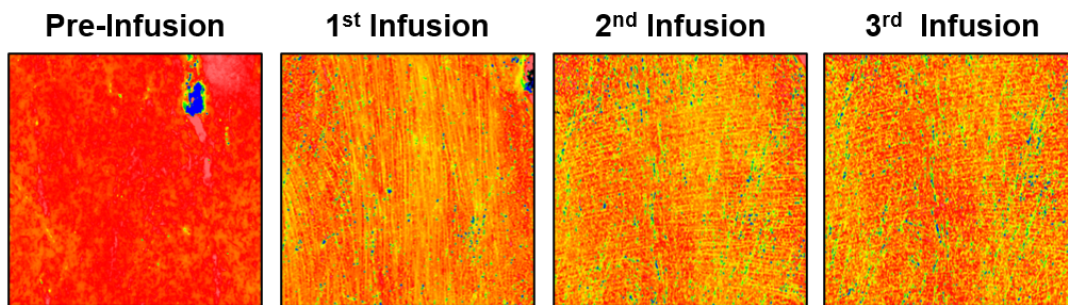
Figure 4.20: Laser profilometry scans of CF-ABS (S2) after infusion showing increasing wear due to fibre imprinting.
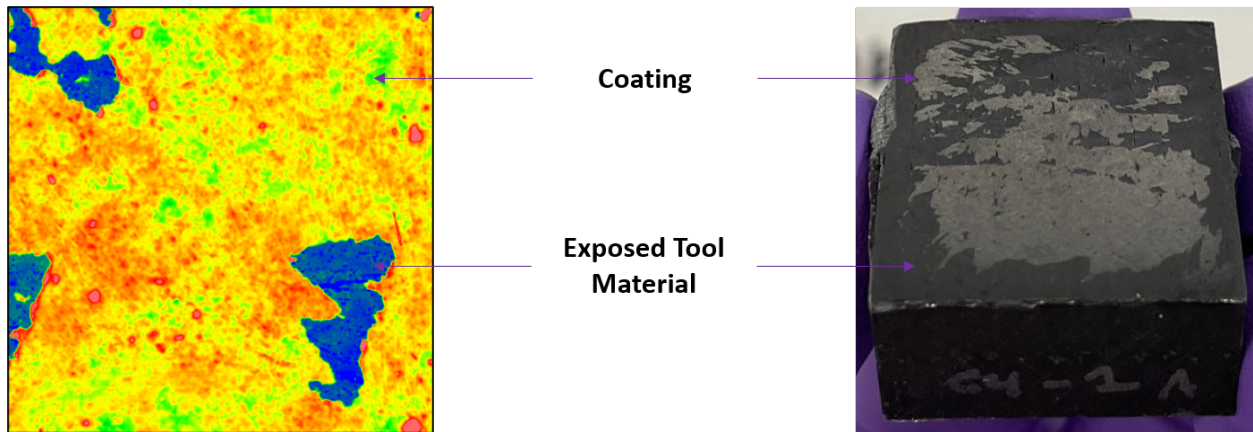
Figure 4.21: Optical image and laser profilometry scan of CF-ABS (C-P) after infusion, highlighting the ability to miss signs of tool wear.

Pseudo Wet-Layup Vacuum Bag Process

The pseudo-WLVB process was fairly repeatable, with composite parts of similar quality being produced with each cycle. However, issues arose due to a combination of the method in which pressure was applied as well as tool "edge effects". During the application of the stone slabs on top of the entire assembly, if they were not placed carefully, the composite parts would "slide" off the tools due to the "free-floating" effect between the tool surface and the composite part resin during initial assembly (Figure 4.22). Furthermore, this same effect led to minor shifting of the plies during compaction which resulted in part dimensions greater than 25.4 mm x 25.4 mm. This "free-floating" effect was mitigated through slight pre-compaction of the plies prior to the application of the weight, ensuring initial consolidation of the plies and removal of any excess resin between the composite part and the tool. However, this additional resin bleed during part compaction was undesirable as after cure, the additional resin along the sides of the tool could potentially lead to additional resistance during demoulding. Though this could potentially be mitigated through decreased resin use, however this runs the risk of under-wetting the dry plies which could, furthermore, potentially decrease wetting of the tool surface [147] which was critical in this work to characterize tool durability. Therefore, in future work this will be addressed through redesign of the tools such that dams/barriers can be incorporated along the perimeter (Appendix A.1).

Figure 4.22: "Free-floating" edge effect during ply compaction leading to misaligned plies.

Demould Testing

Results of demould testing indicate that the durability of hybrid manufactured tools tested was limited by the inherent strength of the tool material (Table 4.8). AL (S1) and GF-Epoxy (S1) tools were relatively easy to demould after all cycles performed, showing no signs of increased resistance to demoulding except for after the 3rd infusion, in which the perceived difficulty had increased for the latter. GF-Epoxy (C-P) tools were difficult to demould for all tests. However there appeared to be no appreciable signs of failure until after the 3rd infusion, after which 1 of 3 tools experienced composite part failure (Figure 4.23a). Tools that experienced PF appeared to be significantly influenced by the edge effect discussed previously, demonstrating the importance of eliminating this in future work through improved specimen design. For almost all hybrid manufactured tools the primary failure mode appeared to be tool failure (Figure 4.23bc), which suggested it was the limiting factor in tool durability. This was potentially exacerbated by the "edge effects" previously discussed. Taking a closer look at this failure mode, all hybrid tools appeared to experience tool failure due to interlayer bond failure in the X/Y direction (i.e. between printed beads). This highlights the importance of optimizing print settings to ensure a robust, repeatable, 3D print with strong interlayer bonding in both the X, Y, and Z directions [89].

Table 4.8: Results of demould testing. E: Easy to demold. M: MEdium effort to demold. H: Hard to demold. TF: Tool failure. PF: Part failure. Further details regarding each identifier can be found in Table 3.7.

Tool Type		Infusion 1	Infusion 2	Infusion 3
AL (S1)	AL-7	E	E	E
	AL-8	E	E	E
	AL-9	E	E	E
GF-Epoxy (S1)	E-9	E	E	M
	E-14	E	E	M
	E-XTRA	E	E	M
GF-Epoxy (C-P)	ECK-7	M	H	M
	ECK-8	H	M	M
	ECK-9	M	M	PF
CF-ABS (C-P)	C4-1A	E	TF	-
	C5-2A	M	TF	-
	C6-2B	TF	-	-
CF-ABS (S2)	C1-3B	E	E	PF
	C3-3A	E	TF	-
	C6-3B	E	TF	-
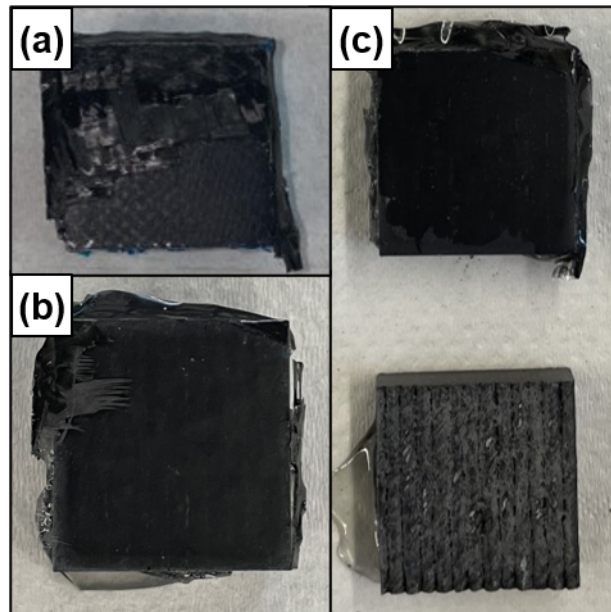
Figure 4.23: (a) GF-Epoxy (C-P) composite part failure after 3rd infusion. Tool failure of (b) CF-ABS (S2) and (c) CF-ABS (C-P).

Analysis of Small-Scale Composite Processing Tests

The relative performance of each tool can be viewed through the changes in surface roughness, where it is seen that higher surface roughness did not always imply poor performance with respect to durability (Figure 4.17). Given the fact that all tool types had different "as-fabricated" surface roughness, to better make a comparison all Sa data was normalized according to the following equation:

$$S_a(Normalized) = \frac{S_a(i)}{S_a(initial)} - 1 \ , \ i = cycle \tag{4.1}$$

$S_a(Normalized)$: Normalized surface roughness [unitless]
$S_a(i)$: Surface roughness for cycle i [μm]
$S_a(initial)$: Initial surface roughness [μm]

This allowed all tools to start at the same initial value (i.e. 0 at 0 cycles), with subsequent values representing the change in surface roughness of the given tool relative to its initial "as-fabricated" surface roughness. Both hybrid tools experienced the first significant change in surface roughness, where the predominant reason for this change appeared to be coating removal. CF-ABS (S2) however had the additional impact of fibre imprinting, which is expected to be due to the inherent mechanical properties of Sealant 2 not offering any significant hardness to the overall tool. Conversely, the Ceramic-Polymer coating demonstrated comparatively higher hardness. It is expected that the former issue (i.e. composite part-coating adhesion) could be improved through two distinct pathways: improved coating adhesion to the tool and/or reduced composite part-coating adhesion by using a mould release agent [24, 61]. Both would prolong the life of the coatings used. However the latter issue of fibre imprinting must be addressed by the inherent mechanical properties of the base tool substrate and/or coating [16, 17]. As a result of the wear incurred by these tools (and the corresponding increase in Sa), both tool types most likely provided poor surfaces for subsequent cycles, leading to increased tool/coating bonding to the composite part and their subsequent early failure.

The remaining tools (i.e. AL (S1), GF-Epoxy (S1), and GF-Epoxy (C-P)) showed minimal change in surface roughness, with only one of the GF-Epoxy (C-P) tools experiencing composite part failure. This failure was most likely due to the edge effects previously described, as visual observation of the available tool surface revealed no distinct difference to the tools that had passed, which was confirmed through laser profilometry. It was interesting to note that even though GF-Epoxy (C-P) tools had the highest initial surface roughness

of all fabricated tools, and was difficult to demould after every infusion, it still maintained its initial surface roughness and showed no appreciable signs of coating degradation. This could potentially be explained by the egg carton topography of the tool surface contributing to decreased adhesion [86, 146], the effort required to demould composite parts largely dominated by the aforementioned edge effects. The performance of AL (S1) and GF-Epoxy (S1) tools from their initial "as-fabricated" state is potentially the result of the coating Sealant 1, as despite being vastly different materials, both showed no signs of wear, and remained easy to demould. This would potentially confirm the manufacturer's advertisement of a high-modulus, durable coating with high adhesion to the base tool substrate, which would indirectly resist adhesion with the composite part during processing (i.e. the tool-coating bond is stronger than the coating-composite part bond) [17].

4.3 Predicting Hybrid Tool Durability: A Summary

For the production of tooling used in composite processing, it is clear that many different properties must be considered and characterized to fully understand and predict its performance and durability. Furthermore, the use of hybrid manufacturing adds an additional dimension in that special attention must be given to the thermal properties of the thermoplastic (or composite thermoplastic) material used during the additive manufacturing stage. As the process is thermoplastic extrusion, performing some type of thermomechanical characterization is essential in understanding the tool material. With an increasing list of properties to characterize for hybrid-manufactured tools, it becomes increasingly apparent that large-scale test methods are infeasible; material and labour costs rising to unsustainable levels.

The work performed in this thesis ultimately gives insight into a small-scale approach to characterize the production and use of large-scale hybrid-manufactured tools by characterizing their properties and performance on 2 key fronts: thermal properties and durability. For the latter of these two, durability was further subdivided into quick, inexpensive pre-screening tests that preluded more labour-intensive small-scale composite processing. It was interesting to note that though the former gave important information on tool durability in its "as-fabricated" state, this did not necessarily give insight into its durability over time with repeated tool use, highlighting the necessity to perform subsequent small-scale composite process testing. The results of the durability test plan can then be further incorporated with thermomechanical characterization results, which serve as additional screening criteria defined by the required thermal properties of the tool application.

The combination of these results ultimately leads to a small-scale quantitative, rigorous framework in which to compare a large quantity of tool-coating combinations, the optimal tool for the required application quickly ascertained by applying weighted decisions for each criterion (ex. Tg, Vacuum Integrity, Chemical Resistance, Hardness) to create a key performance index. The collected results, furthermore, serve as a database that can be referred to when developing novel tool-coating combinations to predict their feasibility at the large-scale.

Chapter 5

Conclusions

With hybrid manufacturing, it is clear that there is an inherent need for low-cost predictive methods to determine the performance of both the additive and subtractive processes and properties of the final tool. Otherwise, due to the plethora of settings for each respective process, significant time is spent iterating to determine the most optimal combination of settings through both. As such, the proposed quantitative, small-scale test method gave a structured approach to determining key process parameters and resultant tool properties through thermal characterization and durability tests that began with a series of pre-screening tests and culminated in a small-scale composite process. The major conclusions for each method were as follows:

Thermal characterization gave fundamental information on the thermal properties of the tool material that ultimately governed its performance both in processing during the additive manufacturing process and final intended tool application. Thermogravimetric analysis gave the maximum processing temperature for the material before its degradation onset, but furthermore showed that this value could change depending on the atmosphere used. On the other side of the processing spectrum, differential scanning calorimetry characterized the glass transition temperatures of the thermoplastic materials used for hybrid tooling, which not only gave insight into the maximum service temperature for the tool but allowed for the development of an extrusion temperature processing window when used in conjunction with TGA results. Lastly, thermomechanical analysis was crucial in characterizing the linear coefficients of thermal expansion of the hybrid tools, which was seen to be significantly influenced by the additive process.

Pre-screening tests gave important information regarding hybrid tool performance in its "as-fabricated" state, in which the three avenues of testing characterized unique elements of chemical resistance, vacuum integrity, and mechanical resistance. Tensiometry was employed to characterize chemical resistance, in which it was shown that contact angle hysteresis could potentially capture the "non-stick" properties of the tool surface which could potential be correlated to the ease of demoulding composite parts during composite processing. Vacuum integrity was assessed through a 5-minute "drop-test" using a custom vacuum fixture, in which it was shown that the ability of a tool to hold vacuum was largely influenced by stringent adherence to directions outlined in the manufacturing protocol. Micro-indentation/hardness testing gave important information on tool ability to resist fiber imprinting and/or accidental scratches. The final analysis of pre-screening test results offered a structured approach to selecting the best performing tool from an initially large group of potential tool/coating combinations.

Small-scale composite processing tests were crucial in characterizing tool degradation over time with each part produced, but furthermore proved invaluable in validating the results of the pre-screening tests. Laser profilometry accurately captured degradation of tool surface with repeated use through changes in surface roughness. The wet-layup vacuum bag process successfully exposed the tool surface to physical/chemical wear present in actual composite process. Demolud testing after each composite part fabrication was straightforward due to the relatively simple 2-stage assessment criteria and showed that hybrid tool performance was predominately dictated by the mechanical strength of the inter-bead bonding.

Chapter 6

Future Work

Though the initial results of this work gave important information regarding tool-coating performance at the small-scale, a few aspects of each test method need to be further improved to validate their use in predicting large-scale performance:

Thermal characterization allowed for the determination of processing and performance limits were ascertained for the hybrid tool materials, however additional thermal characterization techniques could be employed to not only better understand individual properties of the hybrid tool materials but furthermore narrow the extrusion temperature processing window. The processing temperature window determined for each hybrid manufacturing material was relatively large for each material tested, which could potentially be addressed by the use of thermo-rheological characterization to impose greater restrictions on the allowable temperature range.

Pre-screening tests gave important information regarding manufactured tool performance on three key fronts of chemical resistance, vacuum integrity, and mechanical resistance through tensiometry, vacuum "drop" test, and micro-indentation/hardness respectively, however improvements could be made in both specimen design, fabrication, and/or experimental setup. In tensiometry, it is important to ensure that the surface/coating of the tool is homogeneous to maximize the "non-stick" property of the tools. Vacuum integrity results showed poor performance of traditional tools that have already been demonstrated in industry, therefore modification of the tool surface and/or experimental setup is potentially needed to ensure that any vacuum pressure drop is exclusively due to tool permeability. Micro-indentation/Hardness testing results indicated that size and type of indenter could potentially lead to significant variation in hardness value, potentially masking the true hardness of the tool/coating. As such, future work should select an indenter of sufficient size to capture a more homogeneous

picture of tool hardness. In the analysis of pre-screening test results, the ranking criteria used to develop the key performance index should potentially be revisited and redeveloped to better consider the performance of each tool across all pre-screening tests.

Small-scale composite processing tests gave critical information on tool durability over time with repeated use, however the results of the current procedure employed shows clear avenues of improvement to yield more impactful results. Laser profilometry results revealed the potential for small scan areas to not capture full extent of tool wear was identified, which could be addressed in future work through an increased scan area per tool, or potentially the adoption of an alternate technology that is able to scan the entire tool surface. In the pseudo-WLVB process, the method of introducing vacuum pressure was cumbersome and tools tested had simple topography (i.e. flat plates). Given that this was largely due to the small tool size used (25.4 mm x 25.4 mm), a larger tool geometry could be used in future testing such that an actual vacuum source could be employed. Characterization through demould testing was entirely qualitative where quantitative methods would be more preferable. In future work, incorporation of a quantitative technique to characterize the demould force would greatly compliment the small-scale test method.

Improvement in the aforementioned areas would further improve the accuracy and validity of the quantitative, small-scale test suite, solidifying its utility in the characterization of the hybrid-manufacturing process and hybrid-manufactured tools. Furthermore, future work in this area can add to the test suite by incorporating additional characterization tools from the plethora that already exist, using them to address and quantitatively predict other fundamental properties of large-scale tooling at the small-scale.

References

[1] A. C. M. Association. "Benefits of composites." (2022), [Online]. Available: `composiuteslab.com/benefits-of-composites/`.

[2] J. Group. "Benefits of composites." (2022), [Online]. Available: `compositeslab.com/benefits-of-composites/`.

[3] C. Australia. "Benefits of composites." (2021), [Online]. Available: `compositesaustralia.com.au/about-composites/benefits-of-composites/`.

[4] F. Campbell, *Manufacturing Processes for Advanced Composites*. Amsterdam: Elsevier Science, 2003, ISBN: 978-1-85617-415-2. DOI: `doi.org/10.1016/B978-1-85617-415-2.X5000-X`. [Online]. Available: `sciencedirect.com/book/9781856174152/manufacturing-processes-for-advanced-composites#book-info`.

[5] H. Propeller. "How a composite propeller blade is made." (2016), [Online]. Available: `hartzellprop.com/propeller-how-a-composite-propeller-blade-is-made/`.

[6] N. Shultz. "How to protect carbon fiber vehicle parts." (2019), [Online]. Available: `https://www.drivingline.com/articles/how-to-protect-carbon-fiber-vehicle-parts/`.

[7] I. U. of Stuttgart. "Buga fibre pavilion 2019." (2019), [Online]. Available: `https://www.icd.uni-stuttgart.de/projects/buga-fiber-pavilion/`.

[8] E. S. Agency. "Rocket tanks of carbon-fiber-reinforced plastic are proven possible." (2021), [Online]. Available: `phys.org/news/2021-07-rocket-tanks-carbon-fiberreinforced-plastic-proven.html`.

[9] Gurit. "Composites for luxury yachts." (2022), [Online]. Available: `gurit.com/en/our-business/industries--markets/marine/luxury-yachts`.

[10]   Y. Li, Y. Xiao, L. Yu, K. Ji, and D. Li, "A review on the tooling technologies for composites manufacturing of aerospace structures: Materials, structures and processes," *Composites Part A: Applied Science and Manufacturing*, vol. 154, p. 106 762, 2022, ISSN: 1359-835X. DOI: doi.org/10.1016/j.compositesa.2021.106762. [Online]. Available: sciencedirect.com/science/article/pii/S1359835X21004747.

[11]   J. Cadden and P. Sadesky, "Tooling for composites," in *Handbook of Composites*. 1988.

[12]   Solvay. "A unique approach to composite tooling." (2018), [Online]. Available: compositesone.com/wp-content/uploads/Composite-Tooling-Brochure.pdf.

[13]   CompositesWorld. "Materials & processes: Tooling for composites." (2016), [Online]. Available: compositesworld.com/articles/tooling.

[14]   N. Denardo, E. Barocio, B. Brenken, A. Favaloro, and R. B. Pipes, "Economics of composite tooling made via additive manufacturing," *SAMPE Journal*, vol. 52, no. 6, pp. 55–60, 2016, ISSN: 00911062.

[15]   PCMInnovation. "Molds for composites made of metal or composites." (2022), [Online]. Available: pcminnovation.com/en/molds-aerospace-composites/.

[16]   G. Kim *et al.*, "Enhancing surface characteristics of additively manufactured fiber reinforced thermoplastic mold using thermoset coating with ceramic particles," *Surface and Coatings Technology*, vol. 422, p. 127 536, 2021, ISSN: 0257-8972. DOI: doi.org/10.1016/j.surfcoat.2021.127536. [Online]. Available: sciencedirect.com/science/article/pii/S0257897221007106.

[17]   N. Northrup, "Durability of hybrid large area additive tooling for vacuum infusion of composites," MSc Thesis, Brigham Young University, 2019.

[18]   J. Weaver and J. Jones, "Characterization of high-deposition polymer extrusion in hybrid manufacturing," in *Solid Freeform Fabrication*, 2018, pp. 287–290.

[19]   C. Ajinjeru *et al.*, "The influence of dynamic rheological properties on carbon fiber-reinforced polyetherimide for large-scale extrusion-based additive manufacturing," *International Journal of Advanced Manufacturing Technology*, vol. 99, no. 1-4, pp. 411–418, 2018, ISSN: 14333015. DOI: 10.1007/s00170-018-2510-z.

[20]   C. Ajinjeru *et al.*, "The influence of rheology on melt processing conditions of carbon fiber reinforced polyetherimide for big area additive manufacturing," *International SAMPE Technical Conference*, no. September 2018, pp. 1823–1829, 2017.

[21] C. Ajinjeru *et al.*, "Determination of melt processing conditions for high performance amorphous thermoplastics for large format additive manufacturing," *Additive Manufacturing*, vol. 21, no. December 2017, pp. 125–132, 2018, ISSN: 22148604. DOI: `10.1016/j.addma.2018.03.004`. [Online]. Available: `doi.org/10.1016/j.addma.2018.03.004`.

[22] V. Kishore *et al.*, "Predicting sharkskin instability in extrusion additive manufacturing of reinforced thermoplastics," in *Solid Freeform Fabrication*, 2017, pp. 1696–1704.

[23] C. Ajinjeru *et al.*, "The influence of rheology on melt processing conditions of amorphous thermoplastics for big area additive manufacturing (BAAM)," in *Solid Freeform Fabrication Symposium*, 2016, pp. 754–761.

[24] T. Z. Sudbury, R. Springfield, V. Kunc, and C. Duty, "An assessment of additive manufactured molds for hand-laid fiber reinforced composites," *International Journal of Advanced Manufacturing Technology*, vol. 90, no. 5-8, pp. 1659–1664, 2017, ISSN: 14333015. DOI: `10.1007/s00170-016-9464-9`.

[25] D. Moreno Nieto and S. I. Molina, "Large-format fused deposition additive manufacturing: a review," *Rapid Prototyping Journal*, vol. 26, no. 5, pp. 793–799, 2019, ISSN: 13552546. DOI: `10.1108/RPJ-05-2018-0126`.

[26] V. Kunc *et al.*, "Investigation of In-Autoclave Additive Manufacturing Composite Tooling," in *CAMX - Composites and Advanced Materials Expo*, Anaheim, 2016.

[27] B. G. Compton, B. K. Post, C. E. Duty, L. Love, and V. Kunc, "Thermal analysis of additive manufacturing of large-scale thermoplastic polymer composites," *Additive Manufacturing*, vol. 17, pp. 77–86, 2017, ISSN: 22148604. DOI: `10.1016/j.addma.2017.07.006`. [Online]. Available: `doi.org/10.1016/j.addma.2017.07.006`.

[28] D. Marrett. "Thermwood blog." (2022), [Online]. Available: `blog.thermwood.com/`.

[29] W. Systems. "Vacuum bagging techniques." (2010), [Online]. Available: `westsystem.com/wp-content/uploads/VacuumBag-7th-Ed.pdf`.

[30] P. A. Corp. "What is a composite layup tool and what are their benefits for aerospace." (2021), [Online]. Available: `pacificaerospacecorp.com/what-is-composite-layup-tool-and-what-are-their-benefits-for-aerospace`.

[31] K. M. M. Billah, F. A. Lorenzana, N. L. Martinez, R. B. Wicker, and D. Espalin, "Thermomechanical characterization of short carbon fiber and short glass fiber-reinforced ABS used in large format additive manufacturing," *Additive Manufacturing*, vol. 35, no. August, p. 101 299, 2020, ISSN: 22148604. DOI: `10.1016/j.addma.2020.101299`. [Online]. Available: `doi.org/10.1016/j.addma.2020.101299`.

[32] F. A. R. Lorenzana, "Thermal characterization of abs/carbon fiber, abs/glass fiber and petg/glass fiber reinforced composites used in large area additive manufacturing," MSc Thesis, University of Texas at El Paso, 2019.

[33] G. Twigg, A. Poursartip, and G. Fernlund, "Tool–part interaction in composites processing. part i: Experimental investigation and analytical model," *Composites Part A: Applied Science and Manufacturing*, vol. 35, no. 1, pp. 121–133, 2004, ISSN: 1359-835X. DOI: `doi.org/10.1016/S1359-835X(03)00131-3`. [Online]. Available: `sciencedirect.com/science/article/pii/S1359835X03001313`.

[34] M. Szarski and S. Chauhan, "Composite temperature profile and tooling optimization via deep reinforcement learning," *Composites Part A: Applied Science and Manufacturing*, vol. 142, p. 106 235, 2021, ISSN: 1359-835X. DOI: `doi.org/10.1016/j.compositesa.2020.106235`. [Online]. Available: `sciencedirect.com/science/article/pii/S1359835X20304681`.

[35] M. Li, "Temperature and moisture effects on composite materials for wind turbine blades," MSc Thesis, Montana State University-Bozeman, 2000.

[36] V. P. Nikolaev, E. V. Myshenkova, V. S. Pichugin, E. N. Sinitsyn, and A. N. Khoroshev, "Temperature effect on the mechanical properties of composite materials," *Inorganic Materials*, vol. 50, no. 15, pp. 1511–1513, 2014, ISSN: 16083172. DOI: `10.1134/S002016851415014X`.

[37] P. C. Painter, "Essentials of polymer science and engineering / paul c. painter, michael m. coleman.," in *Essentials of polymer science and engineering*. Lancaster, PA: DEStech Publications, Inc., 2008 - 2009, ISBN: 9781932078756.

[38] R. Geissberger, J. Maldonado, N. Bahamonde, A. Keller, C. Dransfeld, and K. Masania, "Rheological modelling of thermoset composite processing," *Composites Part B: Engineering*, vol. 124, pp. 182–189, 2017, ISSN: 1359-8368. DOI: `doi.org/10.1016/j.compositesb.2017.05.040`. [Online]. Available: `sciencedirect.com/science/article/pii/S1359836817302962`.

[39] F. Campbell, "Thermoplastic Composite Fabrication Processes," in *Structural Composite Materials*, ASM International, Nov. 2010, ISBN: 978-1-62708-314-0. DOI: `10.31399/asm.tb.scm.t52870183`. [Online]. Available: `doi.org/10.31399/asm.tb.scm.t52870183`.

[40] R. Akkerman, M. Bouwman, and S. Wijskamp, "Analysis of the thermoplastic composite overmolding process: Interface strength," *Frontiers in Materials*, vol. 7, 2020, ISSN: 2296-8016. DOI: `10.3389/fmats.2020.00027`. [Online]. Available: `frontiersin.org/article/10.3389/fmats.2020.00027`.

[41] W. Qiao and W. Yao, "Modelling of process-induced deformation for composite parts considering tool-part interaction," *Materials*, vol. 13, no. 20, 2020, ISSN: 1996-1944. DOI: `10.3390/ma13204503`. [Online]. Available: `mdpi.com/1996-1944/13/20/4503`.

[42] X. Zeng and J. Raghavan, "Role of tool-part interaction in process-induced warpage of autoclave-manufactured composite structures," *Composites Part A-applied Science and Manufacturing - COMPOS PART A-APPL SCI MANUF*, vol. 41, pp. 1174–1183, Sep. 2010. DOI: `10.1016/j.compositesa.2010.04.017`.

[43] G. Fernlund *et al.*, "Experimental and numerical study of the effect of cure cycle, tool surface, geometry, and lay-up on the dimensional fidelity of autoclave-processed composite parts," *Composites Part A: Applied Science and Manufacturing*, vol. 33, no. 3, pp. 341–351, 2002, ISSN: 1359-835X. DOI: `doi.org/10.1016/S1359-835X(01)00123-3`. [Online]. Available: `sciencedirect.com/science/article/pii/S1359835X01001233`.

[44] D. D. Wright, J. L. Gilbert, and E. P. Lautenschlager, "The effect of processing temperature and time on the structure and fracture characteristics of self-reinforced composite poly(methyl methacrylate)," *Journal of Materials Science: Materials in Medicine*, vol. 10, no. 8, pp. 503–512, 1999, ISSN: 09574530. DOI: `10.1023/A:1008909311523`.

[45] C. Stokes-Griffin and P. Compston, "The effect of processing temperature and placement rate on the short beam strength of carbon fibre–peek manufactured using a laser tape placement process," *Composites Part A: Applied Science and Manufacturing*, vol. 78, pp. 274–283, 2015, ISSN: 1359-835X. DOI: `doi.org/10.1016/j.compositesa.2015.08.008`. [Online]. Available: `sciencedirect.com/science/article/pii/S1359835X15002791`.

[46] D. Saenz-Castillo, M. Martín, S. Calvo, F. Rodriguez-Lence, and A. Güemes, "Effect of processing parameters and void content on mechanical properties and ndi of thermoplastic composites," *Composites Part A: Applied Science and Manufac-*

turing, vol. 121, pp. 308–320, 2019, ISSN: 1359-835X. DOI: `doi.org/10.1016/j.compositesa.2019.03.035`. [Online]. Available: `sciencedirect.com/science/article/pii/S1359835X19301150`.

[47] D. Adams. "Glass transition temperature testing of composites." (2018), [Online]. Available: `compositesworld.com/articles/glass-transition-temperature-testing-of-composites`.

[48] M. Umarfarooq, P. Shivakumar Gouda, G. Veeresh kumar, N. Banapurmath, and A. Edacherian, "Impact of process induced residual stresses on interlaminar fracture toughness in carbon epoxy composites," *Composites Part A: Applied Science and Manufacturing*, vol. 127, p. 105 652, 2019, ISSN: 1359-835X. DOI: `doi.org/10.1016/j.compositesa.2019.105652`. [Online]. Available: `sciencedirect.com/science/article/pii/S1359835X19304014`.

[49] S. Chava and S. Namilae, "Continuous evolution of processing induced residual stresses in composites: An in-situ approach," *Composites Part A: Applied Science and Manufacturing*, vol. 145, p. 106 368, 2021, ISSN: 1359-835X. DOI: `doi.org/10.1016/j.compositesa.2021.106368`. [Online]. Available: `sciencedirect.com/science/article/pii/S1359835X21000920`.

[50] Q. Wu, N. Yoshikawa, N. Morita, and T. Ogasawara, "Investigation of residual stresses induced by composite forming using macro-micro simulation," *Journal of Reinforced Plastics and Composites*, vol. 39, no. 17-18, pp. 654–664, 2020. DOI: `10.1177/0731684420920927`. [Online]. Available: `doi.org/10.1177/0731684420920927`.

[51] J. David A. Darrow and L. V. Smith, "Isolating components of processing induced warpage in laminated composites," *Journal of Composite Materials*, vol. 36, no. 21, pp. 2407–2419, 2002. DOI: `10.1177/0021998302036021784`. [Online]. Available: `doi.org/10.1177/0021998302036021784`.

[52] G. Struzziero, D. Nardi, J. Sinke, and J. J. E. Teuwen, "Cure-induced residual stresses for warpage reduction in thermoset laminates," *Journal of Composite Materials*, vol. 54, no. 22, pp. 3055–3065, 2020. DOI: `10.1177/0021998320908631`. [Online]. Available: `doi.org/10.1177/0021998320908631`.

[53] M. Khalil, E. Bakhiet, and A. El-Zoghby, "Optimum design of laminated composites subjected to hygrothermal residual stresses," *Proceedings of the Institution of Mechanical Engineers, Part L: Journal of Materials: Design and Applications*, vol. 215, no. 3, pp. 175–186, 2001. DOI: `10.1243/1464420011545021`. [Online]. Available: `doi.org/10.1243/1464420011545021`.

[54] J. Timms, S. Bickerton, and P. Kelly, "Laminate thickness and resin pressure evolution during axisymmetric liquid composite moulding with flexible tooling," *Composites Part A: Applied Science and Manufacturing*, vol. 43, no. 4, pp. 621–630, 2012, ISSN: 1359-835X. DOI: `doi.org/10.1016/j.compositesa.2011.12.012`. [Online]. Available: `sciencedirect.com/science/article/pii/S1359835X11004179`.

[55] M. Buntain and S. Bickerton, "Modeling forces generated within rigid liquid composite molding tools. part a: Experimental study," *Composites Part A: Applied Science and Manufacturing*, vol. 38, no. 7, pp. 1729–1741, 2007, ISSN: 1359-835X. DOI: `doi.org/10.1016/j.compositesa.2007.01.012`. [Online]. Available: `sciencedirect.com/science/article/pii/S1359835X0700019X`.

[56] C. Park, "15 - numerical simulation of flow processes in composites manufacturing," in *Advances in Composites Manufacturing and Process Design*, P. Boisse, Ed., Woodhead Publishing, 2015, pp. 317–378, ISBN: 978-1-78242-307-2. DOI: `doi.org/10.1016/B978-1-78242-307-2.00015-4`. [Online]. Available: `sciencedirect.com/science/article/pii/B9781782423072000154`.

[57] S. of Manufacturing Engineers. "Composite tooling design." (), [Online]. Available: `sme.org/globalassets/sme.org/media/training-guides/dv08pub4_study_guide.pdf?_t_tags=language%3Aen%2Csiteid%3A1649ec32-15af-4a13-8a0c-ace198b58648&_t_hit.id=SME_Models_Media_AssetMedia/_6f49d252-e243-4496-bdd7-64644e2e7b93&_t_hit.pos=10`.

[58] U. of Southampton. "Hardness." (2022), [Online]. Available: `southampton.ac.uk/engineering/research/facilities/360/nCATS_facility/hardness.page#:~:text=Hardness%20is%20the%20resistance%20of,to%20plastics%20and%20soft%20tissues.`.

[59] C. Suresh Kumar, V. Arumugam, and C. Santulli, "Characterization of indentation damage resistance of hybrid composite laminates using acoustic emission monitoring," *Composites Part B: Engineering*, vol. 111, pp. 165–178, 2017, ISSN: 1359-8368. DOI: `doi.org/10.1016/j.compositesb.2016.12.012`. [Online]. Available: `sciencedirect.com/science/article/pii/S1359836816318054`.

[60] A. Spruce. "Molding methods & tooling." (), [Online]. Available: `aircraftspruce.ca/catalog/pdf/ComBase.pdf`.

[61] S. L. Clark, "Release agents," in *Handbook of Composites*, G. Lubin, Ed. Boston, MA: Springer US, 1982, pp. 633–638, ISBN: 978-1-4615-7139-1. DOI: `10.1007/978-1-4615-7139-1_23`. [Online]. Available: `doi.org/10.1007/978-1-4615-7139-1_23`.

[62] L. Dorworth. "Avoiding the pitfalls of vacuum infusion processing." (2021), [Online]. Available: `compositesworld.com/articles/avoiding-the-pitfalls-of-vacuum-infusion-processing`.

[63] V. A. International. "Vacuum systems for composite manufacturing." (2018), [Online]. Available: `vacaero.com/information-resources/vac-aero-training/180484-vacuum-systems-for-composite-manufacturing.html#:~:text=In%20order%20to%20create%20a,the%20shape%20of%20the%20mold.`.

[64] Y. Mujahid, N. Sallih, M. Mustapha, M. Z. Abdullah, and F. Mustapha, "Effects of processing parameters for vacuum-bagging-only method on shape conformation of laminated composites," *Processes*, vol. 8, no. 9, 2020, ISSN: 2227-9717. DOI: `10.3390/pr8091147`. [Online]. Available: `mdpi.com/2227-9717/8/9/1147`.

[65] F. Wu, S. Gao, Y. Zeng, Y. Li, Z. Zhao, and C. Shen, "Study on synthesis and demolding performance of polyethylene glycol fatty acid mold release agents," *Polymers for Advanced Technologies*, vol. 32, no. 10, pp. 4061–4069, 2021. DOI: `doi.org/10.1002/pat.5412`. [Online]. Available: `onlinelibrary.wiley.com/doi/abs/10.1002/pat.5412`.

[66] Henkel. "Mold release agents." (2022), [Online]. Available: `henkel-adhesives.com/ca/en/products/industrial-coatings/mold-release-agents.html#:~:text=Mold%20release%20agents%20are%20an,the%20surface%20of%20the%20mold.`.

[67] L. C. Dorworth, "Composite Tooling," in *Composites*, ASM International, Jan. 2001, ISBN: 978-1-62708-195-5. DOI: `10.31399/asm.hb.v21.a0003403`. [Online]. Available: `doi.org/10.31399/asm.hb.v21.a0003403`.

[68] J. Allen, "An investigation into the comparative costs of additive manufacture vs. machine from solid for aero engine parts," in *Cost Effective Manufacture via Net-Shape Processing*, 2006.

[69] J. Watson and K. Taminger, "A decision-support model for selecting additive manufacturing versus subtractive manufacturing based on energy consumption," *Journal of Cleaner Production*, vol. 176, pp. 1316–1322, 2018, ISSN: 0959-6526. DOI: `doi.org/10.1016/j.jclepro.2015.12.009`. [Online]. Available: `sciencedirect.com/science/article/pii/S0959652615018247`.

[70] E. Artetxe *et al.*, "Optimised methodology for aircraft engine ibrs five-axis machining process," *International Journal of Mechatronics and Manufacturing Systems*, vol. 9, no. 4, pp. 385–401, 2016. DOI: `10.1504/IJMMS.2016.082873`. [Online]. Available: `inderscienceonline.com/doi/abs/10.1504/IJMMS.2016.082873`.

[71] J. Barnes, A. Kingsbury, and E. Bono, "Does " low cost " titanium powder yield low cost titanium parts?," Jun. 2016.

[72] FibreGlast. "Mold construction guide." (2022), [Online]. Available: `fibreglast.com/product/mold-construction/Learning_Center`.

[73] B. Morey. "Tooling it up for composites." (2010), [Online]. Available: `sme.org/technologies/articles/2010/tooling-it-up-for-composites/`.

[74] B. Brenken, E. Barocio, A. Favaloro, V. Kunc, and R. B. Pipes, "Fused filament fabrication of fiber-reinforced polymers: A review," *Additive Manufacturing*, vol. 21, pp. 1–16, 2018, ISSN: 2214-8604. DOI: `doi.org/10.1016/j.addma.2018.01.002`. [Online]. Available: `sciencedirect.com/science/article/pii/S2214860417304475`.

[75] J. M. Pappas, A. R. Thakur, M. C. Leu, and X. Dong, "A Comparative Study of Pellet-Based Extrusion Deposition of Short, Long, and Continuous Carbon Fiber-Reinforced Polymer Composites for Large-Scale Additive Manufacturing," *Journal of Manufacturing Science and Engineering*, vol. 143, no. 7, Mar. 2021, ISSN: 1087-1357. DOI: `10.1115/1.4049646`. [Online]. Available: `doi.org/10.1115/1.4049646`.

[76] HAAS. "Vr-8." (2022), [Online]. Available: `haascnc.com/machines/vertical-mills/vr-series/models/vr-8.html`.

[77] A. A. Hassen, J. Lindahl, X. Chen, B. Post, L. Love, and V. Kunc, "Additive manufacturing of composite tooling using high temperature thermoplastic materials," *International SAMPE Technical Conference*, vol. 2016-Janua, no. April 2018, 2016.

[78] P. Liu *et al.*, "Rheology, crystal structure, and nanomechanical properties in large-scale additive manufacturing of polyphenylene sulfide/carbon fiber composites," *Composites Science and Technology*, vol. 168, no. June, pp. 263–271, 2018, ISSN: 02663538. DOI: `10.1016/j.compscitech.2018.09.010`. [Online]. Available: `doi.org/10.1016/j.compscitech.2018.09.010`.

[79] J. Pragana, R. Sampaio, I. Bragança, C. Silva, and P. Martins, "Hybrid metal additive manufacturing: A state–of–the-art review," *Advances in Industrial and Manufacturing Engineering*, vol. 2, p. 100 032, 2021, ISSN: 2666-9129. DOI: `doi.org/10.1016/j.aime.2021.100032`. [Online]. Available: `sciencedirect.com/science/article/pii/S2666912921000027`.

[80] A. Nycz, M. Noakes, B. Post, A. Roschli, S. Babu, and L. Love, "Development and demonstration of large-scale metal additive manufacturing for military vehicle applications - final report," Aug. 2019. DOI: `10.2172/1569396`. [Online]. Available: `osti.gov/biblio/1569396`.

[81] B. V. Reddy, N. V. Reddy, and A. Ghosh, "Fused deposition modelling using direct extrusion," *Virtual and Physical Prototyping*, vol. 2, no. 1, pp. 51–60, 2007, ISSN: 17452759. DOI: 10.1080/17452750701336486.

[82] B. Post, B. Richardson, P. Lloyd, L. Love, S. Nolet, and J. Hannan, "Additive manufacturing of wind turbine molds," Jul. 2017. DOI: 10.2172/1376487. [Online]. Available: osti.gov/biblio/1376487.

[83] A. Roschli *et al.*, "Designing for Big Area Additive Manufacturing," *Additive Manufacturing*, vol. 25, pp. 275–285, 2019, ISSN: 22148604. DOI: 10.1016/j.addma.2018.11.006.

[84] T. D'Amico and A. M. Peterson, "Bead parameterization of desktop and room-scale material extrusion additive manufacturing: How print speed and thermal properties affect heat transfer," *Additive Manufacturing*, vol. 34, no. April, p. 101 239, 2020, ISSN: 22148604. DOI: 10.1016/j.addma.2020.101239. [Online]. Available: doi.org/10.1016/j.addma.2020.101239.

[85] P. Chesser *et al.*, "Extrusion control for high quality printing on big area additive manufacturing (baam) systems," *Additive Manufacturing*, vol. 28, no. C, May 2019. DOI: 10.1016/j.addma.2019.05.020.

[86] M. Shah Mohammadi, M. Ghani, M. Komeili, B. Crawford, and A. Milani, "The effect of manufacturing parameters on the surface roughness of glass fibre reinforced polymer moulds," *Composites Part B: Engineering*, vol. 125, pp. 39–48, 2017, ISSN: 1359-8368. DOI: doi.org/10.1016/j.compositesb.2017.05.028. [Online]. Available: sciencedirect.com/science/article/pii/S1359836816317887.

[87] J. Ahmad, *Machining of Polymer Composites*. New York: Springer New York, 2009, ISBN: 978-0-387-35539-9. DOI: doi.org/10.1007/978-0-387-68619-6. [Online]. Available: link.springer.com/book/10.1007/978-0-387-68619-6#about-book-content.

[88] I. Martínez-Mateo, F. Carrión-Vilches, J. Sanes, and M. Bermúdez, "Surface damage of mold steel and its influence on surface roughness of injection molded plastic parts," *Wear*, vol. 271, no. 9, pp. 2512–2516, 2011, ISSN: 0043-1648. DOI: doi.org/10.1016/j.wear.2010.11.054. [Online]. Available: sciencedirect.com/science/article/pii/S0043164811002766.

[89] C. E. Duty *et al.*, "Structure and mechanical behavior of Big Area Additive Manufacturing (BAAM) materials," *Rapid Prototyping Journal*, vol. 23, no. 1, pp. 181–189, 2017, ISSN: 13552546. DOI: 10.1108/RPJ-12-2015-0183.

[90] "7 - stability of composite shell–type structures," in *Stability and Vibrations of Thin Walled Composite Structures*, H. Abramovich, Ed., Woodhead Publishing, 2017, pp. 253–428, ISBN: 978-0-08-100410-4. DOI: `doi.org/10.1016/B978-0-08-100410-4.00007-7`. [Online]. Available: `sciencedirect.com/science/article/pii/B9780081004104000077`.

[91] K. Karunakaran, V. Pushpa, S. B. Akula, and S. Suryakumar, "Techno-economic analysis of hybrid layered manufacturing," *International Journal of Intelligent Systems Technologies and Applications*, vol. 4, no. 1-2, pp. 161–176, 2008. DOI: `10.1504/IJISTA.2008.016364`. [Online]. Available: `inderscienceonline.com/doi/abs/10.1504/IJISTA.2008.016364`.

[92] D. Homar and F. Pušavec, "The development of a recognition geometry algorithm for hybrid – subtractive and additive manufacturing," *Strojniški vestnik - Journal of Mechanical Engineering*, vol. 63, no. 3, pp. 151–160, 2017, ISSN: 0039-2480. DOI: `10.5545/sv-jme.2016.3924`. [Online]. Available: `sv-jme.eu/article/the-development-of-a-recognition-geometry-algorithm-for-hybrid-subtractive-and-additive-manufacturing/`.

[93] N. A. Sbrugnera Sotomayor, F. Caiazzo, and V. Alfieri, "Enhancing design for additive manufacturing workflow: Optimization, design and simulation tools," *Applied Sciences*, vol. 11, no. 14, 2021, ISSN: 2076-3417. DOI: `10.3390/app11146628`. [Online]. Available: `mdpi.com/2076-3417/11/14/6628`.

[94] T. Cadiou, F. Demoly, and S. Gomes, "A multi-part production planning framework for additive manufacturing of unrelated parallel fused filament fabrication 3d printers," *Designs*, vol. 6, no. 1, 2022, ISSN: 2411-9660. DOI: `10.3390/designs6010011`. [Online]. Available: `mdpi.com/2411-9660/6/1/11`.

[95] L. Wirths, M. Bleckmann, and K. Paetzold, "A structured approach to reduce design iterations in additive manufacturing," *Proceedings of the Design Society*, vol. 1, pp. 231–240, 2021. DOI: `10.1017/pds.2021.24`.

[96] C. Potter, S. Cotts, and F. Wiebke. ().

[97] S. Hunter, "Molybdenum nitrides: Structural and reactivity studies," PhD Thesis, University of Glasgow, 2012. [Online]. Available: `researchgate.net/deref/http%3A%2F%2Ftheses.gla.ac.uk%2F3221%2F`.

[98]   M. Nijman, "Thermal analysis in practice: Tips and hints," in *Thermal Analysis*, N. Fedelich *et al.*, Eds., 2016. [Online]. Available: `mt.com/ca/en/home/library/applications/lab-analytical-instruments/thermal-analysis-tips-and-hints.html`.

[99]   T. A. Instruments. "Thermal analysis." (2011), [Online]. Available: `tainstruments.com/pdf/brochure/2011%20TGA%20Brochure.pdf`.

[100]   S. Tagliati, "Development and characterization of a membrane-based nancalorimeter for low temperatures," PhD Thesis, Stockholm University, 2010. [Online]. Available: `researchgate.net/publication/267985499_Development_and_characterization_of_a_membrane-based_nanocalorimeter_for_low_temperatures`.

[101]   T. A. Instruments. "Ta instruments - tga/sorption sample pan guide," Thermal Analysis Instruments. (), [Online]. Available: `tainstruments.com/pdf/literature/TN072_REV-D-TGA_Sample_Pan_Guide.pdf`.

[102]   R. P. Wool, B. .-. Yuan, and O. J. McGarel, "Welding of polymer interfaces," *Polymer Engineering & Science*, vol. 29, no. 19, pp. 1340–1367, 1989, ISSN: 15482634. DOI: `10.1002/pen.760291906`.

[103]   A. Shrivastava, *Introduction to Plastics Engineering* (Plastics Design Library). William Andrew Publishing, 2018, ISBN: 978-0-323-39500-7. DOI: `doi.org/10.1016/B978-0-323-39500-7.00001-0`. [Online]. Available: `sciencedirect.com/science/article/pii/B9780323395007000010`.

[104]   K. Friedrich and R. Walter, *Structure and Properties of Additive Manufactured Polymer Composites*, C. Soutis, Ed., ed. by S. Advani, ed. by B. Fiedler. Woodhead Publishing, 2020, ISBN: 978-0-12-819535-2. DOI: `doi.org/10.1016/C2018-0-03664-6`. [Online]. Available: `sciencedirect.com/book/9780128195352/structure-and-properties-of-additive-manufactured-polymer-components#book-info`.

[105]   PerkinElmer. "A beginners guide to tma 4000." (2013), [Online]. Available: `resources.perkinelmer.com/corporate/cmsresources/images/44-154961faq_tma_4000.pdf`.

[106]   K. Menard and B. Cassel. "Basics of thermomechanical analysis with tma 4000." (2013), [Online]. Available: `resources.perkinelmer.com/corporate/cmsresources/images/44-154962tch_tma_4000.pdf`.

[107]   D. Price and J. Duncan, "Thermomechanical, dynamic mechanical and dielectric methods," in Feb. 2016, pp. 164–213, ISBN: 978-1-78262-051-8.

[108] Hitachi. "Principle of thermomechanical analysis (tma)." (2022), [Online]. Available: `hitachi-hightech.com/global/products/science/tech/ana/thermal/descriptions/tma.html`.

[109] Y. Xiu, L. Zhu, D. W. Hess, and C. P. Wong, "Relationship between work of adhesion and contact angle hysteresis on superhydrophobic surfaces," *The Journal of Physical Chemistry C*, vol. 112, no. 30, pp. 11 403–11 407, 2008. DOI: `10.1021/jp711571k`. [Online]. Available: `doi.org/10.1021/jp711571k`.

[110] Hideo Nakae, Ryuichi Inui, Yosuke Hirata, and Hiroyuki Saito, "Effects of surface roughness on wettability," *Acta Materialia*, vol. 46, no. 7, pp. 2313–2318, 1998, ISSN: 1359-6454. DOI: `doi.org/10.1016/S1359-6454(98)80012-8`. [Online]. Available: `sciencedirect.com/science/article/pii/S1359645498800128`.

[111] B. Scientific. "Contact angle measurement." (2022), [Online]. Available: `biolinscientific.com/measurements/contact-angle`.

[112] B. Scientific. "Dynamic contact angle." (2022), [Online]. Available: `biolinscientific.com/measurements/dynamic-contact-angle`.

[113] G. Kim, "The effect of additional surface coating on the performance of additively manufactured fiber reinforced composite mold," PhD Thesis, Purdue University, 2020. DOI: `doi.org/10.25394/PGS.12517904.v1`. [Online]. Available: `hammer.purdue.edu/articles/thesis/The_effect_of_additional_surface_coating_on_the_performance_of_additively_manufactured_fiber_reinforced_composite_mold/12517904`.

[114] G. Chardon, H. Chanal, E. Duc, and T. Garnier, "Study of surface finish of fiber-reinforced composite molds," *Proceedings of the Institution of Mechanical Engineers, Part B: Journal of Engineering Manufacture*, vol. 231, no. 4, pp. 576–587, 2017. DOI: `10.1177/0954405415617929`. [Online]. Available: `doi.org/10.1177/0954405415617929`.

[115] G. Dickson and R. McIlhagger, "Assessing the surface finish of polymer composite components," *International Journal of Machine Tools and Manufacture*, vol. 32, no. 1, pp. 51–56, 1992, Proceedings of the 5th International Conference on Metrology and Properties of Engineering Surfaces, ISSN: 0890-6955. DOI: `doi.org/10.1016/0890-6955(92)90060-T`. [Online]. Available: `sciencedirect.com/science/article/pii/089069559290060T`.

[116] J. Marteau, M. Bigerelle, S. Bouvier, and A. Iost, "Reflection on the measurement and use of the topography of the indentation imprint," *Scanning*, vol. 36, no. 1, pp. 115–126, 2014. DOI: `doi.org/10.1002/sca.21107`. eprint: `onlinelibrary.wiley.com/doi/pdf/10.1002/sca.21107`. [Online]. Available: `onlinelibrary.wiley.com/doi/abs/10.1002/sca.21107`.

[117] N. Instruments. "Optical profilometry." (2022), [Online]. Available: `nanoscience.com/techniques/optical-profilometry/`.

[118] G. Mitaľ, J. Dobránsky, J. Ružbarský, and Š. Olejárová, "Application of laser profilometry to evaluation of the surface of the workpiece machined by abrasive waterjet technology," *Applied Sciences*, vol. 9, no. 10, 2019, ISSN: 2076-3417. DOI: `10.3390/app9102134`. [Online]. Available: `mdpi.com/2076-3417/9/10/2134`.

[119] P. de Groot, *Optical Measurement of Surface Topography*, R. Leach, Ed. Berlin, Heidelberg: Springer Berlin Heidelberg, 2011, ISBN: 978-3-642-12011-4. DOI: `doi.org/10.1007/978-3-642-12012-1`. [Online]. Available: `link.springer.com/book/10.1007/978-3-642-12012-1`.

[120] Zygo. "Coherence scanning interferometry (csi)." (2022), [Online]. Available: `zygo.com/support/technologies/csi-techology`.

[121] Keyence. "Sa (arithmetical mean height)." (2022), [Online]. Available: `keyence.com/ss/products/microscope/roughness/surface/parameters.jsp`.

[122] Keyence. "Sz (maximum height)." (2022), [Online]. Available: `keyence.com/ss/products/microscope/roughness/surface/sz-maximum-height.jsp`.

[123] Keyence. "Sq (root mean square height)." (2022), [Online]. Available: `keyence.com/ss/products/microscope/roughness/surface/sq-root-mean-square-height.jsp`.

[124] A. B. Varotsis. "Injection molding spi surface finishes." (2022), [Online]. Available: `https://www.hubs.com/knowledge-base/injection-molding-spi-surface-finishes/`.

[125] HUBS. "The manufacturing & design guide: Injection molding." (2022), [Online]. Available: `https://www.hubs.com/guides/injection-molding/#design-for-injection-molding`.

[126] A. Roschli, A. Messing, M. Borish, B. K. Post, and L. J. Love, "ORNL Slicer 2: A novel approach for additive manufacturing tool path planning," in *Solid Freeform Fabrication*, 2017, pp. 896–902.

[127] C. E. Duty *et al.*, "A Viscoelastic Model for Evaluating Extrusion-Based Print Conditions," in *Solid Freeform Fabrication Symposium*, 2017, pp. 495–506.

[128] T. A. Instruments. "Ta instruments - thermal analysis." (2006), [Online]. Available: `http://www.tainstruments.com/pdf/TGA%20Brochure.pdf`.

[129] A. International, "Standard test method for transition temperatures and enthalpies of fusion and crystallization of polymers by differential scanning calorimetry," in *ASTM Volume 08.02: Plastics (II): D3222–D5083*. 2015.

[130] C. Demaria and P. Hubert, *Measurement of the coefficient of thermal expansion of al6061-t6*, 2017.

[131] A. International, "Standard test method for linear thermal expansion of solid materials by thermomechanical analysis," in *ASTM Volume 14.01: Statistical Methods; Hazard Potential Of Chemicals; Thermal Measurements; Manufacture Of Pharmaceutical And Biopharmaceutical Products; Healthcare Informatics*. 2012.

[132] F. Silva, R. Martinho, M. Andrade, A. Baptista, and R. Alexandre, "Improving the wear resistance of moulds for the injection of glass fibre–reinforced plastics using pvd coatings: A comparative study," *Coatings*, vol. 7, no. 2, 2017, ISSN: 2079-6412. DOI: `10.3390/coatings7020028`. [Online]. Available: `https://www.mdpi.com/2079-6412/7/2/28`.

[133] ZEUS, *Thermal degradation of plastics*, 2005. [Online]. Available: `http://www.appstate.edu/~clementsjs/polymerproperties/zeus_thermal_degradation.pdf`.

[134] J. Shah, B. Snider, T. Clarke, S. Kozutsky, M. Lacki, and A. Hosseini, "Large-scale 3D printers for additive manufacturing: design considerations and challenges," *International Journal of Advanced Manufacturing Technology*, vol. 104, no. 9-12, pp. 3679–3693, 2019, ISSN: 14333015. DOI: `10.1007/s00170-019-04074-6`.

[135] M. Toledo. "Abs glass transition by dsc." (), [Online]. Available: `https://www.mt.com/ca/en/home/supportive_content/matchar_apps/MatChar_HB251.html`.

[136] J. Moore, "Acrylonitrile-butadiene-styrene (abs) - a review," *Composites*, vol. 4, no. 3, pp. 118–130, 1973, ISSN: 0010-4361. DOI: `https://doi.org/10.1016/0010-4361(73)90585-5`. [Online]. Available: `https://www.sciencedirect.com/science/article/pii/0010436173905855`.

[137] Omnexus. "Glass transition temperature." (2022), [Online]. Available: `https://omnexus.specialchem.com/polymer-properties/properties/glass-transition-temperature`.
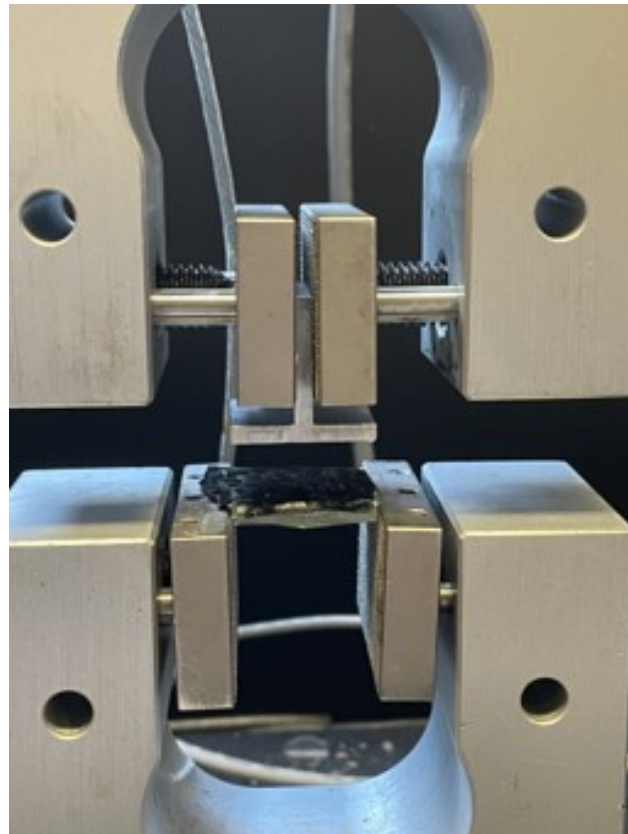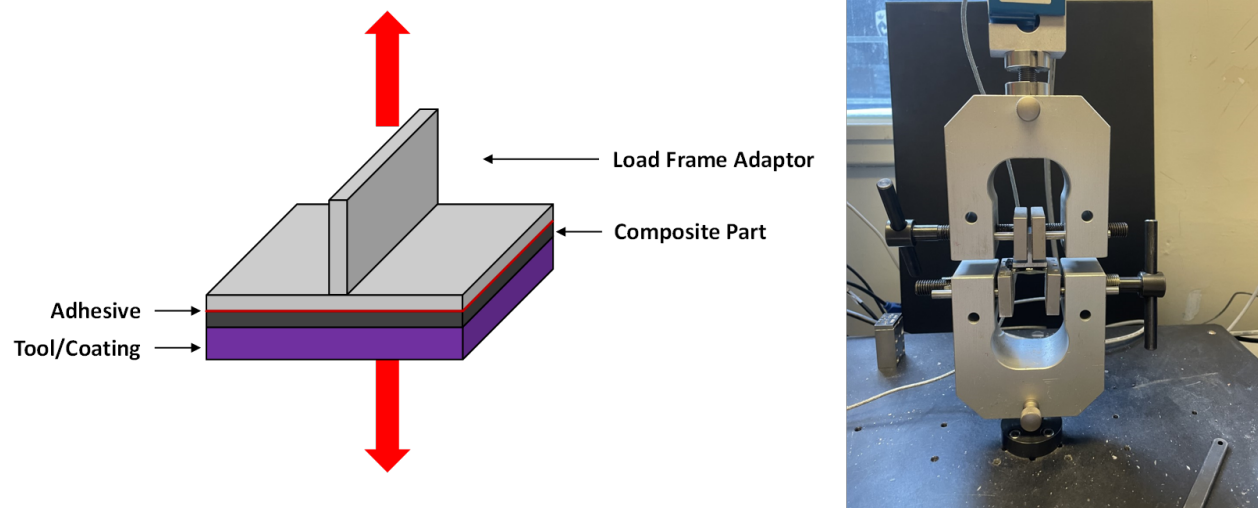
[138] Z. Lan *et al.*, "Color changes and mechanical properties of glass fiber reinforced polycarbonate composites after thermal aging," *Polymers*, vol. 14, no. 2, 2022, ISSN: 2073-4360. DOI: `10.3390/polym14020222`. [Online]. Available: `https://www.mdpi.com/2073-4360/14/2/222`.

[139] D. Adams. "Glass transition temperature testing of composites." (2018), [Online]. Available: `https://www.compositesworld.com/articles/glass-transition-temperature-testing-of-composites`.

[140] A. A. Hassen *et al.*, "Simulation assisted design for an additively manufactured autoclave tool accounting for an anisotropic expansion," *CAMX 2019 - Composites and Advanced Materials Expo*, pp. 1–10, 2020.

[141] S. Kim *et al.*, "Analysis on part distortion and residual stress in big area additive manufacturing with carbon fiber-reinforced thermoplastic using dehomogenization technique," *CAMX 2019 - Composites and Advanced Materials Expo*, pp. 1–14, 2019.

[142] S. Gantenbein, K. Masania, W. Woigk, J. P. Sesseg, T. A. Tervoort, and A. R. Studart, "Three-dimensional printing of hierarchical liquid-crystal-polymer structures," *Nature*, vol. 561, no. 7722, pp. 226–230, 2018, ISSN: 14764687. DOI: `10.1038/s41586-018-0474-7`.

[143] S. Sgobba, "Materials for high vacuum technology, an overview," *CAS - CERN Accelerator School: Vacuum in Accelerators*, pp. 117–144, 2006. DOI: `http://dx.doi.org/10.5170/CERN-2007-003.117`.

[144] "Chapter 2 microstructure and mechanical properties of materials," in *Microstructure and Wear of Materials*, ser. Tribology Series, K.-H. Z. Gahr, Ed., vol. 10, Elsevier, 1987, pp. 8–47. DOI: `https://doi.org/10.1016/S0167-8922(08)70720-X`. [Online]. Available: `https://www.sciencedirect.com/science/article/pii/S016789220870720X`.

[145] J. Lopez, "Microhardness testing of plastics: Literature review," *Polymer Testing*, vol. 12, no. 5, pp. 437–458, 1993, ISSN: 01429418. DOI: `10.1016/0142-9418(93)90016-I`.

[146] M. Herring, J. Mardel, and B. Fox, "The effect of material selection and manufacturing process on the surface finish of carbon fibre composites," *Journal of Materials Processing Technology*, vol. 210, no. 6, pp. 926–940, 2010, ISSN: 0924-0136. DOI: `https://doi.org/10.1016/j.jmatprotec.2010.02.005`. [Online]. Available: `https://www.sciencedirect.com/science/article/pii/S0924013610000385`.

[147]   M. Mehdikhani, L. Gorbatikh, I. Verpoest, and S. V. Lomov, "Voids in fiber-reinforced polymer composites: A review on their formation, characteristics, and effects on mechanical performance," *Journal of Composite Materials*, vol. 53, no. 12, pp. 1579–1669, 2019. DOI: 10.1177/0021998318772152. [Online]. Available: https://doi.org/10.1177/0021998318772152.

Appendix

A.1   Custom Demould Testing Setup

In the preliminary design and planning for the demold testing, a custom demold test setup was devised which would quantitatively characterize the force required to demold the fabricated composite part from the tool (Figure 6.1). This setup consisted of a load frame adaptor adhesively bonded to the top of the composite part, which was then loaded into a mechanical testing frame and pulled in tension recording the applied load until the composite part was demolded or failure occurred. A "threshold value" of 222 kN (approximately 50 lbf) was defined as "reasonable" maximum force a technician could apply during demolding, any force value above this constituting failure of the tool. Initial testing of the design however revealed that the predominate failure mode appeared to be cohesive in the adhesive between the adaptor and composite part (Figure 6.2), occurring during the first iteration of demold testing (i.e. after the first iteration of composite processing). Though initially thought to be a result of poor adaptor bonding, the measured forces at failure well exceeded 600 N, which was well above the defined threshold value. As such, it was expected that this was most likely due to the "edge effects" previously discussed, therefore future work looks to address this issue by eliminating it in an updated tool design and test setup (Figure 6.3).
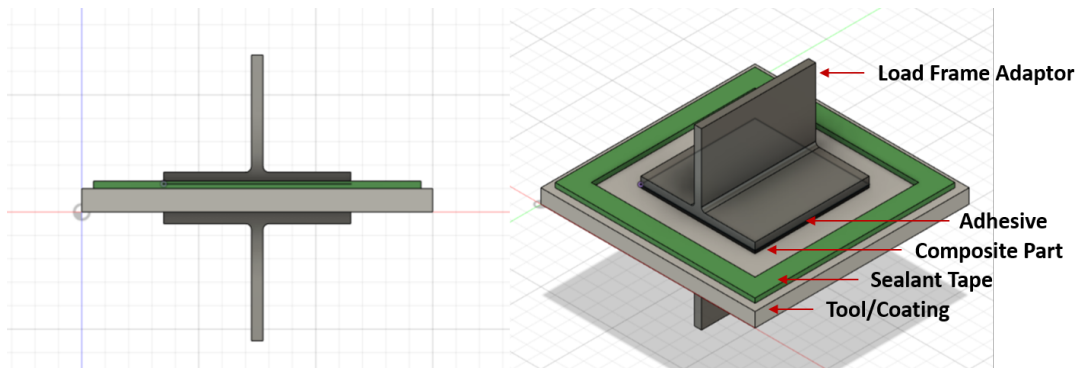
Figure 6.1: Initial design of the custom demold test.

Figure 6.2: Cohesive failure of the adhesive used to bond the adaptor to the composite part.

Figure 6.3: Updated design of the custom demold test.

A.2 Custom Procedure for GF-PC Tool Tensiometry

During the tensiometry tests for GF-PC tools, there appeared to be some degree of attraction between the reverse osmosis water droplet and the tool surface (or repulsion between the droplet and the needle) that would cause the droplet to interfere with contact angle measurement. To prevent this issue, for all subsequent droplets the needle was positioned directly above the specimen surface prior to droplet formation (Figure 6.4a). This had limited success however, as instead of remaining directly below the needle with the needle centre in the droplet, the droplet with instead jump to the side of the needle (Figure 6.4bc). When the needle position was attempted to be re-centered, in some cases the droplet would appear to be repelled by the needle being pushed along the surface of the specimen. To circumnavigate the aforementioned issue, the needle was laterally removed from the droplet, raised above the droplet's edge, repositioned over the centre, and vertically lowered back into the droplet. Despite these modifications to the procedure, for many subsequent tests the droplet would again jump/grow to the side of the needle.as soon as they drop the increased in size.
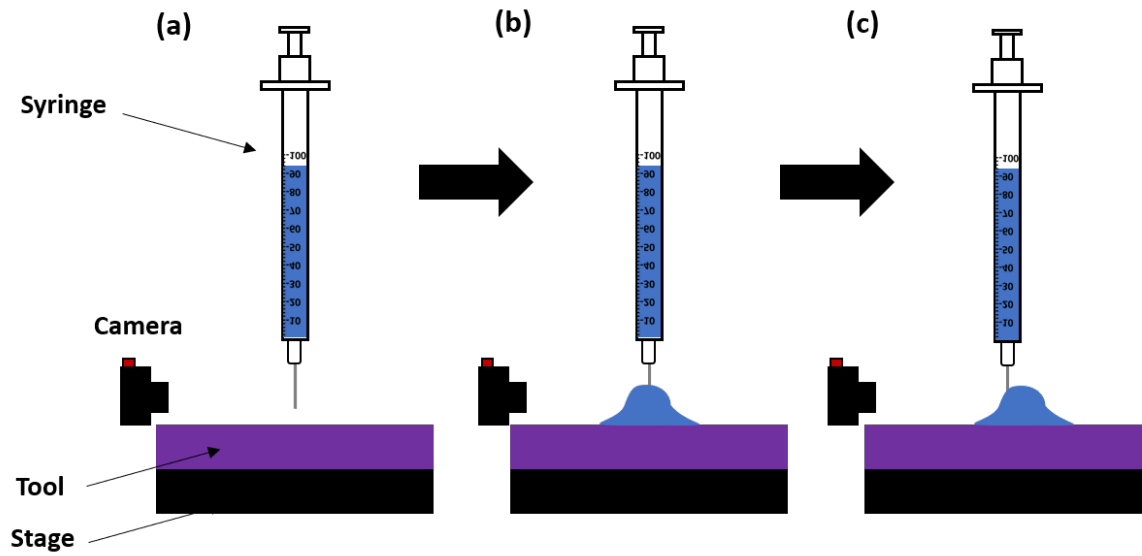
Figure 6.4: Shifting droplet phenomenon during droplet formation on GF-PC tools. (a) Initial position of needle prior to droplet formation. (b) Initial droplet formation. (c) Final droplet position after initial droplet formation.